

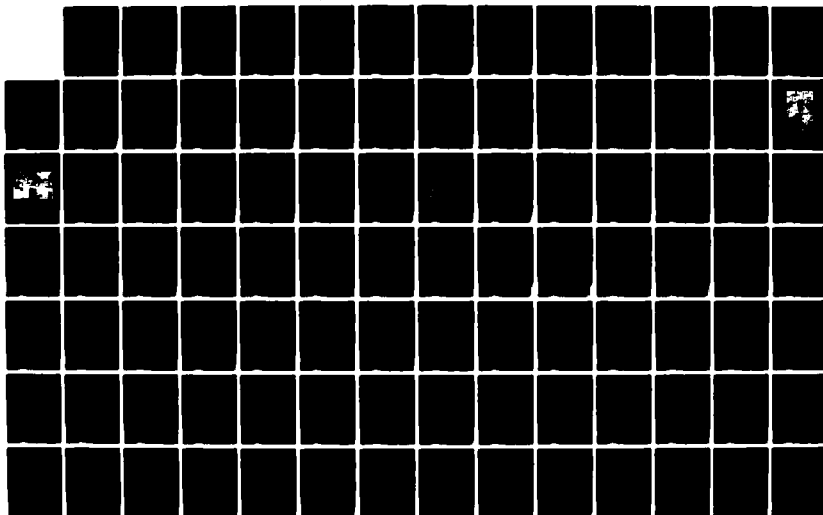
AD-A147 449

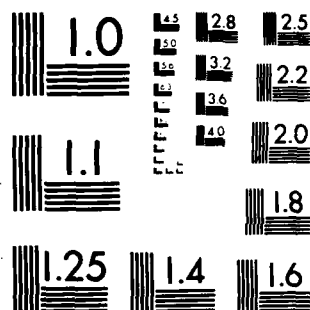
X-RAY AND BACKSCATTERING ANALYSIS OF ION IMPLANTATION
PHENOMENA IN GAAS A. (U) CALIFORNIA INST OF TECH
PASADENA M A NICOLET ET AL. 04 AUG 84 MDA903-82-C-0348

1/3

UNCLASSIFIED

F/G 20/12 NL





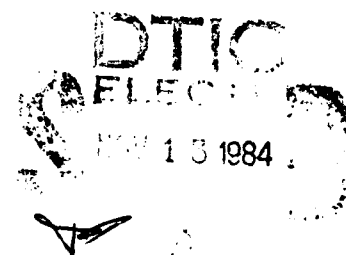
MICROCOPY RESOLUTION TEST CHART
NATIONAL BUREAU OF STANDARDS-1963-A

AD-A147 449

DTIC FILE COPY

"X-RAY AND BACKSCATTERING ANALYSIS
OF ION IMPLANTATION PHENOMENA IN
GAAs AND RELATED COMPOUNDS"

FINAL TECHNICAL REPORT
CONTRACT No. MDA 903-82-C-0348



APPROVED FOR PUBLIC RELEASE
DISTRICT OF COLUMBIA (A)

84 11 09 042

"X-Ray and Backscattering Analysis of Ion Implantation
Phenomena in GaAs and Related Compounds"

FINAL TECHNICAL REPORT

| | |
|-----------------------------|--|
| ARPA Order Number: | 4550 |
| Contractor: | California Institute of Technology |
| Effective Date of Contract: | August 5, 1982 |
| Contract Expiration Date: | August 4, 1984 |
| Reporting Period: | August 5, 1982-August 4, 1984 |
| Contract Number: | MDA 903-82-C-0348 |
| Principal Investigators: | Professor M-A. Nicolet (818) 356-4803 Professor T. Vreeland, Jr. (818) 356-4431 |

"The views and conclusions contained in this document are those of the authors and should not be interpreted as representing the official policies, either expressed or implied, of the Defense Advanced Research Projects Agency or the U.S. Government".

Sponsored by

Defense Advanced Research Projects Agency (DoD)

ARPA Order No. 4550

Under Contract No. MDA 902-82-C-0348 issued by

Department of Army, Defense Supply Service

Washington,

Washington, D. C. 20310



A-1

TABLE OF CONTENTS

| | <u>Page</u> |
|--|-------------|
| 1. Introduction | 2 |
| 2. Methods | 2 |
| a. Sample Preparation | 2 |
| b. X-Ray Diffraction | 3 |
| c. Backscattering Spectrometry | 4 |
| d. Transmission Electron Microscopy | 5 |
| 3. Room Temperature Implantation in Si, Ge, and GaAs | 5 |
| a. Dose Dependence of Strain | 5 |
| b. Dependence of Strain on Nuclear Energy Deposition | 7 |
| i) Low doses: profiles | 7 |
| ii) Low doses: variation with ion species | 8 |
| iii) All doses | 8 |
| c. TEM | 11 |
| 4. Implantation in GaAs - Other Temperatures | 11 |
| a. Low Temperature | 11 |
| b. High Temperature | 12 |
| 5. Annealing of Implanted GaAs | 12 |
| a. Room Temperature Implantation | 12 |
| b. Low Temperature Implantation | 13 |
| c. Multiple Implantation | 14 |
| 6. Other III-V Compounds | 16 |
| 7. III-V Strained Layers and Superlattices | 18 |
| 8. List of Participants | 41 |
| 9. References | 43 |
| Appendix A: A List of Publications with Sponsorship of DARPA | 45 |
| Appendix B: Reprints and preprints of Publications | 47 |

X-RAY AND BACKSCATTERING ANALYSIS OF ION IMPLANTATION IN GaAs AND RELATED COMPOUNDS

Final Technical Report

1. Introduction

→ This report

We present ~~here~~ an overview of a two-year study of the structure of III-V semiconductor materials with a powerful new analysis technique (kinematic modeling of double-crystal x-ray diffraction), complemented by two well-established techniques (backscattering spectrometry and transmission electron microscopy). The kinematic modeling approach to x-ray diffraction was developed at Caltech by Speriosu^(P) for studies of magnetic garnets, but clearly had great additional potential for studying the crystalline structure of semiconductors. We have used these three techniques ^{ways} to study ion implantation and annealing phenomena in uniform III-V semiconductors and extended the kinematic modeling of x-ray diffraction for high precision analysis of bilayer and multilayer epitaxial III-V systems. In the latter application, this method has proven to be superior to all other known techniques.

2. Methods

a. Sample Preparation

(100) Si, Ge, and III-V wafers were obtained from standard sources, and cleaned and etched lightly before processing. Heteroepitaxial structures, which were analyzed as-grown only, were provided by various outside collaborators.

For ion implantation, samples were mounted with thermally-conducting paste on a temperature-controlled carousel. To avoid channeling of the incoming ions, they were rotated 7° away from normal about an axis lying about 22° from a [100] plane. Implantation currents were kept at $0.1 \mu\text{A}/\text{cm}^2$ to within $\pm 30\%$.

Annealing was conducted in flowing forming gas for 60 min at 420°C .

b. X-Ray Diffraction

A double-crystal x-ray spectrometer was designed and constructed for this project. It is shown in Fig. 1. X-rays from a tube with a Fe target are collimated and diffracted by a first crystal which has been adjusted to a Bragg angle near that chosen for the sample. This serves to reduce the beam divergence and select the characteristic K_α line. The first crystals were Si for the Si samples, and GaAs for the Ge and III-V samples. The beam from the first crystal is then allowed to impinge on the sample with a spot size of $\sim 1 \text{ mm} \times 1 \text{ mm}$, set with slits. X-rays diffracted from the sample are detected with a NaI(Tl) detector. The sample is first oriented by hand close to the chosen Fe $K_{\alpha 1}$ (400) reflection angle and then rotated finely through typically less than 1° , by a microprocessor-controlled step-scan apparatus, with a step size of 0.0001° . The reflected intensity is

normalized to the incident intensity to give the reflecting power. This is recorded as a function of angle to give a so-called "rocking curve".

To analyze this data, theoretical rocking curves are generated from trial distributions of crystal strain and damage by means of a kinematic model for the diffraction. These are computed repeatedly with iterative manual adjustments of the strain and damage profiles until good fits to the experimental data are obtained. By this method, one can determine profiles of strain (ϵ) to high accuracy, and profiles of damage (U) to a moderate precision (see Ref. 1 for details). In all of the present work on uniform layers, U (in Å) was found to be equal to about $0.3 \times \epsilon^\perp$ (in %), where ϵ^\perp is the strain perpendicular to the sample surface.

Computer codes for accepting rocking curve data from the step-scan system, and for generating the theoretical rocking curves were written under the present contract. Also, complete plotter graphics programs were written for comparing experimental and theoretical rocking curves, and displaying the corresponding profiles of strain and damage. Finally, an attempt was made to write a program for automatic iterative fitting of the rocking curves, but because of the large number of parameters involved, it was successful only for simple profiles. Since an experienced operator was faster than the automatic routine for such profiles, the routine was clearly not useful.

c. Backscattering Spectrometry

Backscattering spectrometry (BSS) was conducted in an

evacuated target chamber with 1.5 MeV He^+ ions from either an old van de Graaff accelerator or our new Pelletron accelerator. The ions are collimated to a spot of $\sim 1.5 \text{ mm} \times 1.5 \text{ mm}$, and allowed to impinge close to normal to the top surface of the sample. Backscattered ions are detected by a Si surface barrier detector mounted at a scattering angle of 170° . Signals from the detector are sorted according to energy to give backscattering spectra. The sample is rotated finely about two axes until the beam is incident on the (100) axis for "axially channeled" spectra or misoriented by 7° from the axis and rotated continuously about the beam axis for "random" spectra. A high vacuum beam line (shown in Fig. 2) was designed and installed on the Pelletron for this purpose.

d. Transmission Electron Microscopy

Selected implanted samples were analyzed by transmission electron microscopy (TEM) by A. K. Rai at Universal Energy Systems, Inc., Dayton, Ohio. They were prepared by jet thinning with methyl bromide solution from the unimplanted side and observed in plan view with the microscope operating at 300 kV. (200) reflection bright field micrographs were recorded, as well as transmission electron diffraction (TED) patterns.

3. Room Temperature Implantation in Si, Ge and GaAs

a. Dose Dependence of Strain

We reported some results for room temperature Si-implantation in Si, Ge and GaAs, analyzed by x-ray rocking

curves, at an early date⁽²⁾. In Si and Ge, the distributions of strain and defects have the same approximately - Gaussian shapes, which increase in magnitude linearly with irradiation dose, until the material goes amorphous. Thus the maximum strain increases linearly with dose, as is shown in Fig. 3. For GaAs, the situation is markedly different. We now discuss those results in detail.

Figure 4 shows a typical series of rocking curves, obtained from 300 keV Ne-implanted GaAs, together with calculated fits and the corresponding distributions of strain and damage. In part A, the strain profile is approximately Gaussian and, as will be shown later, closely follows the distribution of energy deposited in the lattice by atomic displacements. Its maximum is about 0.25%. In part B of Fig. 4, the dose has been increased by a factor of 6.6. But the strain does not increase by this factor. Rather, it saturates strongly at a value near 0.45%. The fact that U (the measure of net point defects created) is saturating in the same way as the strain suggests that self-annealing is the cause of the saturation. At a dose of 5×10^{14} ions/cm² (part C), there is a drastic change in the strain and damage profiles. In a 3000 Å thick region at the depth of the broad peak in the distributions for the lower doses, the strain now rises sharply to 0.8%, while at other depths the profile is nearly the same as it was in part B. In this region the damage also rises, but we do not have the resolution to determine whether it is still strictly linear with the strain. This dramatic phenomenon was reproduced with all of the ion

species that we investigated (C, Ne, Si, P, Te). Its cause is not yet clear. At a dose of 1×10^{15} ions/cm² (part D of Fig. 4) the surface half of the layer has been rendered amorphous ($U = 0.4 \text{ \AA}$), but a 3000 \AA thick strained layer remains. The rocking curve for this sample no longer has the rapid oscillations exhibited in those for lower irradiation doses. Similar behavior was observed at doses close to those necessary for amorphizing the sample with the other irradiating ions. This indicates that the lateral coherence (or uniformity) of the layer has deteriorated. Specifically, we calculate that there are variations of $\sim 0.01\%$ in the strain and/or variations of ~ 2 arcmin in orientation. A similar series of strain and damage profiles, but this time for 300 keV Si⁺ implantation, is shown in Fig. 5 and corresponding backscattering spectra are shown in Fig. 6. The maximum strain-versus-dose curve from this series is that included in Fig. 3 for GaAs.

b. Dependence of Strain on Nuclear Energy Deposition

(i) Low Doses: Profiles

The linear rise of maximum strain with dose seen at low doses (see Fig. 3) suggests in this regime the strain may be related simply to parameters which scale linearly with dose. Possible candidates include the amount of energy deposited by a collision cascade in nuclear interactions per unit depth (F_D), or the local concentration of implanted ions. In Fig. 7, we compare the strain profile obtained with 300 keV Si⁺ ions at a dose of 2×10^{13} ions/cm² with calculated distributions of F_D and the Si concentration⁽³⁾. The agreement between the shapes of the strain

and F_D curves suggests that the source of the strain is the energy deposited in nuclear interactions.

(ii) Low Doses: Variation with Ion Species.

Another way of testing the hypothesis that at low doses the strain is linear with F_D is to compare doses for different ion species resulting in the same (below- saturation) strain. We have determined experimentally the doses corresponding to 0.1% peak strain for implantation with Te^{++} , P^+ , Si^+ , Ne^+ , C^+ , and H^+ . If the relation between strain and F_D is unique, there should be an inverse relationship between dose and F_D for various implanted species. Figure 8 shows fairly convincingly that this is indeed the case.

(iii) All Doses

We showed earlier that at higher doses the strain profile becomes almost flat, and at higher doses still, develops a large peak. Thus it is clearly no longer scaling with F_D . Nevertheless, it is of interest to determine whether there is a unique relationship between the strain that is actually measured at a depth x and the total energy in nuclear interactions deposited there, E_d .

$$E_d(x) = F_{D,\phi}(x)\phi$$

where ϕ is the implantation dose and $F_{D,\phi}(x)$ is the energy deposited in nuclear interactions for a unit dose. We have done this for several different ion species as follows. The strain profile $\epsilon_0(x)$ measured at the lowest dose ϕ_0 for which reasonable

statistics could be obtained was taken to be proportional to the exact $F_D(x)$ profile, i.e.

$$F_{D,\phi}(x) = C\epsilon_0(x)/\phi_0$$

where C is an unknown constant. In all cases the x -dependence so obtained for $F_{D,\phi}(x)$ was close to the heat of calculated F_D profile, but since the calculations have uncertainties of the order of 20%, the strain profile was thought to give a more reliable shape for F_D . Thus, at all doses, E_d is proportional $\epsilon_0(x)$, scaled with ϕ :

$$E_d(x) = C(\phi/\phi_0)\epsilon_0(x)$$

Now for each irradiation dose we have a histogram for $\epsilon(x)$ versus x . Calculating E_d/C for each x , we obtain a series of $(E_d/C, \epsilon)$ points. Results for the 300 keV Ne^+ irradiation at room temperature and constant flux of $0.1 \mu\text{A}/\text{cm}^2$ are shown in Fig. 9, in which the series of points for each irradiation dose is represented by a different symbol. We see that except for one small deviation (which may result from a slight change in irradiation flux) all of the points lie on a single curve. This means that the strain is indeed a unique function of the total energy deposited locally.

However, as expected from our earlier plots of maximum strain versus dose, the dependence of the strain on E_d is far from linear. The strain initially rises linearly with E_d

(region I) up to a value of about $\epsilon = 0.25\%$. Then the strain increases more and more slowly with E_d , until it saturates at about 0.43% at $E_d \sim 1$ unit and stays almost constant up to $E_d \sim 3$ units (region II). At higher E_d , the strain begins to rise again (region III) and continues to about 0.8% (region IV), at which level the GaAs becomes amorphous. These regions are analogous to the regions marked in Fig. 3. Similar curves were obtained for irradiations of other ions in GaAs. By contrast, for elemental semiconductors the curves were approximately linear for all doses.

The strain that is observed in these ion-implanted semiconductors is most likely caused by atoms that have been displaced from their lattice sites (i.e. point defects) tending to expand the lattice isotropically. The implanted region is constrained horizontally by the undamaged underlying crystal, so it can expand only in the direction perpendicular to the sample surface. This is supported by the fact that in magnetic garnets, as well as Si, Ge and for low dose implantations in GaAs, the strain distribution is found to give the same shape as that calculated for F_D , and the damage deduced from the x-ray rocking curves always scales linearly with the strain.

Presumably, in region I the number of atoms remaining a significant distance from lattice sites is approximately proportional to deposited energy E_d , with the result that ϵ increases linearly with E_d . The saturation of ϵ in region II may be the result of self-annealing of displacement damage. In region III the GaAs strain is about 0.43% which is

close to the known yield value of tensile strain in undamaged, externally-stressed $\langle 110 \rangle$ GaAs⁽⁴⁾. It is in this regime that the loss of coherence in the rocking curves becomes apparent. A possible explanation for this may be the onset of plastic deformations, or the formation of extended defects.

c. TEM

A transmission electron microscopy study was conducted on the Si-implanted GaAs samples of Fig. 3. The bright field micrographs in regions I and II were featureless. In region III they show a spotty structure, suggesting the presence of damage clusters. This adds support to the hypothesis of self-annealing in regions II and III. In region IV, similar spotty structure is evident in the bright field mode while faint rings begin to appear in the TED pattern, indicating the onset of amorphous regions. However, no evidence for extended defects could be found. For higher doses in region IV, the amorphous rings become stronger, indicating a thickening of the amorphous layer.

4. Implantation in GaAs - Other Temperatures

a. Low Temperature

GaAs was implanted at a temperature of ~ 90 K with 300 keV P^+ ions, with six different doses below that required for amorphicity. The strain and damage profiles had exactly the same shape as observed for room temperature implantation and they evolved with increasing dose in the same way. The only

observable difference for the room temperature behavior was that the rate of increase of the strain and damage with dose were slightly higher. We attribute this to a lower rate of self-annealing at the lower temperature.

b. High Temperature

Implantation of 300 keV Si ions in GaAs was carried out at 290°C to doses of 1×10^{13} to 1×10^{15} Si/cm². X-ray rocking curves of these implants are shown in Fig. 10. Inspection of these rocking curves reveals that the strain and damage profiles are originally approximately Gaussian and then saturate at higher doses, just as for the lower temperature implantations. Also, the maximum strain in these samples is less than their counterparts implanted at room temperature by almost a factor of two. This can be easily seen by employing the relation $\Delta\theta = -\epsilon \tan\theta_B$, where $\Delta\theta$ is the shift of the strained layer peak from the substrate peak, ϵ is the strain and $\theta_B = 43^\circ$ for the Fe K _{α} (400) reflection in GaAs. The maximum strain in the sample implanted with 1×10^{15} Si/cm² at 290°C is almost equal to that implanted with Si ions of the same energy at room temperature, but to a dose of only 1×10^{13} /ions cm².

5. Annealing of Implanted GaAs

a. Room Temperature Implantation

Figure 11 shows rocking curve and BSS measurements of GaAs implanted at room temperature with 500 keV Te⁺⁺ to doses of 5×10^{12} and 1×10^{14} at/cm². At 5×10^{12} at/cm² (part A), the

usual Gaussian-shaped strain and damage profiles are observed from the x-ray rocking curve while BSS with channeling detects little change from single crystallinity. At 1×10^{14} ions/cm² (part B), BSS shows that a 2200 Å layer has been amorphized while x-ray diffraction senses only the region of steeply-graded strain lying between the amorphous layer and deeper perfect single crystal. The strain in this region ranges from 0.5% to zero in $\sim 500\text{\AA}$.

Figure 12 shows the results of annealing these samples at 420°C for 60 min. The sample that was implanted with 5×10^{12} Te ions/cm² (part A) has regrown, leaving a ~ 2000 Å region that is very slightly strained (0.03%). Again, BSS could sense no departure from perfect crystallinity. In the sample implanted to 1×10^{14} Te ions/cm² (part B) a thin layer at the amorphous/crystalline interface has regrown with excellent epitaxy, as has been observed before⁽⁵⁾, but the remainder is heavily damaged. Note that the x-ray data shows that the highly-strained interface region has regrown almost perfectly.

b. Low Temperature Implantation

A sample implanted at liquid nitrogen temperature with 300 keV P to a dose of 1×10^{13} ions/cm² was also annealed. The maximum strain was the same as that in the sample that was implanted at room temperature with Te to a dose of 5×10^{12} ions/cm² (see Fig. 11). X-ray analysis showed that the damaged layer had been completely regrown. Thus as we have observed previously in channeling studies⁽⁵⁾ thermal regrowth in GaAs implanted below room temperature is independent of the

temperature of the implantation.

c. Multiple Implantation

In section 3.a we noted that as implanted GaAs approaches amorphicity, it no longer diffracts x-ray coherently. This suggests that there may be variations in the orientations of pieces of material with dimensions of the order of hundreds of unit cells, probably accompanied by misfit dislocations. Now it has been shown that in lattice-mismatched epitaxially-grown films, misfit dislocations can be avoided by incorporating a graded profile of strain⁽⁶⁾. We have seen that for an implantation to a dose sufficient to cause amorphization, the transition between the region of zero strain in the single crystal, to the region of very high strain just adjacent to the amorphous layer occurs over a few hundred Å (e.g. Fig. 11(b)). We therefore suggested in the proposal for this project that if the transition could be made to extend over several thousand Å, thus reducing the strain gradient, the transition to plastic behavior might be avoided and the low-temperature regrowth could be improved. The reduction in the gradient of the strain was to be achieved by means of a multiple-energy implantation. We explored this possibility as follows.

We chose Te as the doping ion because it is a heavy dopant. An energy of 500 keV was selected to produce an amorphous layer thickness of about 2000 Å. For this and greater layer thicknesses, the rocking curve is very sensitive to lateral non-uniformities, as might be created by extended defects. Neon was chosen for the multiple energy implants because it is

chemically inert, but light enough to penetrate substantially further than the Te for production of the layer of graded strain. Energies and doses were 1×10^{14} Ne/cm² at 60 keV, 1×10^{14} Ne/cm² at 140 keV and 2×10^{13} Ne/cm² at 300 keV. The x-ray strain and damage profiles, plus the backscattering spectra for this "triple Ne" implantation alone are shown in Fig. 13(a). Figure 13(b) shows the results for "triple Ne" followed by a 500 keV Te implantation to 1×10^{14} Te/cm². We see that the Te has generated an amorphous layer to a depth of ~ 1500 Å. However, we also note that the rocking curve has lost all of the oscillations that were present for the lower-dose Te implantation (see Fig. 11(a)), i.e. the graded strain layer has failed to prevent the plastic deformations. Figure 14 shows the results of annealing for 60 min in forming gas at 420°C. The "triple Ne" sample regrew almost completely, but the sample with "triple Ne" plus Te remained highly damaged in the region penetrated by the Te. In fact it regrew no better than the Te implant with no graded-strain layer (see Fig. 12(b)). Thus our attempt to improve the low temperature regrowth of GaAs was unsuccessful. It is not clear whether this is because our hypothesis about the role of extended defects in disrupting low-temperature regrowth is incorrect, or because we simply failed to prevent them from occurring.

Our detailed analyses of ion implanted GaAs by x-ray rocking curves under various conditions have produced much information on the roles of the ion species, of the irradiation temperature and of subsequent annealing in the build-up and

evolution of strain and damage in an implanted layer. But two main questions still remain unanswered. One is the explanation of the sharp strain spikes that are observed at high doses, and that is obviously related to the very non-linear build-up of strain with dose. An extension of the work summarized in Fig. 9 to low temperatures should clarify whether self-annealing plays a role. The other issue is to explain how the crystals break up into incoherent domains as amorphicity is approached. A comparison with Ge or Si would be helpful.

6. Other III-V Compounds

Ion implantation was also investigated in (100) InP and (100) GaP wafers. The ions used were Ne, Si, P, Fe, and As, in the dose range of 5×10^{13} to 2×10^{15} cm², for energies of 200-300 keV at temperatures of -180, 20, 200, 290, 400, and 450°C. The results obtained so far are preliminary in the sense that their reproducibility has not been verified.

Channeling analysis of the implanted InP samples showed only small departures from single crystallinity, except for Fe irradiation at room temperature (the heaviest ion used and so analyzed), for which a minimum yield of $\sim 42\%$ was found. There is a discrepancy here between our results and those reported in the literature⁽⁷⁻¹⁰⁾. Our results agree with the generally accepted notion that InP undergoes significant self-annealing at room temperature⁽¹¹⁾. Our channeling analyses were all carried out weeks after the irradiation, which possibly explains the

observed discrepancy. In contrast, all x-ray rocking curves were obtained immediately after the implantation. If these results are affected by self-annealing at all, then it must be by that part of the self-annealing that occurs during the irradiation.

All rocking curves clearly show that the strain induced in InP by implantation is slightly below $10^{-2}\%$, which is the smallest strain we have detected for any semiconductor, other parameters being equal. To improve the sensitivity, we resorted to a non-symmetrical x-ray reflection on (511). This trick improves the sensitivity, and has very recently been described also in the literature⁽¹²⁾.

The other most noticeable fact about InP is that the strained layer is spacially ill-defined in depth. More surprisingly yet, the polarity of this strain can change. It is positive for Si (see Fig. 15) and negative for P (see Fig. 16). These strain distributions seem to appear only above a certain irradiation temperature. With Si for a dose of $(0.5-5) \times 10^{14} \text{ cm}^{-2}$, the positive strain is observed only at 290°C (see Fig. 15). With Fe, the strain appears only at 400°C and it is negative. There is a positive component in all cases as well. It is visible only when the other one is absent, as Fig. 17 shows for Si irradiation at -180 and 20°C. A few irradiations were also carried out on GaP. The results tend to follow the same general trend as in InP.

Future experiments should take into consideration that self-annealing may take place at room temperature. Specifically, analyses should be performed immediately after

irradiation, or in-situ. Low temperature irradiation should be emphasized. The dose range should be extended below 10^{13} ions/cm² in an attempt to see if a range of conditions exists that yields results comparable to those we found in GaAs. Finally, TEM studies would be very desirable to clarify the structural features of the strained layers identified.

7. III-V Strained Layers and Superlattices

In the second contract year of this project, a significant effort was undertaken along two lines not anticipated in the original proposal: (i) a number of strained layers and superlattices were analyzed in detail by rocking curves, and (ii) the capabilities of rocking curves and channeling analysis for the characterization of these synthetic materials were compared. These investigations were made possible largely by the collaboration of other groups who provided the samples, and by an IBM Grant that supported an additional research fellow for 12 months, thus providing additional manpower at no cost to the contract.

A detailed analysis of x-ray double crystal rocking curve spectra of superlattices has been carried out⁽¹³⁾. Relationships are derived between the structure of the rocking curve and the structure of the superlattice, based on the kinematical model of x-ray diffraction. These relationships allow direct determination of the structure of the superlattice, without the

need to resort to computer fitting or Fourier transformations. The method is applied to a GaAlAs/GaAs and a AlSb/GaSb superlattice to obtain depth profiles of perpendicular and parallel strain. The thickness of the period of modulation and the average strain are determined with a precision of $\sim 1\%$. The detailed structure of the period is determined to $\sim 5\%$. With Vegard's law and elasticity theory, strain profiles can be converted into composition profiles.

We have also used superlattices to compare MeV He backscattering and channeling with x-ray rocking curves⁽¹⁴⁾. Through the combined use of the two techniques, depth profiles of strain, composition and crystalline quality have been determined. An example of an $\text{Al}_x\text{Ga}_{1-x}\text{As}/\text{GaAs}$ strained-layer-superlattice is considered. The thicknesses of the individual periods in these strained-layer-superlattice structures were accurately measured by backscattering spectrometry. The values so obtained were used in the detailed calculations of x-ray rocking curves. An excellent agreement between measured and calculated curves was achieved. Transition regions at the interfaces of the various layers in the strained-layer-superlattice structures were also detected and measured by both techniques. The two techniques complement each other well. Backscattering and channeling provide accurate information on the thickness, composition and atomic profiles of the uppermost periods of a superlattice, as long as each sublayer exceeds the depth resolution (~ 100 to 200 \AA). Variations in the period thickness are also readily detectable, but backscattering lacks the ability to see down into

the substrate for superlattices exceeding a few 1000 Å in total depth. Strain is time-consuming to measure by channeling, and the sensitivity is quite poor ($\sim 1\%$) compared to x-ray rocking curves, which are capable of detecting strains below $10^{-3}\%$. In addition, rocking curves can typically sample the substrate through several microns of material, which gives a precise reference that channeling data lack. Rocking curves are also easy to execute, because they can be done in air.

A major drawback of backscattering and channeling for the analysis of strained layers has been exposed in the course of an investigation of GaSb/AlSb superlattices⁽¹⁵⁾. X-ray spectra for the strain present at an unirradiated spot on the crystal is in excellent agreement with the value calculate by elasticity theory, but a region of the same sample that had been exposed to He bombardment for backscattering analysis had strain values that were smaller. The He ion bombardment reduced the strain by 50% and created lateral inhomogeneities in the crystal structure. X-rays are much less destructive to strained epitaxial layers than MeV He ions.

We also applied x-ray rocking curve and backscattering analyses to a $\text{Al}_{0.88}\text{Ga}_{0.12}\text{As}/\text{GaAs}$ superlattice before and after heat treatment at 600°C for 1 h⁽¹⁶⁾. The structure had 10 periods, each consisting of alternating layers of GaAs (270 Å) and $\text{Al}_{0.88}\text{Ga}_{0.12}\text{As}$ (140 Å). In vacuum, the heat treatment produced no detectable change, but when a source of Zn vapor was added, the structure was transformed into a uniform single $\text{Al}_x\text{Ga}_{1-x}\text{As}$ layer. The average perpendicular strain of the whole

layer (0.085%), and its crystalline quality are conserved, however. The redistribution of Al and Ga concentrations is thus a consequence of Zn diffusion in the strained layer superlattice. This result raises serious questions about doping in strained layer superlattices. It also points out a way by which the diffusion of impurities can be measured in such superlattices.

Rocking curves can yield both parallel and perpendicular strain profiles. This feature is especially useful in the study of buffer layers⁽¹⁷⁾. A superlattice of 30 alternating layers of $\text{GaAs}_{0.14}\text{P}_{0.86}$ and GaP grown on a 1 μm buffer layer of $\text{GaAs}_{0.07}\text{P}_{0.93}$ on (100) GaP exhibited a parallel strain of 0.19% relative to the substrate throughout the superlattice and the buffer layer, with a transition region where that strain drops to zero at the interface with the substrate confined to less than 10% of the buffer thickness. This fact suggests that the buffer and the superlattice are crystallographically decoupled from the underlying substrate by misfit dislocations. The perpendicular strain was 0.26% in the buffer, and + 0.80% and - 0.19% in the superlattice $\text{GaAs}_x\text{P}_{1-x}$ and GaP layers, respectively. From these values, the unstrained lattice constants of the buffer layer and of the superlattice layers can be inferred, and the compositions can be obtained via Vegard's law. The x-ray rocking curve method is a fast and powerful tool to determine the complete state of strain of epitaxial multilayers.

We have also applied x-ray rocking curves to investigate the 2500 Å thick layer of $\text{Al}_x\text{Ga}_{1-x}\text{As}$ used as a window on GaAs solar concentrator cells⁽¹⁸⁾. The measured perpendicular strain of

0.231% translates to a concentration of $x = 0.87$ (using bulk AlAs and GaAs lattice parameters, Vegard's law, and the elastic constants of GaAs), which agreed well with the design value of 0.88. In addition, a transition region of about $280 \pm 50 \text{ \AA}$ was detected in which the perpendicular strain was rising at a finite slope from zero and that reflected the changing growth conditions at the onset of the Al supply in the metalorganic chemical vapor deposition reactor. Since strain is uniquely related to the concentration of Al, an Al profile can be derived from the measurement over the whole range of the epitaxial film with a depth resolution of about 50 \AA . Multilayered $\text{Al}_x\text{Ga}_{1-x}\text{As}/\text{GaAs}$ superlattices grown in the same reactor were also analyzed in the same fashion⁽¹⁹⁾. Within each period of 410 \AA , the Al distribution was skewed, reflecting a sharp rise of Al when the Al-organic gas is injected into the reactor, but a slow decrease of Al when the supply is cut off and the residual gas must be pumped out. These results show the effectiveness of x-ray rocking curves in the analysis of epitaxial structures. In view of the expected major importance of strained layer superlattices in future advanced electronic device design, the development of such a tool is relevant. X-ray rocking curves analysis is compatible with on-line monitoring of routine production; even in-situ analysis of the sample during the growth process is conceivable.

The general conclusion that can be drawn from our applications of channeling and rocking curve analyses of epitaxial thin-film structures is that x-ray rocking curves are

the preferred tool for a first analysis. The technique is fast, requires no vacuum, uses little elaborate or bulky hardware, and generates less damage than backscattering analysis. The latter provides atomic distributions directly, however, while the strain profiles of a rocking curve have to be interpreted with Vegard's law and elasticity theory to derive atomic profiles. Strain, however, can be related much more directly to lattice mismatches and epitaxial registry than can backscattering profiles. Herein lies the main advantage of the x-ray rocking curve technique.

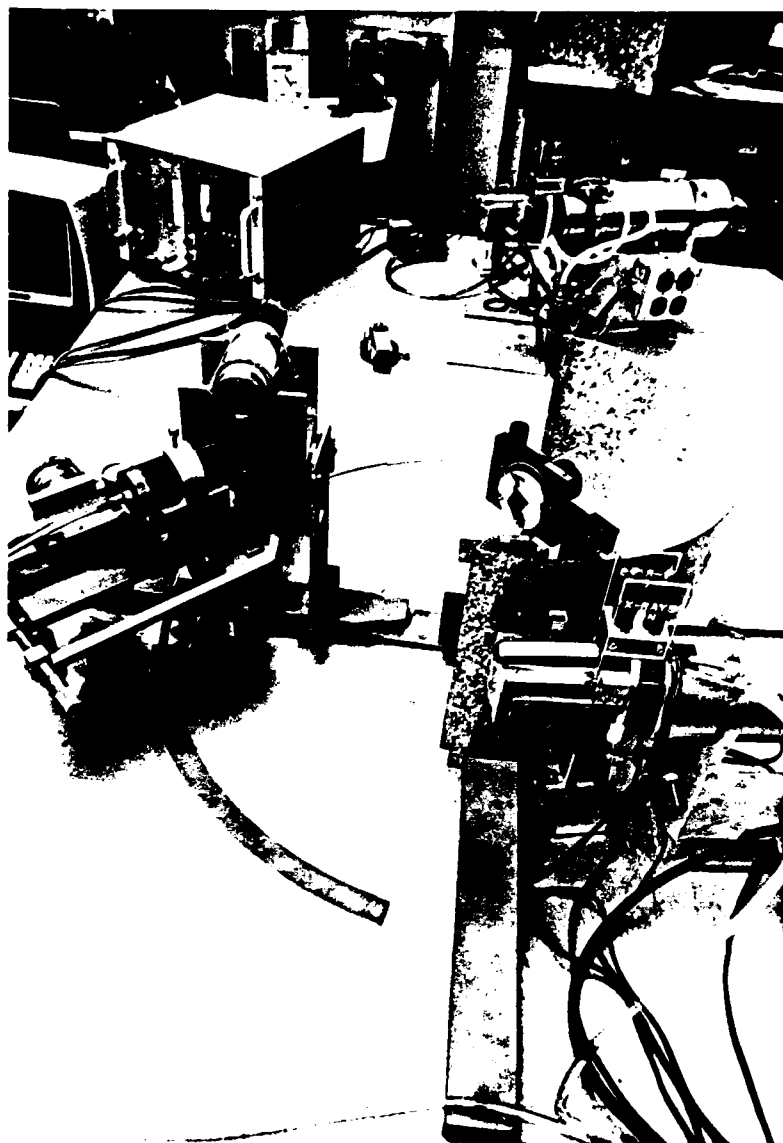


Fig. 1 Double crystal x-ray spectrometer.



Fig. 2 Beam line for backscattering spectrometry.

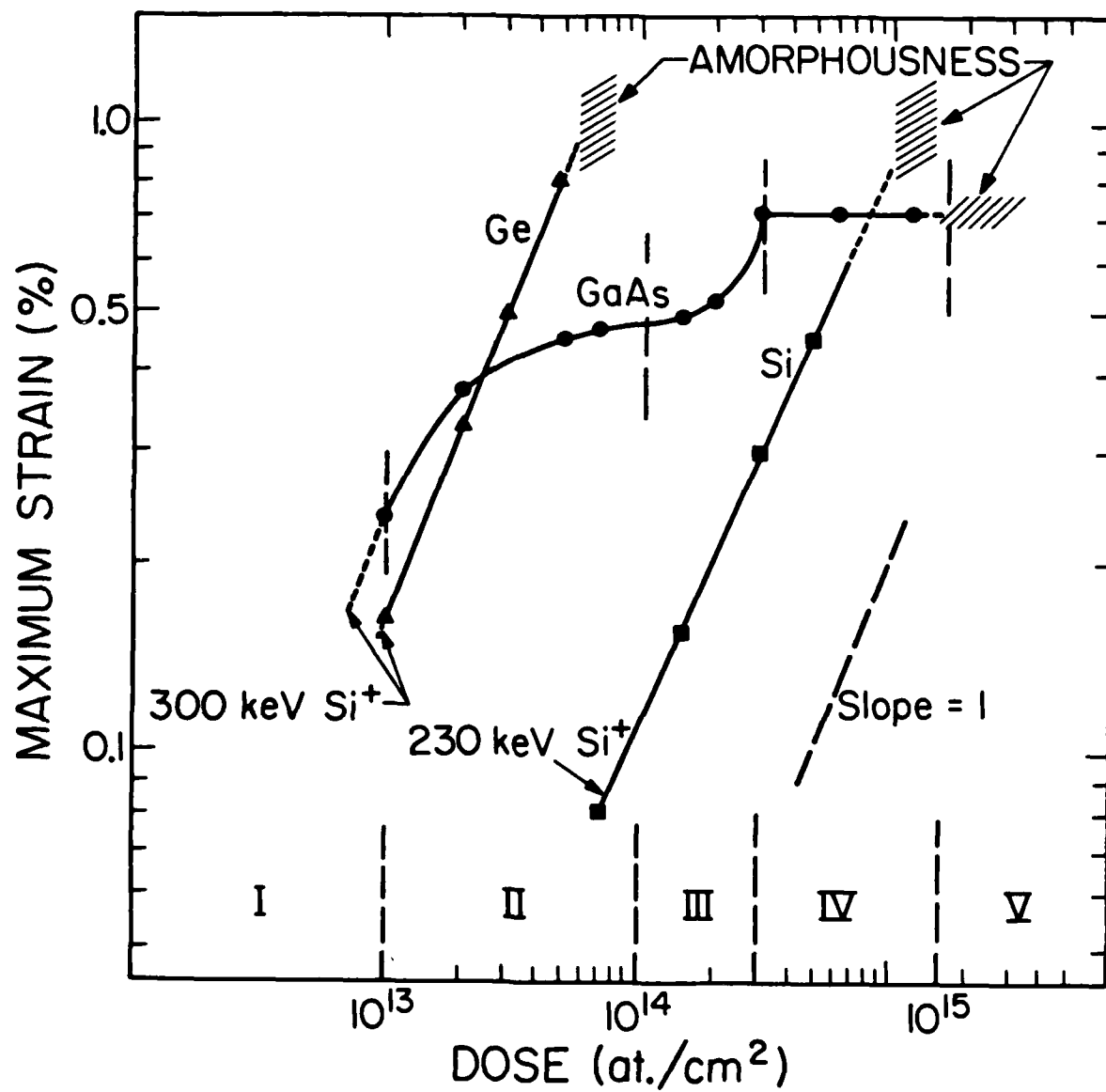


Fig. 3 Maximum strain as a function of dose for room temperature implantation of Si ions into Si, Ge and GaAs. The Roman numerals identify regions of differing strain/dose behavior in GaAs.

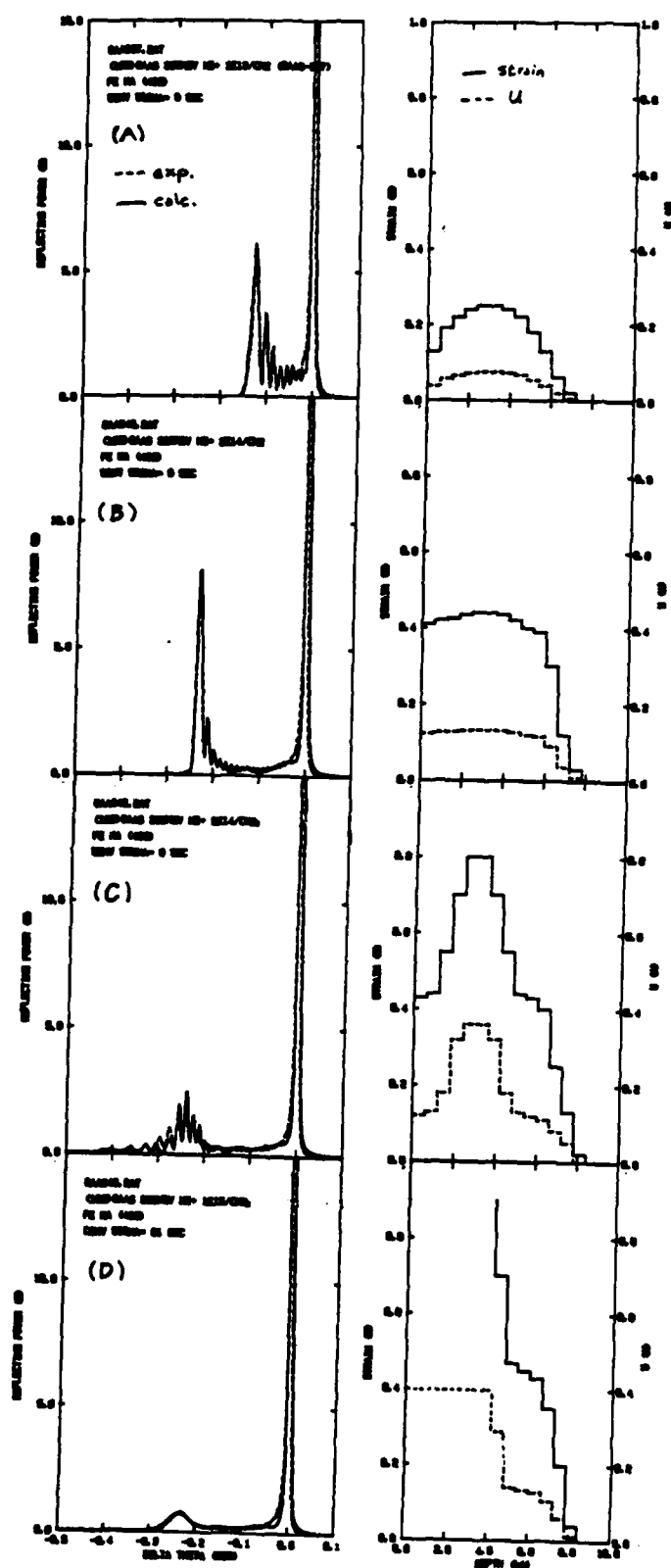


Fig. 4 Implantation of 300 keV Ne⁺ into GaAs at room temperature. Left-hand side: Experimental rocking curves (dashed lines) and calculated fits (solid lines). Right-hand side: Corresponding profiles of strain (solid lines) and damage (dashed lines).

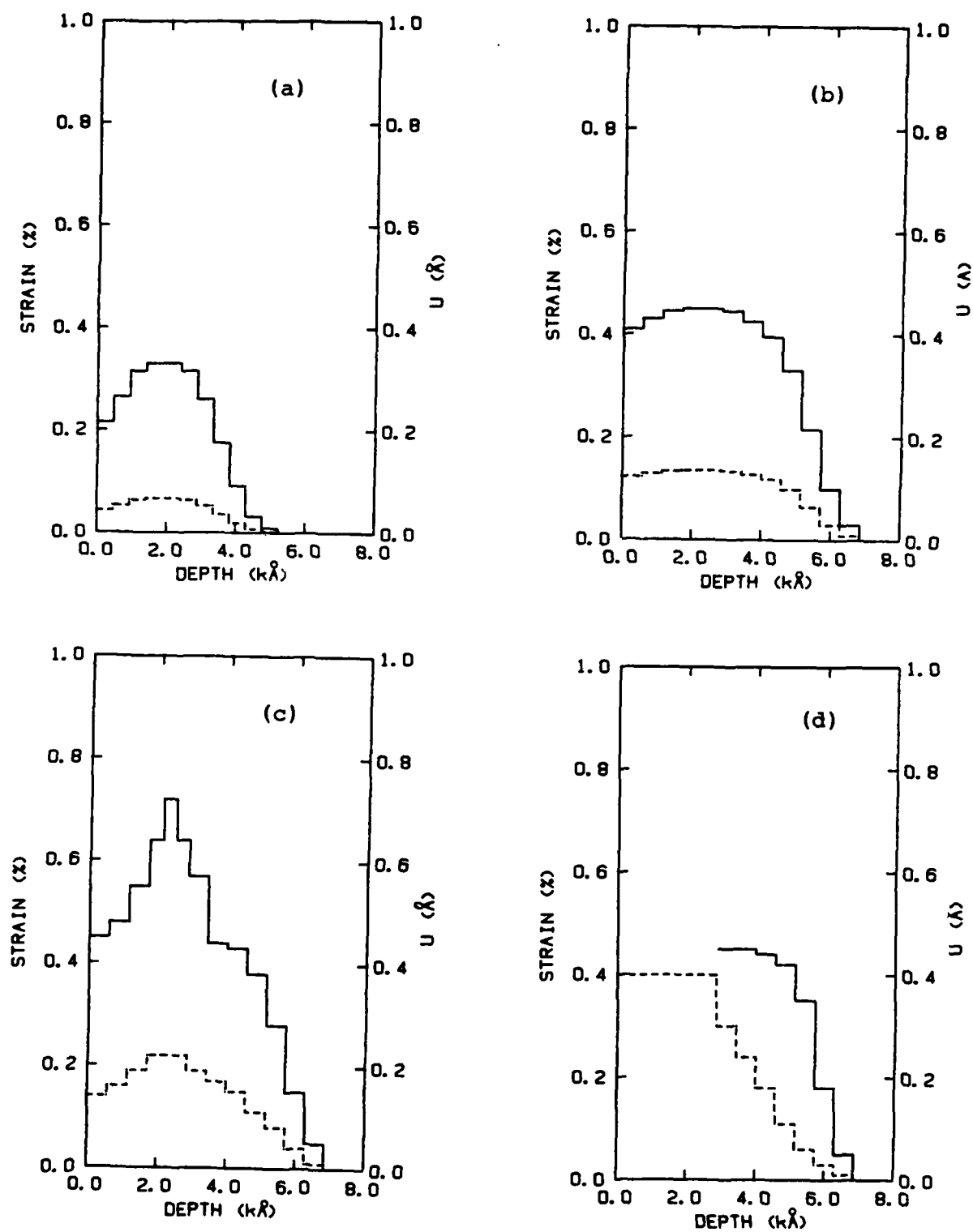


Fig. 5. Strain (solid lines) and damage (dashed lines) profiles in GaAs for R.T. 300 keV Si^+ implantation. Doses are (a) 2×10^{13} , (b) 1.5×10^{14} , (c) 3.0×10^{14} , (d) 1.2×10^{15} ions/ cm^2 .

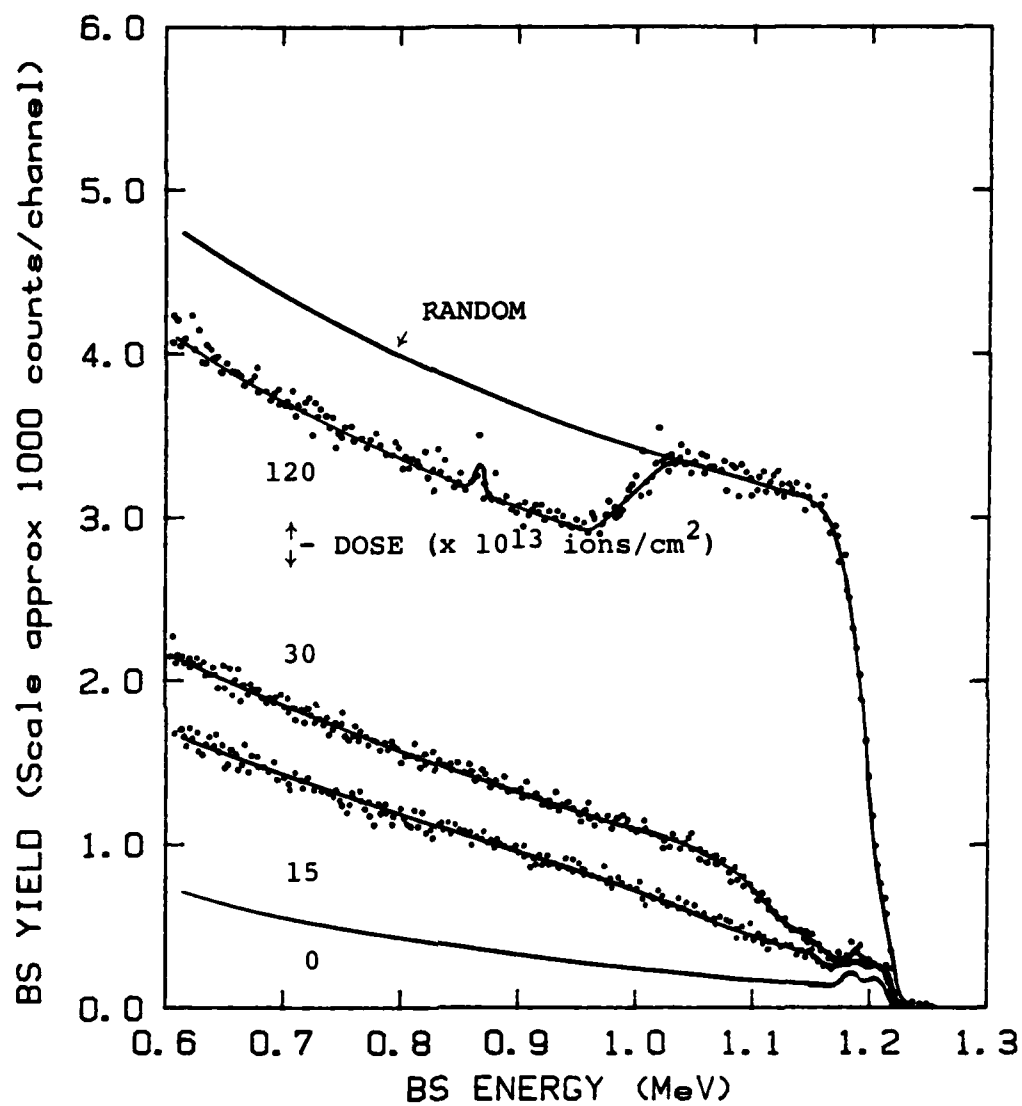


Fig. 6. Channeling spectra for the samples of Fig. 5 parts b, c, and d. Spectra for random orientation, and (100) axially-aligned orientation of an unimplanted sample are also shown.

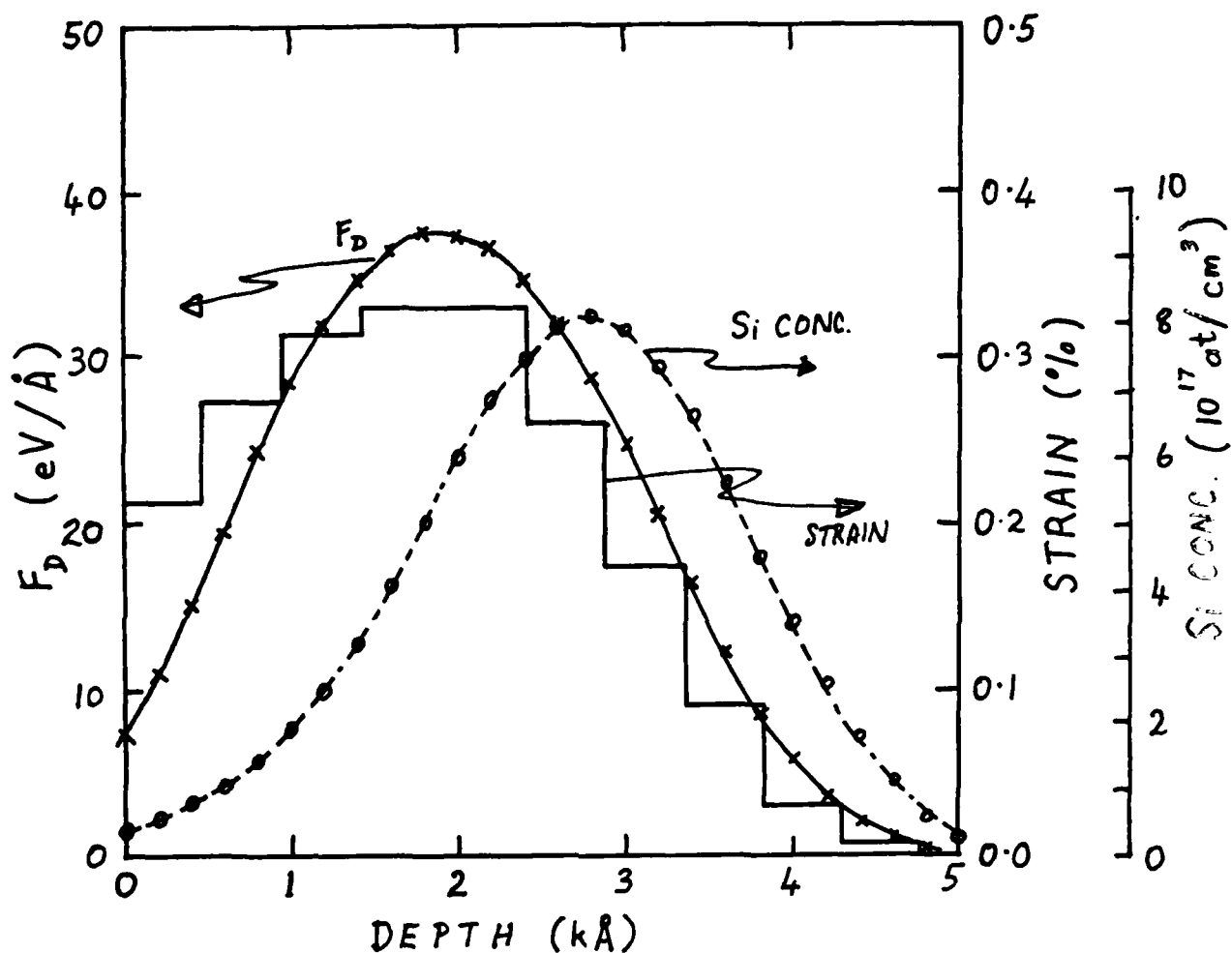


Fig. 7. Comparison of profiles of strain, nuclear energy deposition density (F_D) and Si concentration for implantation of 300 keV Si^+ to 2×10^{13} ions/cm².

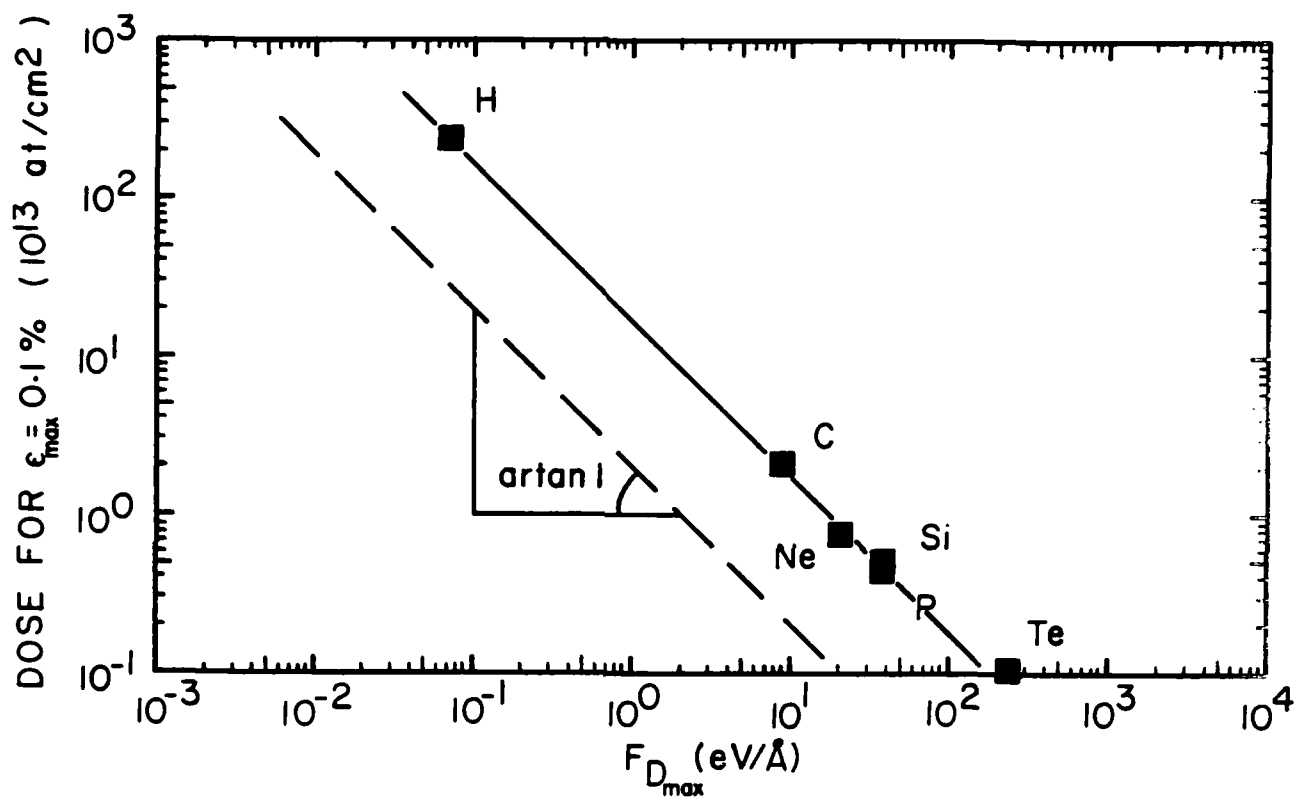


Fig. 8 Dose required for a peak strain of 0.1%, plotted against maximum density of energy deposited in atomic displacements, for six species implanted into GaAs.

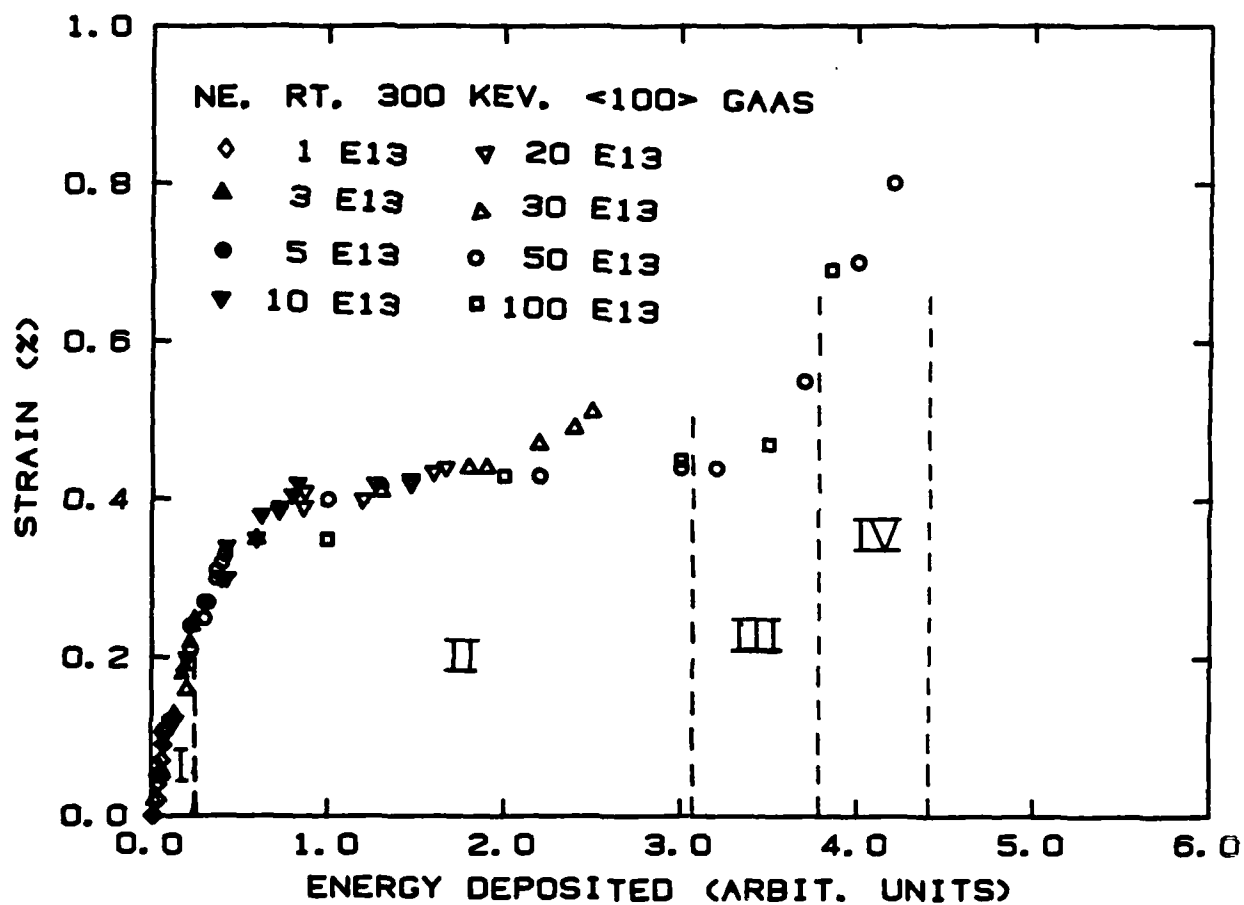


Fig. 9 Strain versus $E_d (= \phi F_D)$ for all room temperature 300 keV Ne^+ implantations into GaAs, at all depths.

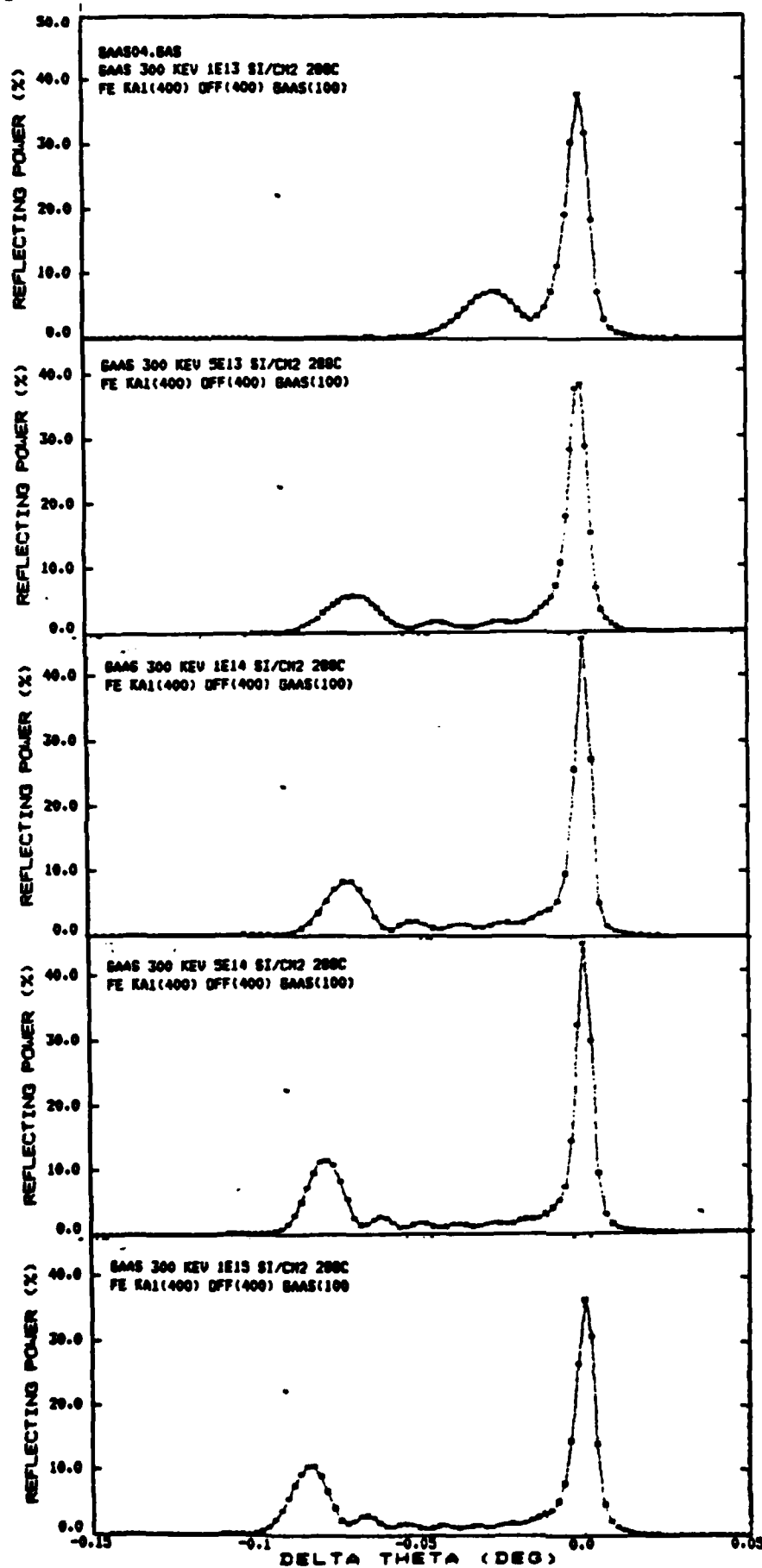


Fig. 10 Plots of x-ray rocking curves of the Fe $K_{\alpha 1}$ (400) symmetric reflection obtained from GaAs samples implanted with 300 keV Si ions at 290°C to doses from 1×10^{13} to 1×10^{15} Si/cm²

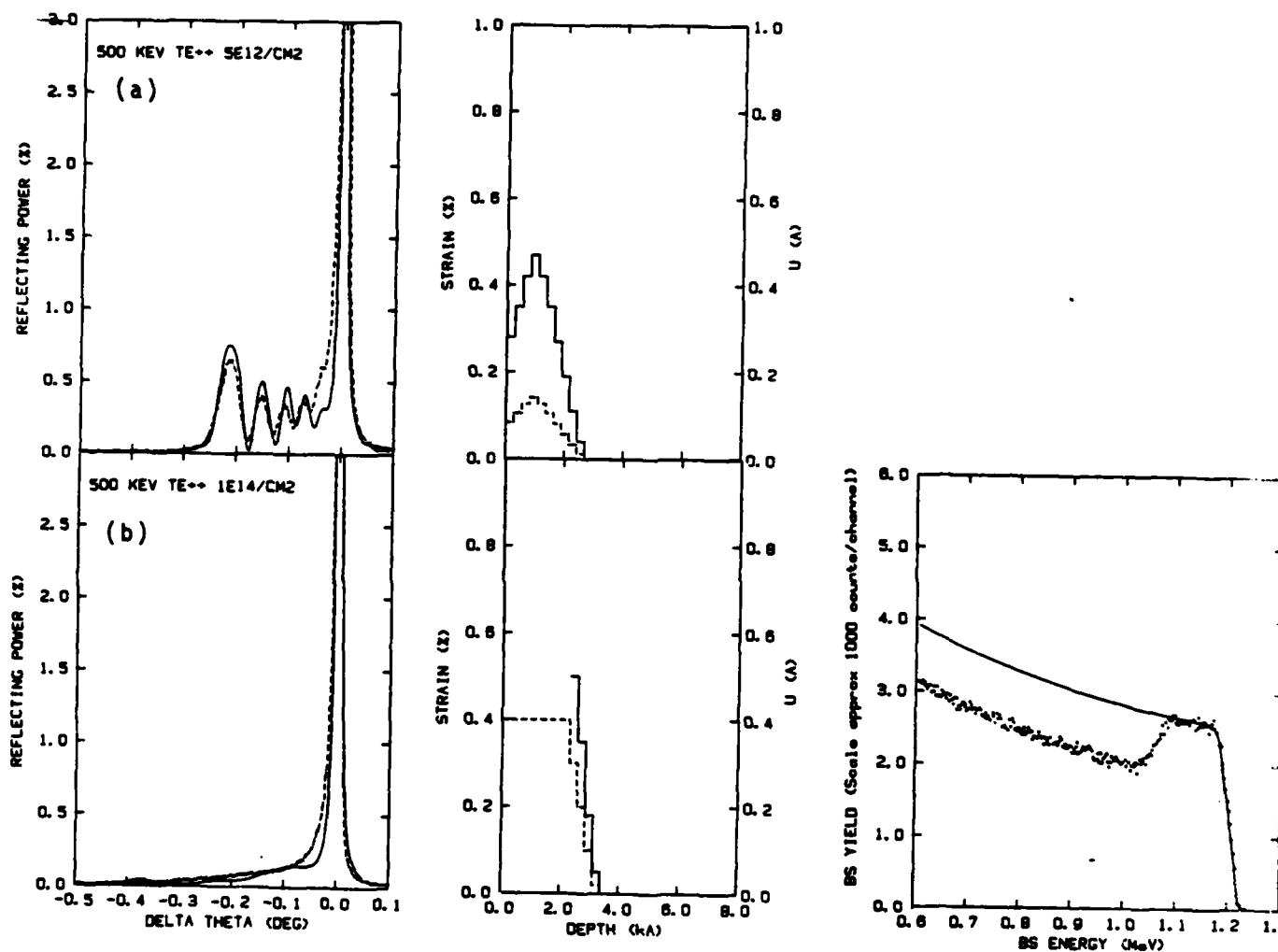


Fig. 11 Rocking curves and strain and damage profiles for two doses of Te implantation in GaAs. Also shown for the higher dose is the channeled BSS spectrum (data points) and the random spectrum (solid line).

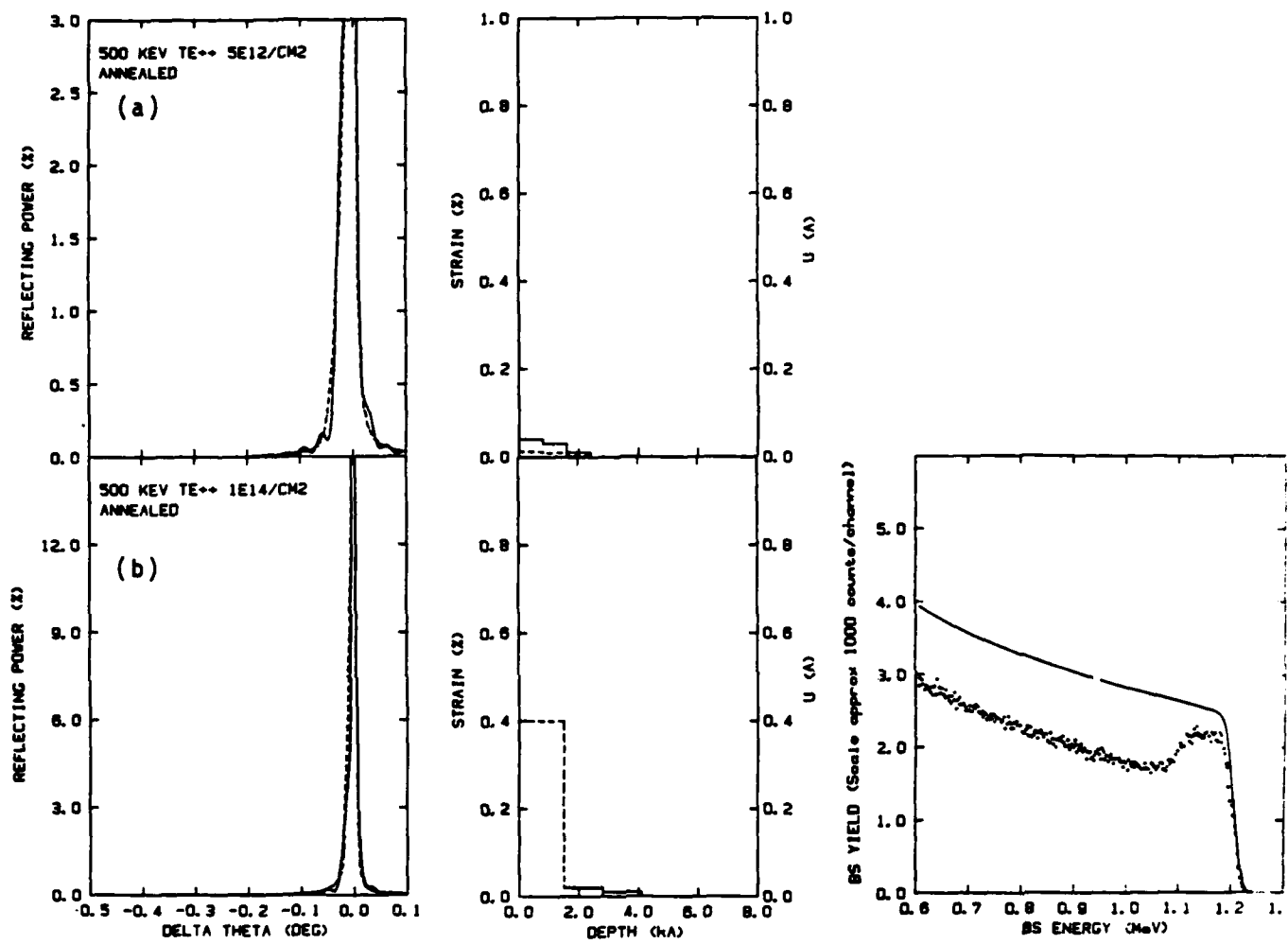


Fig. 12 Rocking curves and strain and damage profiles for the implantation of Fig. 11, after annealing at 420°C for 60 min. Again the BSS spectrum for the higher implantation dose is also included.

AS IMPLANTED <100> GaAs

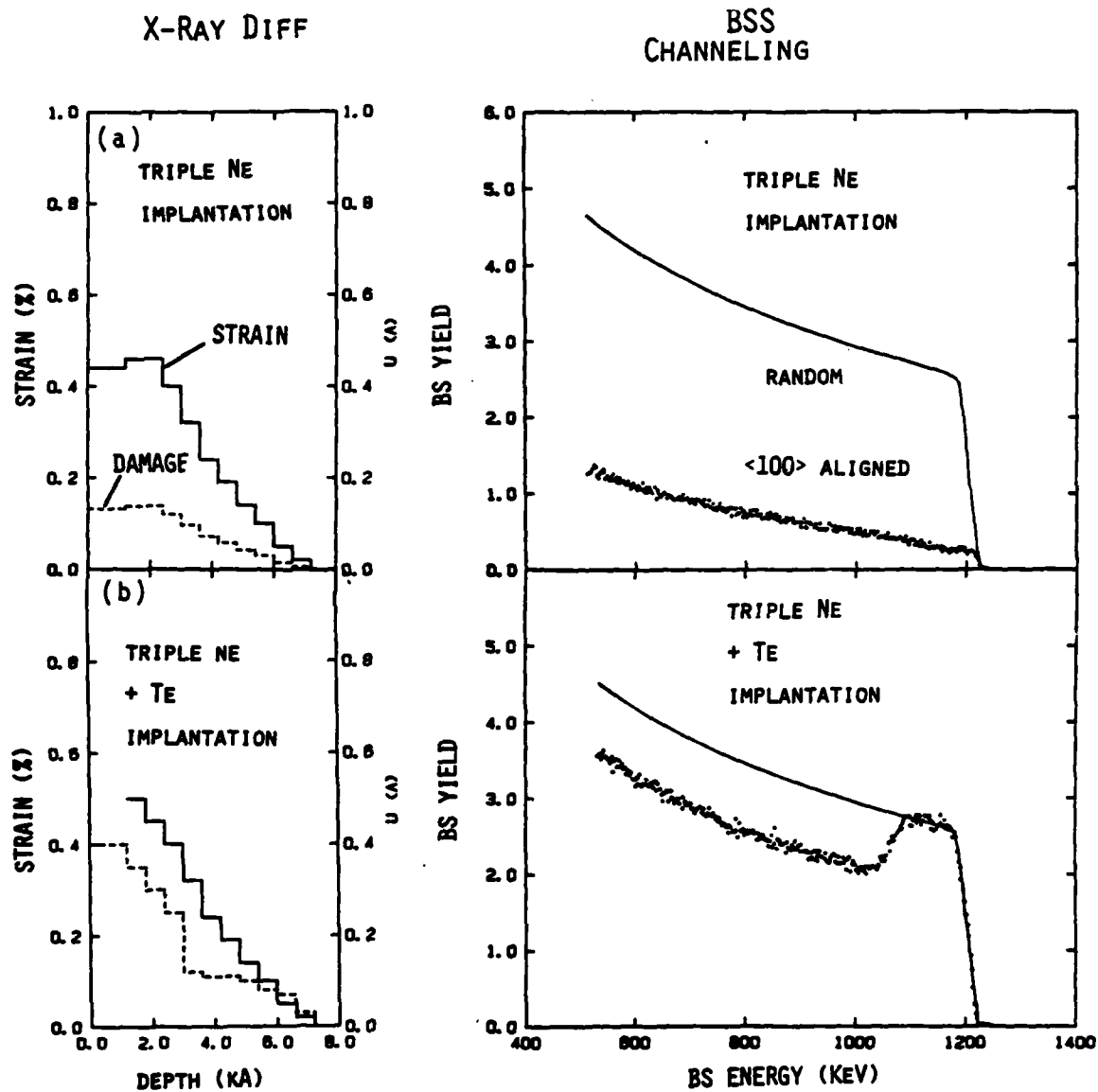


Fig. 13 Strain and damage profiles and BSS spectra for GaAs implanted with (a) "triple Ne", i.e. 1×10^{14} Ne/cm² at 60 keV, 1×10^{14} Ne/cm² at 140 keV and 2×10^{13} Ne/cm² at 300 keV, and (b) "triple Ne" plus 1×10^{14} Te ions/cm² at 500 keV.

ANNEALED 60 MIN, 420°C

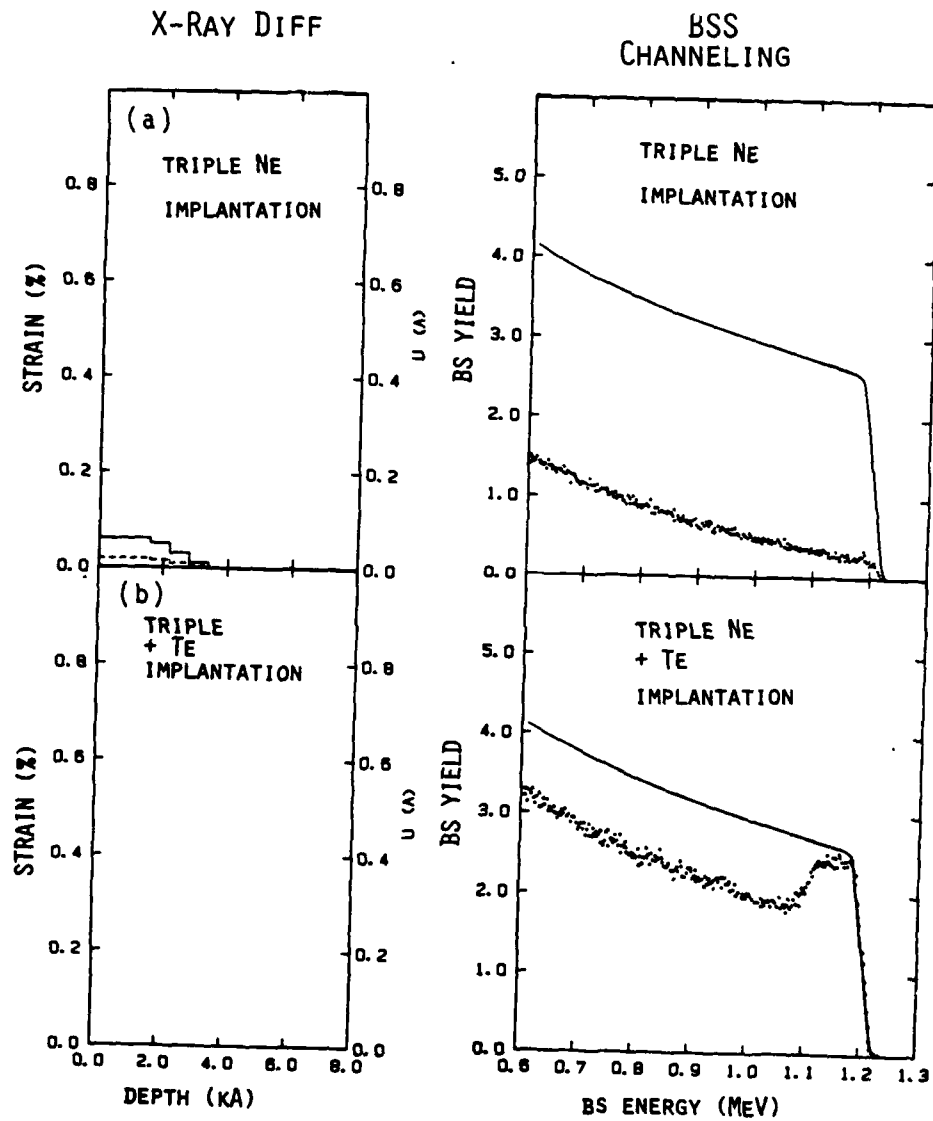


Fig. 14 Strain and damage profiles and BSS spectra for the samples of Fig. 13 after annealing at 420°C for 60 min.

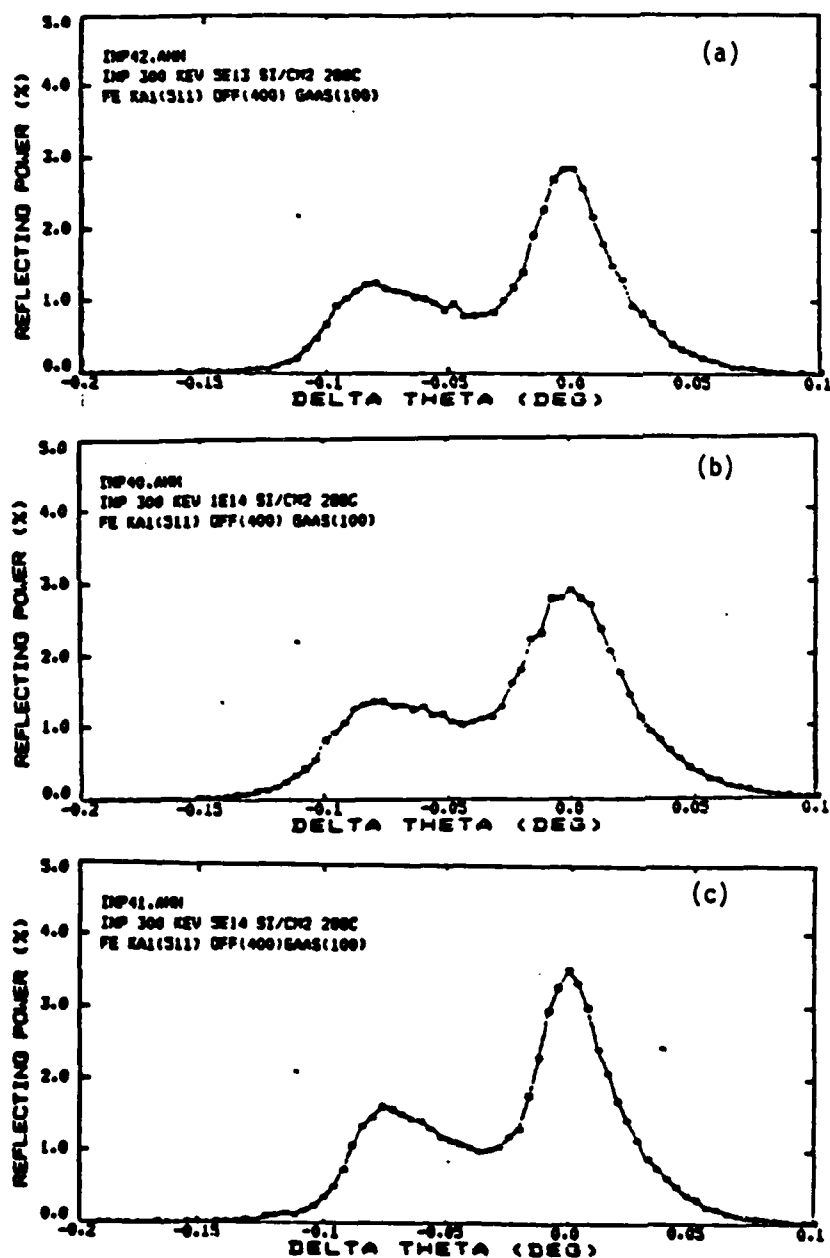


Fig. 15 Plots of Fe K α_1 (511) asymmetric reflection x-ray rocking curves from InP implanted with 300 keV Si ions at 288°C with doses of 5, 10 and 50 $\times 10^{13}$ ions/cm² (parts a - c, respectively). Notice the secondary peak represents a damaged layer on the negative side of the substrate peak, which indicates positive strain through the relation $\Delta\theta = -\langle\epsilon\rangle\tan\theta_B$.

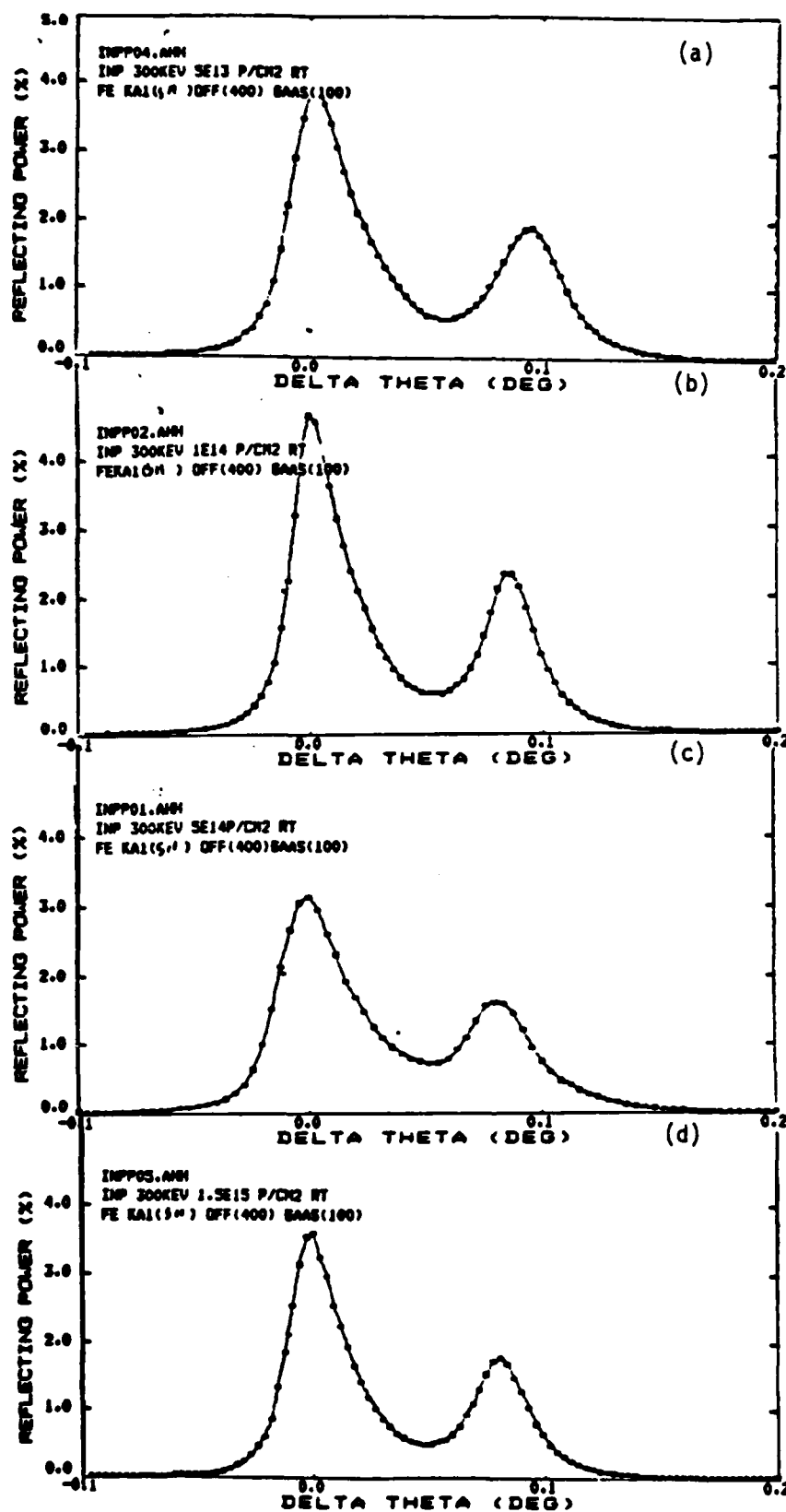


Fig. 16 Plots of $\text{Fe K}_{\alpha 1}$ (511) asymmetric reflection of x-ray rocking curves from InP implanted with 300 keV P ions at room temperature with doses of 5, 10, 50 and 150 $\times 10^{13}$ ions/cm² (parts a-d, respectively). Here the strain is negative.

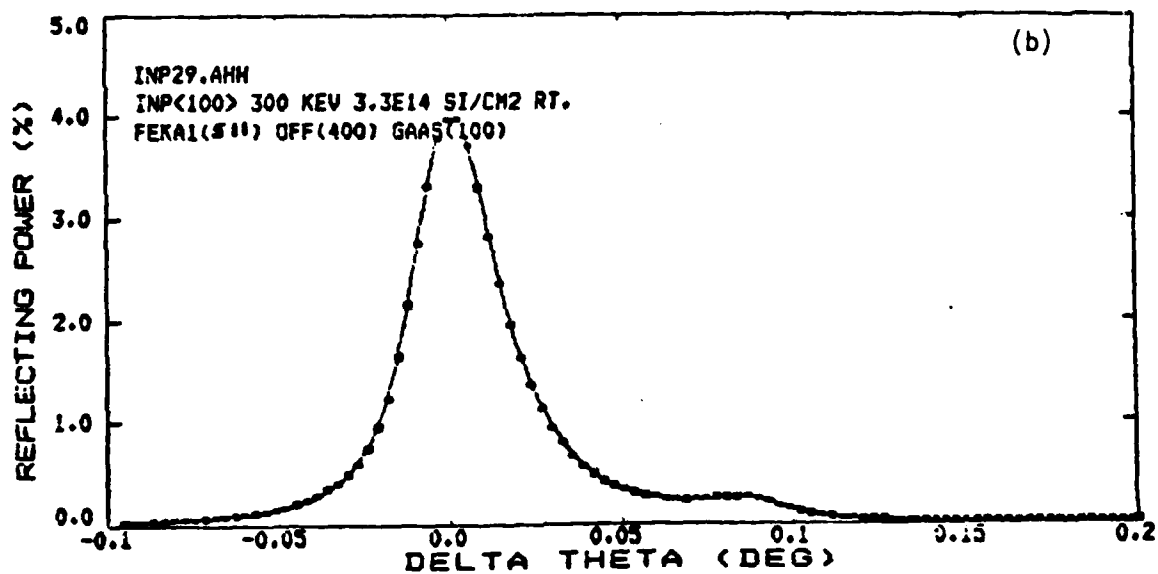
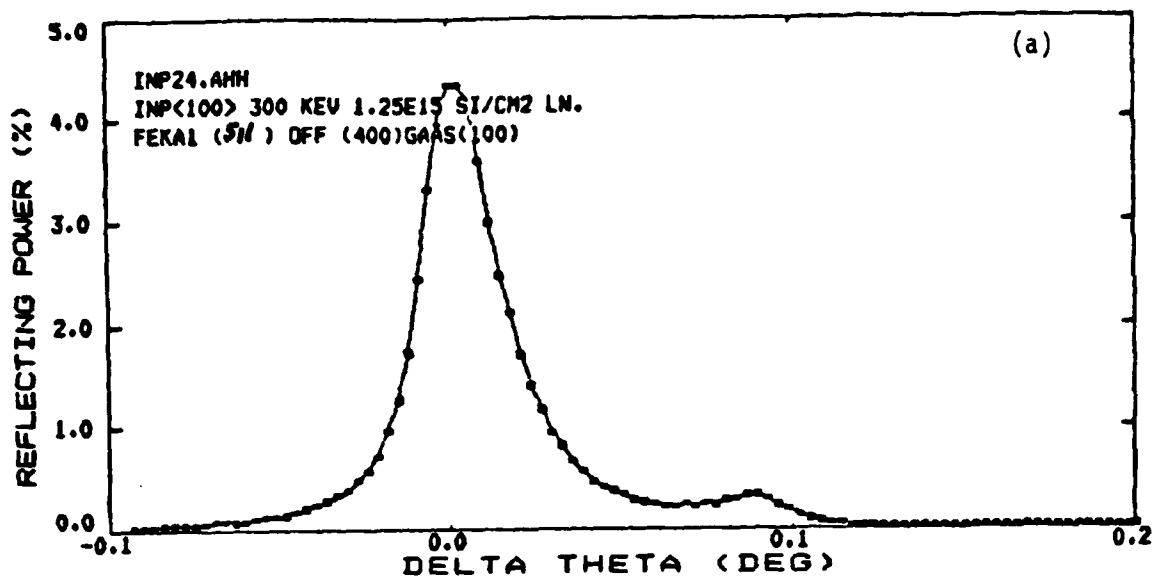


Fig. 17 X-ray rocking curves for the Fe $K_{\alpha 1}$ (511) asymmetric reflection on InP implanted with 300 keV Si ions at 20°C and -180°C. The doses were 1.25×10^{15} ions/cm² (part a) and 3.3×10^{14} ions/cm² (part b).

8. List of Participants

The following were engaged in the work under Contract
MDA 903-82-C-0348:

| <u>Investigator</u> | <u>Status</u> | <u>Present Address</u> |
|---------------------|----------------------------------|---|
| J. H. Barrett | Collaborator | Oak Ridge National Lab., Oak Ridge, Tennessee |
| R. M. Biefeld | Collaborator | Sandia National Lab., Albuquerque, New Mexico |
| W. K. Chu | Collaborator | University of North Carolina, Chapel Hill, North Carolina |
| T. G. Finstad | Collaborator | University of North Carolina, Chapel Hill, North Carolina |
| R. Gorris | Technician | Caltech |
| A. H. Hamdi | Research Fellow | Caltech |
| M-A. Nicolet | Professor | Caltech |
| B. M. Paine | Senior Res. Fellow | Caltech |
| C. K. Pan | Collaborator | University of North Carolina, Chapel Hill, North Carolina |
| M. Parks | Secretary | Caltech |
| S. T. Picraux | Collaborator | Sandia National Lab., Albuquerque, New Mexico |
| V. S. Speriosu | Post-doctoral Research Fellow | IBM Research Division, San Jose, California |
| J. L. Tandon | Visiting Associate | Caltech |
| T. Vreeland, Jr. | Professor | Caltech |
| Y. C. M. Yeh | Collaborator | Applied Solar Energy Corporation, City of |

D. C. Zheng

Collaborator

Industry, California

University of North
Carolina, Chapel Hill,
North Carolina

References

1. V. S. Speriosu, J. Appl. Phys. 52, 6094 (1981).
2. V. S. Speriosu, B. M. Paine, M-A. Nicolet, and H. L. Glass, Appl. Phys. Lett. 40, 604 (1982).
3. K. B. Winterbon, Ion Implantation Range and Energy Distributions, (Plenum, New York, 1975), Vol. 2.
4. H. Booyens, J. S. Vermaak, and G. R. Proto, J. Appl. Phys. 49, 5435 (1978).
5. M. G. Grimaldi, B. M. Paine, M-A. Nicolet, and D. K. Sadana, J. Appl. Phys. 52, 4038 (1981).
6. G. A. Rozgonyi, P. M. Petroff, and M. B. Panish, Appl. Phys. Lett. 24, 251 (1974).
7. E. F. Kennedy, Appl. Phys. Lett. 38, 375 (1981).
8. D. E. Davies, J. Cryst. Growth, 54, 150 (1981).
9. P. Auvray, A. Guivarch, H. L. Haridon, G. Pelous, M. Salvi, and P. Henoc, J. Appl. Phys. 53, 6202 (1982).
10. T. H. Zhang, R. G. Elliman, and G. Carter, Nucl. Instrum. and Meth. 209, 761 (1983).
11. M. Slater, presented at the Ion Beam Modification of Materials Conference, Ithaca, New York (July 1984); to be published in Nucl. Instrum. and Meth.
12. U. Pietsch, J. Bak-Misiuk, and V. Gottschalch, phys. stat. sol. (a) 82, K137 (1984).
13. V. S. Speriosu and T. Vreeland, Jr., J. Appl. Phys. (in press).
14. A. H. Hamdi, V. S. Speriosu, J. L. Tandon, and M-A.

Nicolet, (submitted to Phys. Rev. B).

15. C. K. Pan, D. C. Zheng, T. G. Finstad, W. K. Chu, V. S. Speriosu, M-A. Nicolet, and J. H. Barrett, to be published in Phys. Rev. B.
16. A. H. Hamdi, J. L. Tandon, and M-A. Nicolet, to be published in Materials Letters.
17. V. S. Speriosu, M-A. Nicolet, S. T. Picraux, and R. M. Biefeld, Appl. Phys. Lett. 45, 223-225 (1984).
18. V. S. Speriosu, J. L. Tandon, Y. C. M. Yeh, and M-A. Nicolet, to be published in J. Appl. Phys.
19. A. H. Hamdi, V. S. Speriosu, M-A. Nicolet, J. L. Tandon, and Y. C. M. Yeh, to be published in J. Appl. Phys.

APPENDIX A: A List of Publications with Sponsorship of DARPA

- 1) V. S. Speriosu and T. Vreeland, Jr., "X-Ray Rocking Curve Analysis of Superlattices", Journal of Applied Physics (in press).
- 2) V. S. Speriosu, M-A. Nicolet, S. T. Picraux, and B. M. Biefeld, "Depth Profiles of Perpendicular and Parallel Strain in a $\text{GaAs}_x\text{P}_{1-x}/\text{GaP}$ Superlattice", Applied Physics Letters, 45 (3), 223 (1984).
- 3) V. S. Speriosu, M-A. Nicolet, J. L. Tandon, and Y. C. M. Yeh, "Interfacial Strain in $\text{Al}_x\text{Ga}_{1-x}\text{As}$ Layers on GaAs", submitted to Journal of Applied Physics.
- 4) A. H. Hamdi, V. S. Speriosu, M-A. Nicolet, J. L. Tandon, and Y. C. M. Yeh, "Analyses of Metalorganic Chemical Vapor Deposition-Grown $\text{Al}_x\text{Ga}_{1-x}\text{As}/\text{GaAs}$ Strained Superlattice Structures by Backscattering Spectrometry and X-Ray Rocking Curves", submitted to Journal of Applied Physics.
- 5) C. K. Pan, D. C. Zheng, T. G. Finstad, W. K. Chu, V. S. Speriosu, M-A. Nicolet, and J. H. Barrett, "A Structure of GaSb/AlSb Strained Layer Superlattice", submitted to Physical Review B.
- 6) A. H. Hamdi, J. L. Tandon, and M-A. Nicolet, "Analysis of Zn-Diffused $\text{Al}_{0.88}\text{Ga}_{0.12}\text{As}/\text{GaAs}$ Superlattice Structure by X-Ray Rocking Curves and Backscattering Spectrometry", to be published in Materials Letters.
- 7) A. H. Hamdi, V. S. Speriosu, J. L. Tandon, and M-A. Nicolet,

"Combined Use of Ion Backscattering and X-Ray Rocking Curves
in the Analysis of Superlattices", submitted to Physical
Review B.

APPENDIX B: Reprints and preprints of Publications

X-RAY ROCKING CURVE ANALYSIS OF SUPERLATTICES

V. S. Speriosu^{a)} and T. Vreeland, Jr.
California Institute of Technology
Pasadena, California 91125

ABSTRACT

We present detailed analyses of x-ray double-crystal rocking curve measurements of superlattices. The technique measures depth profiles of structure factor, and profiles of perpendicular and parallel strains relative to the underlying substrate. In addition to providing a detailed picture of the state of stress, the profiles are a direct measure of the composition modulation. The thickness of the period of modulation and the average strain are determined with a precision of $\sim 1\%$. The detailed structure of the period is determined to $\sim 5\%$. We obtain an expression relating the structure of the rocking curve to the structure of the period. This expression allows analytic determination of the structure without Fourier transformation or computer fitting. We show the influence of small random fluctuations in layer thicknesses and strains. The technique is applied to a 15 period GaAlAs/GaAs and a 10 period AlSb/GaSb superlattice grown on $\langle 100 \rangle$ GaAs and $\langle 100 \rangle$ GaSb substrates, respectively. In the former, the thickness of the period was 676 \AA and the perpendicular strain varied between zero for the GaAs layer and 0.249% for the layer with peak (93%) Al concentration. Transition regions, $\sim 100 \text{ \AA}$ thick, with continuously varying composition, were found between

the GaAs and the $\text{Ga}_{0.07}\text{Al}_{0.93}\text{As}$ layers. Fluctuations in structural properties were less than 5% of the average. The AlSb/GaSb superlattice had a period of 610 Å with sharp transition regions between the layers and negligible fluctuations from period to period. The perpendicular strains were -0.03% and 1.25%, respectively, for the GaSb and AlSb layers. A uniform parallel strain of 0.03% was found throughout the superlattice. Nonzero parallel strain indicates that a small fraction of the misfit between the superlattice and the substrate is plastically accommodated by net edge dislocations lying in a narrow region (a few hundred Å thick) at the interface with the substrate. The net number of edge dislocations was calculated to be $\sim 1 \times 10^4/\text{cm}^2$. The measured perpendicular strains were in excellent agreement with the values calculated from bulk lattice parameters, elastic properties and the parallel strain. For both superlattices, the standard deviation of random atomic displacements away from perfect crystal sites was below 0.1 Å, in agreement with reported ion channeling and electron diffraction measurements of superlattices. The rocking curve method is a major tool for quantitative analysis of superlattices.

1. INTRODUCTION

Superlattices⁽¹⁾ are a class of epitaxial materials grown by periodic depth modulation of the composition. Recent improvements in growth methods have produced superlattices of nearly perfect crystallinity whose electrical and optical properties can be tailored for various applications. Since the free lattice parameters of the alternating layers are frequently unequal, the modulation of the composition results in a modulated strain. Electrical and optical properties of these devices depend on the state of strain as well as on the composition modulation⁽²⁾. The strain in lattice mismatched superlattice layers has been the subject of a series of measurements by ion channeling⁽³⁻⁶⁾ and electron diffraction⁽⁷⁾. Ion channeling has detected periodic changes in crystal channel direction corresponding to distortions of the crystallographic unit cells in the superlattice layers. If a number of nontrivial basic assumptions are made⁽⁴⁻⁶⁾ concerning the geometry of the distortion, the change in channel direction can be interpreted as a measure of the relative strain in the alternating layers. Electron diffraction has measured absolute distortion in such layers⁽⁷⁾, but with limited precision. Although capable of measuring strain values from 10^{-8} upward, x-ray diffraction has remained relatively unused in the study of superlattices.

Bragg case double-crystal x-ray rocking curves are highly sensitive to strain in epitaxial structures, as shown by their application to semiconductor heterostructures⁽⁸⁻¹¹⁾, diffusion

layers⁽¹²⁻¹⁴⁾ and ion-implanted layers⁽¹⁵⁻¹⁹⁾. Quantitative analysis^(12-14,16) of experimental rocking curves can provide depth profiles of strain with a precision often approaching 2% of quoted values. In general, no assumptions need be made about the geometry of lattice distortion. In epitaxial layers, the scattering of x-rays can be modeled⁽¹⁶⁾ to very good approximation by the single-scattering or kinematical theory. The mathematical simplicity of this theory enables rapid computer calculation of rocking curves corresponding to arbitrary structures. By fitting experimental curves, the actual structure can be obtained. The rocking curve method is rapid, nondestructive, requires no sample preparation, and is exceedingly simple.

In an early paper⁽²⁰⁾, Segmüller et al. gave detailed interpretations of rocking curves of GaAs/AlAs superlattices. Excellent agreement was found between measured intensities and intensities calculated using periodic modulation of strain and structure factor. The modulation was a step function corresponding to the nominal modulation in composition. The strain included a component due to elastic accommodation of the misfit between AlAs and GaAs. More recently, the Fourier transform relationship between the rocking curve on one hand, and the strain and structure factor distributions on the other, was used to measure interdiffusion in annealed GaAs/AlAs superlattices⁽²¹⁾. Due to the small mismatch in lattice parameter between GaAs and AlAs, nonzero strain in directions parallel to the surface was neither expected nor considered in

detail in the above references.

In this paper, the diffraction model presented in Ref. (16) is applied to superlattices. Relationships are obtained between the structure of the rocking curve and the structure of the superlattice. These relationships allow direct determination of the structure of the superlattice, without the need to resort to computer fitting or Fourier transformation. In addition to strains in the direction perpendicular to the surface, profiles of parallel strain and structure factor are included in the model. The sensitivity of the rocking curve to the structure of the superlattice period and the effect of random fluctuations from period to period are demonstrated. The method is applied to a GaAlAs/GaAs and an AlSb/GaSb superlattice to obtain depth profiles of perpendicular and parallel strain. Finally, Vegard's law and elasticity theory are used to convert the strain profiles into composition profiles.

II. REFLECTING POWER OF A SUPERLATTICE

It is convenient to define the x-ray strains of an epitaxial film with respect to the substrate, since these are determined directly from the rocking curve. Denoting the film and the substrate by f and s respectively, for an arbitrary set of planes there is, in general, a difference $\Delta d = d_f - d_s$ in interplanar d -spacing. The difference depends on the particular deformation as well as on the planes. In principle, the strain $\tilde{\epsilon}$ is a tensor with unequal normal and shear components. For cubic crystals of

arbitrary orientation, such as $\langle 311 \rangle$, it is necessary to consider shear strains (22,8). But for layers grown along $\langle 100 \rangle$, $\langle 110 \rangle$ or $\langle 111 \rangle$ directions, the principal strains are perpendicular and parallel to the layer. In these directions, the x-ray strains ϵ^\perp and ϵ'' are the fractional differences in interatomic spacing between the film and the substrate. The strains are related to the difference in d-spacing through:

$$\frac{\Delta d}{d_s} = \epsilon^\perp \cos^2 \psi + \epsilon'' \sin^2 \psi \quad (1)$$

where ψ is the angle between the planes and the surface. For perfectly coherent epitaxy $\epsilon'' \equiv 0$ regardless of the mismatch between the free film and the free substrate. Even under partial relaxation ($\epsilon'' \neq 0$), this condition imposes stresses of opposite signs in the layer and substrate, and in the simplest case produces tetragonal distortions and bending. Second order variations of ϵ'' with direction in the plane of the layer occur for non-orthotropic orientations. Since the thickness of the substrate is usually two orders of magnitude greater than the thickness of the layer, the strains in the substrate are usually two orders of magnitude smaller than those in the film. To a good approximation, the substrate is unstrained and one may substitute the free substrate interplanar spacing d_s° for d_s in eq. (1). If the free lattice parameter of the film is known, it is a simple matter to convert the x-ray strain, defined relative to the substrate, to the strain of elasticity theory, defined

relative to the free film. In a later section, we apply elasticity theory to calculate the elastic strains of the superlattice, the substrate elastic strain and the bending radius of the structure.

For diffraction calculations, a uniform epitaxial layer is described by its thickness t , structure factor F , perpendicular and parallel strains ϵ^\perp and ϵ'' , and normal absorption coefficient μ . With respect to the inward normal to the surface, the direction cosines of the incident and diffracted waves are γ_0 and γ_H , respectively. The angle between the diffracting planes and the surface is ψ . Associated with the epitaxial layer and the particular reflection are the quantities A and γ ⁽²³⁾.

$$A = \frac{r_e \lambda |F| t}{V \sqrt{|\gamma_0 \gamma_H|}} \quad (2)$$

$$\gamma = - \sqrt{\frac{\gamma_0}{|\gamma_H|}} \frac{\pi V \sin 2\theta_B}{r_e \lambda^2 |F|} \cdot \Delta\omega \quad (3)$$

where r_e is the classical electron radius, λ is the x-ray wavelength, V is the volume of the unit cell and θ_B is the Bragg angle of the substrate. The differential angle $\Delta\omega$ is:

$$\Delta\omega = \theta - \theta_B + (\epsilon^\perp \cos^2 \psi + \epsilon'' \sin^2 \psi) \tan \theta_B \pm (\epsilon^\perp - \epsilon'') \sin \psi \cos \psi \quad (4)$$

where θ is the grazing angle of incidence with respect to the

diffracting planes. The + or - sign is chosen according to whether the angle of incidence with respect to the surface is $\theta_B - \psi$ or $\theta_B + \psi$, respectively. In eq. (4), the first term involving strains represents a change in d-spacing while the second is due to the rotation of the planes. Equation (4) differs in two ways from eq. (6) in Ref. (16). One is due to the inclusion of parallel strain. In addition, the dependence on ψ in eq. (4) is valid for any Bragg case $\theta_B + \psi$, whereas eq. (6) in Ref. (16) is valid only for $\theta_B + \psi \leq \pi/2$ (24).

An arbitrary depth profile of strains and structure factor can, for computational convenience and with sufficient accuracy, be represented by a discrete structure of N laminae. The normalized amplitude diffracted by such a structure is (16):

$$E_N = i \sqrt{\frac{\gamma_0}{|\gamma_H|}} \sum_{j=1}^N a_j e^{-i(A_j \gamma_j + \phi_j)} \frac{\sin A_j \gamma_j}{\gamma_j} \quad (5)$$

where

$$a_j = \exp\left[-\mu \frac{\gamma_0 + |\gamma_H|}{2|\gamma_0 \gamma_H|} \sum_{i=j+1}^N t_i\right]$$

$$a_N = 1$$

$$\phi_j = 2 \sum_{i=1}^{j-1} A_i \gamma_i$$

$$\phi_1 = 0$$

and each lamina j has its own A_j and Y_j .

A superlattice is a special case of the arbitrary laminar structure. In its simplest form, the superlattice period consists of two layers, labeled a and b , each with its own thickness, strains, structure factor and the corresponding A_a , Y_a and A_b , Y_b . For M superlattice periods and neglecting normal absorption, the diffracted amplitude (eq. (5)) becomes:

$$E_M = i \sqrt{\frac{Y_0}{|Y_H|}} e^{-i\beta} F_s \frac{\sin[M(A_a Y_a + A_b Y_b)]}{\sin(A_a Y_a + A_b Y_b)} \quad (6)$$

where

$$\beta \equiv (M-1)(A_a Y_a + A_b Y_b) + A_a Y_a, \quad \text{and}$$

$$F_s \equiv \frac{\sin A_a Y_a}{Y_a} + e^{-i(A_a Y_a + A_b Y_b)} \frac{\sin A_b Y_b}{Y_b} \quad (7)$$

The quantity F_s can be regarded as the structure factor of one superlattice period. The sinusoidal term in the numerator of eq. (6) produces zeroes with a period $\Delta\theta_M$ given by:

$$M \Delta(A_a Y_a + A_b Y_b) = \pi$$

or

$$\Delta\theta_M = \frac{\lambda |\gamma_H|}{M(t_a + t_b) \sin 2\theta_B} \quad (8)$$

from which the total thickness, $M(t_a + t_b)$, of the superlattice can be determined. However, for typical samples ($\sim 1 \mu\text{m}$ thick) lateral nonuniformities frequently result in a convolution of the rapid oscillations. The more slowly-varying sinusoidal term in the denominator of eq. (6) produces observable peaks at:

$$A_a \gamma_a + A_b \gamma_b = n\pi \quad (9)$$

hence, the peaks are labeled $0, \pm 1, \pm 2$, etc. The spacing $\Delta\theta_p$ between the peaks yields the superlattice periodicity p :

$$p \equiv t_a + t_b = \frac{\lambda |\gamma_H|}{\Delta\theta_p \sin 2\theta_B} \quad (10)$$

The superlattice zeroeth order peak is located at an angle $\Delta\theta_0$ from the substrate peak. From eq. (9)

$$\begin{aligned} -\Delta\theta_0 &= k_1 \langle \epsilon^{\perp} \rangle + k_2 \langle \epsilon^{\parallel} \rangle \\ k_1 &= \cos^2 \psi \tan \theta_B \pm \sin \psi \cos \psi \\ k_2 &= \sin^2 \psi \tan \theta_B \mp \sin \psi \cos \psi \end{aligned} \quad (11)$$

where $\langle \rangle$ denotes depth averaging (over the superlattice period) and the sign is chosen as described above. The amplitude of the n th order peak is proportional to the superlattice structure factor (eq. (7)) evaluated at angles determined by eq. (9), using n as a subscript,

$$F_{sn} = \sin A_a Y_{an} \left(\frac{1}{Y_{an}} - \frac{1}{Y_{bn}} \right)$$

$$= \frac{\sin A_a Y_{an}}{A_a Y_{an}} \left(A_a + \frac{A_b}{1 - \frac{n\pi}{A_a Y_{an}}} \right) \quad (12)$$

Since Y_{an} is related to Y_{a0} through eqs. (10) and (3), equation (12) depends on A_a , A_b and Y_{a0} only. For $n = 0$, this reduces to

$$F_{s0} = \frac{\sin A_a Y_{a0}}{A_a Y_{a0}} (A_a + A_b) \quad (13)$$

$$\approx (A_a + A_b), \quad A_a Y_{a0} \ll 1$$

Thus, the amplitude of the zeroeth order peak measures $F_a T_a + F_b T_b$ where F_a and F_b are the crystallographic structure factors of layers a and b , respectively. The approximation in eq. (13) is quite good for typical strong reflections and products of strain modulation and period thickness below $\sim 1\% \times 300 \text{ \AA}$. In these cases, the zeroeth order peak is more intense than higher

order peaks. For larger strains and thicknesses, the approximation in eq. (13) breaks down and the zeroth order peak may be less intense than higher order peaks. In a later section, we give examples of both regimes.

From eq. (6), it is clear that the basic structure of the rocking curve is determined by the structure of the superlattice period. The number of peaks, their locations and relative amplitudes are independent of the number of periods, provided this number is greater than 1. For M periods and negligible absorption, the overall intensity of the rocking curve goes as M^2 . A perfect superlattice is described by 6 parameters: t_a , t_b , $\tilde{\epsilon}_a$, $\tilde{\epsilon}_b$, F_b/F_a and M . To determine these parameters, one can use equations (8), (10), (11), (13) and eq. (12) evaluated for the ± 1 peaks. The locations and amplitudes of peaks corresponding to $|n| > 1$ are completely determined by the six parameters. To separate the components of $\tilde{\epsilon}_a$ and $\tilde{\epsilon}_b$, one needs at least two rocking curve measurements. The availability of a large number of intense reflections with varying degrees of asymmetry enables the verification of the internal consistency of the depth profiles of strain and structure factor. In fact, the present method can be extended to arbitrary deformations, including shear strains. For each additional strain component, an additional rocking curve measurement is needed.

The solution of the six simultaneous equations is straightforward provided the condition in eq. (13) is satisfied. Since this is not always the case, it may be necessary to consider higher order peaks. Alternatively, since the condition

of eq. (13) depends on the Bragg angle and on ψ as well as on the strain and thickness, it is almost always possible to use a reflection where the zeroth order peak is the most intense. In practice, the number of periods and the approximate composition modulation are known from the growth conditions. One can calculate a priori F_a and F_b from the nominal composition. This reduces the number of unknowns to four without changing the number of equations (six). Thus for a perfect or nearly perfect superlattice, we are able to determine its structure by following a specified algorithm and are not dependent on computer fitting.

If the structure of the superlattice period has more detail than the bilayer model assumed above, it is nevertheless clear that the form of eq. (6) remains valid. By straightforward extension, eqs. (6) and (7) can describe diffraction in superlattices with an arbitrary number of sublayers in one period. For each additional sublayer, the intensity of an additional high-order peak must be considered. However, equations (10) and (11), which determine the periodicity and the average strain, remain applicable regardless of the structure of the period.

Real superlattices are imperfect. The strain and thickness values fluctuate from period to period. One result of this is that the periodicity determined from eq. (6) is noncommensurate with crystallographic unit cells. If the number of periods is small and the fluctuations are arbitrarily large, the rocking curve rapidly loses the structure predicted by eq. (6). In such cases, one can return to eq. (5), which is valid for arbitrary

depth profiles in thin layers, and match the experimental rocking curve with the aid of a computer. Although convergence to a good fit cannot be guaranteed, the sensitivity of the rocking curve to the strain profile ensures that a good fit can only be obtained with the "true" profile^(16,19). The importance of obtaining a good fit (examples may be found in Refs. 10-14, 16 and 19) cannot be overemphasized.

For small fluctuations and a large number of periods, one can describe the frequency of the particular fluctuation by a probability ρ . If the thickness of layer a varies, corresponding to a variation ΔA in A_a , and the probability of ΔA is a Gaussian with standard deviation U_A , it is straightforward to show that the average structure factor $\langle F_{sn} \rangle$ is given by:

$$\langle F_{sn} \rangle = e^{-2Y_{an}^2 U_A^2} F_{sn}^* \quad (14)$$

where F_{sn}^* corresponds to no fluctuation. The exponential term is analogous to a Debye-Waller factor. Since $|Y_{an}|$ increases with n , high order peaks are diminished much more than low order peaks. The intensity lost at each peak will, of course, be seen in the rise of the background intensity between the peaks. From symmetry, a fluctuation in A_b produces a similar result. If both A_a and A_b fluctuate, the structure factors of high order peaks diminish even more rapidly. The influence of strain fluctuations is less transparent, but we shall show by example that it also decreases the intensity of high order peaks.

From a practical point of view, the existence of transition

regions in the superlattice period and the possibility of fluctuations from period to period are of great interest. To explore these possibilities in real samples, we adopt an approach combining analytic determination with trial-and-error fitting. The locations and intensities of the three low-order peaks yield the structure of the superlattice assuming a bilayer distribution in each period and perfect periodicity. These values of strains, structure factors and thicknesses provide an initial distribution for a calculated rocking curve. Discrepancies between measured and calculated intensities of high-order peaks are then minimized by trial-and-error fitting. The structure of the experimental curve will suggest whether the discrepancies are due to fluctuations from period to period, to transition regions in each period, or both.

The frequent presence^(4,7,25) of a buffer layer grown between the superlattice and the substrate also necessitates a departure from analytic structure determination. For a buffer of arbitrary composition modulation, it is not possible to derive simple relationships between the rocking curve and the superlattice-cum-buffer structure. If the buffer is uniform, as is often the case, it will contribute an additional peak to the rocking curve. The location and intensity of this peak yield the strain and thickness of the buffer⁽²⁵⁾.

For calculations of rocking curves, as in Ref. (16), the reflecting power of the epitaxial structure is added to that of the substrate, adjusted for normal absorption in the epitaxial structure. The substrate reflecting power is obtained using only

the σ -component of the dynamical theory⁽²³⁾ result for thick, nonabsorbing, perfect crystals. For computational speed we neglect the substrate π -component which is always narrower than the σ -component. For the same reason we do not interfere the amplitude of the epitaxial structure with that of the substrate. These omissions do not produce observable errors since the plane-wave solutions are always convolved with Gaussians whose widths are greater than the Darwin width⁽²³⁾.

III. EXPERIMENT

Superlattice samples were provided to us by external sources. The $\text{Ga}_x\text{Al}_{1-x}\text{As}/\text{GaAs}$, $x \approx 0.1$, sample was grown⁽²⁶⁾ by metalorganic chemical vapor deposition (MOCVD) on a $\langle 100 \rangle$ GaAs substrate. The nominal number of layers and layer thickness were 30 and 200 Å, respectively (15 periods, 400 Å per period). The AlSb/GaSb sample was grown⁽²⁷⁾ by molecular beam epitaxy (MBE) on a $\langle 100 \rangle$ GaSb substrate. The nominal number of layers and layer thickness were 20 and 300 Å, respectively (10 periods, 600 Å per period). For both kinds of superlattices, the substrates were found to be oriented $\sim 2^\circ$ off the $\langle 100 \rangle$ -axis. The actual misorientation was taken into account for the values of ψ , γ_0 , and γ_H .

Double-crystal x-ray rocking curves were obtained using the $\text{Fe K}_{\alpha 1}$ (200), (400) and (422) reflections and the $\text{Cu K}_{\alpha 1}$ (422) reflection. With the exception of the (200) reflection, the Bragg angle is near 45° and the σ -component is dominant⁽²³⁾. The

symmetric (200) and (400) reflections are sensitive to ϵ^{\perp} only, while the asymmetric (422) reflections measure both ϵ^{\perp} and ϵ^{\parallel} (see eq. (4) above). Depending on asymmetry and Bragg angle the sensitivity to ϵ^{\parallel} is either lower or greater than that to ϵ^{\perp} . The use of more than one reflection permits verification of the internal consistency of the strain profiles. The x-ray beam was first collimated and rendered nearly monochromatic by (400) reflection in $\langle 100 \rangle$ Si or GaAs for the Fe $K_{\alpha 1}$ (200), (400) and (422) reflections and by (333) reflection in $\langle 111 \rangle$ Si for the Cu $K_{\alpha 1}$ (422) reflections. With the exception of the (200) reflection, the Bragg angles of the first crystal and the sample are nearly equal and the rocking curve is insensitive to the finite width of the $K_{\alpha 1}$ line. Even for the (200) reflection, with the $K_{\alpha 2}$ line blocked by the slits, the broadening due to the use of dispersive setting did not significantly affect the measured curve. In all cases, the divergence of the beam incident on the sample was less than 20 arcsec. Except for the (422), $\gamma_0 < |\gamma_H|$ reflection, the spot size at the sample was limited by a set of slits to 0.5 mm x 1 mm or less. For the (422), $\gamma_0 < |\gamma_H|$ reflection, due to the low grazing angle of incidence, the spot size was greater than the size of the sample, viciating absolute measurement of reflecting power. The incident beam intensity was 10^4 to 10^5 counts/sec, depending on the reflection and spot size. Rocking curves were obtained using a microprocessor-controlled diffractometer with a step-scan resolution of 10^{-4} deg.

IV. RESULTS AND DISCUSSION

The two kinds of superlattices discussed below are examples of extreme cases of strain variation likely to be found in practice. For the GaAlAs/GaAs superlattice, the maximum strain is below 0.3%, while for the AlSb/GaSb superlattice, the strain modulation is greater than 1%. In both cases, the nominal thickness of the period is large (400-600 Å) so that for the AlSb/GaSb superlattice the condition in eq. (13) above is not satisfied, i.e., the zeroeth order peak is less intense than higher order peaks. For the GaAlAs/GaAs superlattice, the zeroeth order peak is the most intense. The calculated curves were obtained using eq. (11) in Ref. (16) with structure factors based on nominal composition and tabulated atomic scattering factors⁽²⁸⁾, see Table I. Normal absorption coefficients were averaged over the superlattice period.

A. GaAlAs/GaAs Superlattice

Figure 1(a) shows measured (dashed line) and calculated (solid line) Fe K_{α1} (400) rocking curves of the GaAlAs/GaAs superlattice. In the experimental curve, in addition to the substrate peak (located at zero), seven superlattice peaks are clearly visible. These are obviously not the rapid oscillations of eq. (8), but peaks given by eq. (9) above. Their spacing yields an average superlattice period thickness $p = 676 \pm 2$ Å. The location $\Delta\theta_0 = -0.0641^\circ$ of the zeroeth order peak yields, through eq. (11), $\langle \epsilon \rangle = 0.118\%$. The (400) rocking curve gives

no information on ϵ'' , but previous work has shown^(29,30,8) that it is zero for epitaxial AlAs layers, up to several microns thick, grown on GaAs.

Assuming that the nominal GaAs layer is indeed GaAs, its perpendicular (and parallel) strain must be zero. The task of determining the strain profile in the superlattice period is thus reduced to determining the thickness and strain of the GaAlAs layer. Using the ratio of the amplitude of the +1 peak to that of the zeroeth peak and the appropriate structure factors from Table I, eq. (12) yields a thickness and strain of 320 Å and 0.249%, respectively, for the GaAlAs layer. The same values are obtained using the ratio of the amplitude of the -1 peak to that of the zeroeth peak. The agreement between these two determinations shows that the initial assumption of zero strain in the GaAs layer is valid. Had this assumption been false, the +1 and -1 peaks would have yielded different thicknesses and strains for the GaAlAs layer. The calculated rocking curve of Fig. 1(a) was obtained from this initial strain and structure factor distribution. The calculated curve reproduces very well the locations of the observed peaks as well as the intensities of the three low-order peaks. The slight discrepancy in the intensities of the +1 and -1 peaks is due to the small error in thickness and strain obtained from eq. (12) which neglected absorption, whereas the calculated curve in the figure includes normal absorption. For high-order peaks, the calculated curve generally predicts more intensity than is observed. Since random fluctuations in layer thickness were shown to decrease high-order

more than low-order peaks, one may suppose that the discrepancy is due to such fluctuations. Figure 1(b) reproduces the experimental curve of Fig. 1(a) and shows a calculated curve corresponding to random fluctuations of about 5% in layer thicknesses. The agreement with the measured curve is better although certain discrepancies persist. In Fig. 1(c), the calculated curve includes 5% fluctuations in both layer thicknesses and strain values. This results in a further diminution of high-order peaks, but does not eliminate all discrepancies. Larger fluctuations would only decrease the quality of the fit. In fact, careful examination of Fig. 1(a) shows that the discrepancy is due to the existence of transition regions in the superlattice period, rather than to fluctuations from period to period. This is best seen for the intensities of the +3 and +4 peaks (located at $\Delta\theta \approx 0.25^\circ$ and $\Delta\theta \approx 0.4^\circ$, respectively). The calculated curve matches the +4 peak reasonably well, but overestimates the intensity of the +3 peak. Clearly random fluctuations decrease the intensity of the +4 peak more than that of the +3 peak (Figs. 1(b) and (c)). A much better overall fit, shown in Fig. 1(d), is obtained using the four-layer period of Table II. These values were accepted as sufficiently accurate after a trial-and-error procedure involving about 10 iterations. The strain distribution and the structure factor distribution indicate the self-consistent result that the Al concentration varies continuously between the nominal GaAlAs and GaAs layers. Before discussing this result in more detail, we turn to the Fe $K_{\alpha 1}$ (200) rocking curve of the same sample.

Figure 2(a) shows the measured (dashed line) and a calculated (solid line) Fe $K_{\alpha 1}$ (200) rocking curve. Ten superlattice peaks are evident in the experimental curve. Since the Bragg angle for the (200) reflection is only 20.04° , the zeroeth order peak is not well-separated from the substrate peak (see eq. (4) above). Because in this case the structure factor for GaAs is only 6.64, the substrate peak is very weak and appears as a shoulder on the superlattice zeroeth peak. In addition, the low structure factor of the GaAs layers means that effectively only the GaAlAs layers are diffracting. For this reflection, the superlattice acts as if only the GaAlAs layers, separated by nondiffracting material, were present. Thus the rocking curve is very sensitive to the details of the GaAlAs portion of the period, and is less sensitive to the GaAs portion. The calculated curve corresponds to the same strain profile as was used in Fig. 1(a). As before, the step-function distribution gives a reasonably good fit to the experimental curve. The discrepancies are reduced if the four-layer period of Table II is used in the calculation, as shown in Fig. 2(b). Further improvement in the quality of the fit can only be obtained by introducing even finer detail in the structure of the period.

Despite the difference in their structure, the Fe $K_{\alpha 1}$ (400) and (200) rocking curves yield the same structure for the superlattice period. The thickness of the period and the average strain are determined to a precision of $\sim 1\%$. Consideration of only the three lowest-order peaks determines the amplitude of the strain modulation and the relative thickness of the layers to

$\sim 15\%$. If a good fit is obtained for high-order peaks, as in Figs. 1(d) and 2(b), the structure of the period, including transition regions, is determined to a precision of $\sim 5\%$.

The thickness of the period (676 \AA) is very different from the nominal thickness (400 \AA). Since the growth rate during MOCVD is determined by the availability of Ga, an error in its concentration will result in an error in estimated layer thickness. The present reactor was calibrated⁽²⁶⁾ for much thicker (2000 \AA) layers where the finite rise-time of the system was short compared to the total growth duration. The effects of finite rise-time are also evident in the $\sim 150 \text{ \AA}$ (Table II) transition regions between the uniform GaAlAs ($x = 0.249\%$) and GaAs ($x = 0.00\%$) layers.

B. AlSb/GaSb Superlattice

Figure 3 shows experimental and calculated Fe $K_{\alpha 1}$ (400) rocking curves. In addition to the substrate peak, the measured curve contains 14 clearly visible superlattice peaks. As mentioned earlier, due to the combination of large strain modulation and large thickness of the period, the zeroeth order peak is less intense than higher order peaks. This situation presents the practical problem of identifying the zeroeth order peak. The simplest way to resolve the dilemma is to calculate a rocking curve using data based on the nominal composition modulation. The actual thickness of the period, $610 \pm 2 \text{ \AA}$, is determined directly from the measured curve. Using the appropriate structure factors from Table I, the nominal thickness

ratio of 1:1 in the bilayer model of the period, and assuming zero perpendicular strain in the GaSb layer, one can calculate rocking curves corresponding to various values of perpendicular strain in the AlSb layer. Comparison with the experimental curve immediately shows that the strain in the AlSb layer is around 1.2%, while the strain in the GaSb layer is indeed close to zero. Consequently, the zeroeth order peak is at $\Delta\theta_0 \approx -0.29^\circ$ in Fig. 3. This result may be verified by comparing calculated and measured intensities of all peaks. The good agreement shown in Fig. 3 was obtained by trial-and-error adjustment in the structure of the period. For this sample, the structure is very nearly a step function, see Table III. The thickness of the transition region between the two layers is at most 5% of the thickness (305 Å) of the layers. The perpendicular strains are $(1.25 \pm 0.02)\%$ and $(-0.03 \pm 0.02)\%$ for the AlSb and GaSb layers, respectively. Negative perpendicular strain in the GaSb layer implies positive parallel strain, as we show below.

The Fe $K_{\alpha 1}$ (200) rocking curves of Fig. 4 yield slightly different values for the period thickness (625 Å) and the strain of the AlSb layer (1.23%). Even though for this reflection $\theta_B = 18.5^\circ$, the condition of eq. (13) is still not satisfied and the zeroeth peak, at $\Delta\theta_0 \approx -0.1^\circ$, is less intense than higher order peaks. The agreement between the shapes of calculated and measured curves is very good, but the calculated curve is everywhere about a factor of two more intense than the measured curve. The discrepancy is not accounted for, but suggests an error in the calculated structure factors or in the measurement

of the incident beam intensity, or both.

The Fe $K_{\alpha 1}$ (422), $\gamma_0 > |\gamma_H|$ rocking curves are shown in Fig. 5. Note the much narrower intrinsic width of these curves compared to those of Figs. 3 and 4. The thickness of the period deduced from Fig. 5 is the same as the value obtained with the (400) reflection. For Fe $K_{\alpha 1}$ (422), with $\gamma_0 > |\gamma_H|$, eq. (4) shows that the sensitivity to parallel strain is ~ 3.5 times greater than that to perpendicular strain. Using the values ϵ^\perp obtained with (400) and/or (200), the (422) curve yields $\epsilon'' = -(0.03 \pm 0.02)\%$ for both layers of the period, see Table III.

The sense of asymmetry is reversed for the Cu $K_{\alpha 1}$ (422), $\gamma_0 < |\gamma_H|$ reflection of Fig. 6. In this case, the sensitivity to ϵ^\perp is much greater than that to ϵ'' . As mentioned above, for this reflection the angle of incidence with respect to the sample is only $\sim 2^\circ$ and the x-ray spot size was greater than the size of the sample. Thus the experimental reflecting power was easily underestimated. Nevertheless, the measured and calculated curves have the same shape, confirming the strain profiles obtained with the other reflections. Thus all four rocking curves (Figs. 3 through 6), measured at different Bragg angles, with different asymmetries and different wavelengths, correspond to the same structure of the period (Table III).

The presence of nonzero parallel strain implies the breakdown of perfect coherency between the epitaxial structure and the substrate. In the direction perpendicular to the surface, for $\epsilon'' = 0.03\%$ there are three fewer atomic planes in the superlattice for every 10^4 planes in the substrate. Since ϵ''

is uniform throughout the superlattice layers, the partial crystallographic decoupling occurs in a narrow (a few hundred angstroms thick) region at the interface between the superlattice and the substrate. A parallel strain of 0.03% corresponds to a net number of $\sim 1 \times 10^4$ $a/2$ $\langle 011 \rangle$ edge dislocations/cm² localized in a narrow region at the interface with the substrate. A much larger parallel strain (0.19%) was measured⁽²⁵⁾ in a GaAs_xP_{1-x}/GaP, $x = 0.14$, superlattice grown on a 1 μ m GaAs_yP_{1-y}, $y = 0.061$, buffer on $\langle 100 \rangle$ GaP. The buffer plays a major role in decoupling the superlattice from the substrate.

C. Point Defects and Lateral Inhomogeneities

In addition to providing depth profiles of strain, experimental rocking curves contain information about point defects and lateral inhomogeneities⁽¹⁶⁻¹⁹⁾. A measure of point defects is obtained from comparison of experimental intensity with that predicted using perfect-crystal structure factors. Point defects lead to a decrease in the magnitude of the structure factor. If point defects are described by a probability distribution of incoherent atomic displacements away from perfect-crystal sites, the standard deviation U of the distribution is readily obtained from the measured curve^(16,19). For the present samples, structure factors were calculated assuming no point defects other than those due to random interchange of Ga and Al corresponding to the local composition. The good agreement between measured and calculated curves obtained above indicates that for both samples the standard

deviation U is less than 0.1 \AA . This is consistent with the general result obtained by channeling⁽³⁻⁶⁾ and electron diffraction⁽⁷⁾ on a variety of superlattices.

Lateral inhomogeneities in composition and extended defects such as dislocations produce lateral variations in strain and undulations in atomic planes. A measure of this undulation is the width of the function used to convolve the plane-wave, planar structure rocking curve. As mentioned earlier, the divergence of the beam incident on the sample was in all cases below 20 arcsec. An increase over this value in the width of the convolving function indicates lateral inhomogeneity in the sample. The calculated curves shown above were convolved with Gaussians of from 30 to 75 arcsec standard deviations. Thus for both samples, there are undulations of ~ 1 arcmin in atomic planes.

D. Elastic Strains and Determination of Composition

The problem of the distribution of elastic strains in the epitaxial layer and substrate is similar to the bi-metal strip problem whose solution may be found in standard texts⁽³¹⁾. The final state of strain may be thought of as resulting from a three-step process: (1) the epitaxial layer is strained to match the in-plane interatomic spacing of a rigid substrate; (2) under the action of the epitaxial layer the nonrigid substrate and layer are strained without bending by an amount yielding zero net force on the structure, but nonzero bending moment; (3) the structure acquires curvature when the bending moment is removed. For imperfectly coherent epitaxy (i.e., the x-ray $\epsilon'' \neq 0$), the

structure relaxes as if the initial misfit were decreased by the x-ray parallel strain. From Vegard's law for alloyed materials, the (free) lattice parameter varies linearly with composition. Assuming that elastic properties⁽²²⁾ also vary linearly with composition, one can calculate elastic strains for arbitrary combinations of epitaxial layer and substrate. Comparison of calculated and measured strains allows determination of the composition.

Using the commonly accepted^(30,20,8) misfit of 1.4×10^{-3} between AlAs and GaAs, and the x-ray strain of layer b in Table II, we obtain a peak Al concentration $x = 0.935$. In layers a and c, the concentration of Al scales with the strain. For the 500 μm thick GaAs substrate, the radius of curvature is calculated to be -25.5 m. At the interface with the superlattice, the elastic perpendicular and parallel strains of the substrate are -0.001% and +0.001%, respectively.

Using lattice parameter values⁽³²⁾ of 6.095 Å and 6.135 Å for GaSb and AlSb, respectively, and the measured x-ray $\epsilon'' = 0.03\%$, we calculate x-ray perpendicular strains of -0.027% and 1.27% for the GaSb and AlSb layers, respectively. The agreement with measured values, Table III, is very good. At the interface with the superlattice, the substrate perpendicular and parallel elastic strains are -0.004% and 0.004%, respectively. For the 500 μm thick substrate, the calculated bending radius is -7.5 m.

For both superlattice samples, the deformation of the substrate is only a few percent of that of the epitaxial structure. This validates the (general) use of the free

substrate lattice parameter in the comparison of x-ray and elastic strains in epitaxial structures on thick substrates.

V. CONCLUSION

We have given a simple expression relating the structure of the superlattice period to the structure of the rocking curve. The form of this expression shows at a glance the existence of equally-spaced peaks whose intensities are determined by the structure of the superlattice period. The location and intensity of the zeroeth (and frequently largest) peak measure the depth-averaged properties of the superlattice. For a perfectly periodic superlattice whose period is a step function, consideration of the three lowest-order peaks provides an analytic determination of the period. For more complicated structures, including transition regions between the layers of the period, one must consider the intensities of higher-order peaks. Small, random fluctuations in layer thicknesses and strains decrease the intensities of high-order peaks with relatively small changes for low-order peaks. The treatment above includes depth profiles of structure factor and perpendicular and parallel strains. Extension to arbitrary deformations, including shear strains, is straightforward. For each additional strain component, an additional rocking curve measurement is needed. The availability of a large number of intense reflections allows verification of the internal

consistency of the profiles. The strain profiles, referred to the unit cell of the underlying substrate, are absolute.

We have analyzed a GaAlAs/GaAs and an AlSb/GaSb superlattice. The former is an example of small modulation of strain (GaAlAs on GaAs is frequently called "unstrained") while in the latter the amplitude of strain modulation is 1.28%. Combination of large perpendicular strain and total thickness (6100 Å) in the AlSb/GaSb superlattice produced a departure from perfectly coherent epitaxy. In this sample, a uniform parallel (in-plane) strain of 0.03% was measured. The parallel strain is accommodated by misfit dislocations ($\sim 1 \times 10^4/\text{cm}^2$) localized in a narrow region at the interface with the substrate. The measured perpendicular strain was in excellent agreement with the value calculated from bulk lattice parameters, elastic constants and the measured parallel strain. In the GaAlAs/GaAs superlattice, the Al content was determined from Vegard's law and elasticity theory.

For the samples studied above, the periodicity and average strain were measured with a precision of $\sim 1\%$. The relative thickness of the layers and the strain modulation are known to $\sim 5\%$. Since for both samples the thickness of the period was large (~ 600 Å), one may ask whether the high precision obtained above will hold for samples with periodicities of 100 Å or less. We believe that this will remain true, because of the availability of a large number of asymmetric reflections. In the generalized A and Y coordinates used above, the structure (i.e., number, spacing and relative intensities of peaks) of the

rocking curve is invariant. One may choose the particular reflection by considering sensitivity and convenience.

The x-ray rocking curve method enjoys a number of advantages over ion channeling, Rutherford backscattering, electron diffraction, and Auger electron spectroscopy, all of which have been used to measure properties of superlattices. The complexity and cost of the apparatus are an order of magnitude lower. The measurement of rocking curves is simple, rapid, and reproducible. The measurement does not destroy the sample. In epitaxial layers, the precision of composition determination is at least as good as that obtained by other techniques. For measurement of strain profiles, the rocking curve is unmatched by either channeling or electron diffraction.

ACKNOWLEDGMENTS

Dr. Bruce M. Paine contributed in a major way to the setting up of our diffractometer and data acquisition and analysis system. During the initial critical stages of the development, Dr. Paine guided us successfully through a morass of hardware and software problems. Since then we have relied on him for general troubleshooting and advice on programming. We are grateful to John Melvin for supplying us with an initial graphics package and to Frank Cosso and Prakash Kasiraj for systems programs. Professor M-A. Nicolet encouraged us at every step of this study. The work was supported by the Defense Advanced Research Projects

Agency (S. Roosild) under Contract [MDA 903-82-C-0348].

TABLE I. Absolute Values of Structure Factors.

| Reflection | GaAs | $\text{Al}_{0.9}\text{Ga}_{0.1}\text{As}$ | GaSb | AlSb |
|-----------------------|-------|---|-------|-------|
| Fe K_{α} (400) | 157.9 | 116.9 | 214.2 | 166.9 |
| (200) | 6.64 | 61.05 | 72.4 | 131.1 |
| (422) | - | - | 191.2 | 150.1 |
| Cu K_{α} (422) | - | - | 191.3 | 151.6 |

TABLE II. Strain and Structure Factor Distributions in the Average Period of the GaAlAs/GaAs Superlattice. Strain is Defined Relative to the Substrate, See eq. (1) Above.

| Layer | Thickness (Å) | $\epsilon^{\frac{1}{2}}$ (%) | $ F_{400} $ | $ F_{200} $ |
|-------|---------------|------------------------------|-------------|-------------|
| a | 150 | 0.180 | 128.3 | 46.0 |
| b | 170 | 0.249 | 116.9 | 61.05 |
| c | 100 | 0.103 | 136.5 | 35.1 |
| d | 256 | 0.000 | 157.9 | 6.64 |

TABLE III. Strain Distributions in the Average
Period of the AlSb/GaSb Superlattice.
Strain is Defined Relative to the Substrate,
See eq. (1) Above.

| Layer | Thickness (Å) | ϵ^{\perp} (%) | ϵ^{\parallel} (%) |
|-------|---------------|------------------------|----------------------------|
| a | 305 | 1.25 | 0.03 |
| b | 305 | - 0.03 | 0.03 |

REFERENCES

- a) Present Address: IBM, San Jose Research Laboratory, 5600
Cottle Road, San Jose, California 95193.
1. L. Esaki and L. L. Chang, Phys. Rev. Lett. 33, 495 (1974).
 2. G. C. Osbourn, J. Appl. Phys. 53, 1586 (1982).
 3. F. W. Saris, W. K. Chu, C. A. Chang, R. Ludeke, and L. Esaki, Appl. Phys. Lett. 37, 931 (1980).
 4. S. T. Picraux, L. R. Dawson, G. C. Osbourn, R. M. Biefeld, and W. K. Chu, Appl. Phys. Lett. 43, 1020 (1983).
 5. W. K. Chu, J. A. Ellison, S. T. Picraux, R. M. Biefeld, and G. C. Osbourn, Nucl. Instr. Meth. 218, 81 (1983).
 6. W. K. Chu, C. K. Pan, and C.-A. Chang, Phys. Rev. B, Rapid Comm. 28, 4033 (1983).
 7. J. M. Brown, N. Holonyak, Jr., M. J. Ludowise, W. T. Dietze, and C. R. Lewis, Appl. Phys. Lett. 43, 863 (1983).
 8. W. J. Bartels and W. Nijman, J. Cryst. Growth, 44, 518

(1978).

9. W. J. Bartels and H. Veenliet, Inst. Phys. Conf. Ser. No 45: Chapter 3, 229 (1979).
10. V. S. Speriosu and H. L. Glass, U.S./France Seminar on Topography, Snowmass, Colorado, 1983.
11. V. S. Speriosu, M-A. Nicolet, J. L. Tandon, and Y. C. M. Yeh, Appl. Phys. Lett., MS #L-4676.
12. J. Burgeat and D. Taupin, Acta Crystallogr. A24, 99 (1968).
13. A. Fukuhara and Y. Takano, Acta Crystallogr. A33, 137 (1977).
14. B. C. Larson and J. F. Barhorst, J. Appl. Phys. 51, 3181 (1980).
15. K. Komenou, I. Hirai, K. Asama, and M. Sakai, J. Appl. Phys. 49, 5816 (1978).
16. V. S. Speriosu, J. Appl. Phys. 52, 6094 (1981).
17. V. S. Speriosu, B. M. Paine, M-A. Nicolet, and H. L. Glass, Appl. Phys. Lett. 40, 604 (1982).

18. B. M. Paine, V. S. Speriosu, L. S. Wielunski, H. L. Glass, and M-A. Nicolet, Nucl. Instr. Meth. 191, 80 (1981).
19. V. S. Speriosu and C. H. Wilts, J. Appl. Phys. 54, 3325 (1983).
20. Armin Segmüller, P. Krishna, and L. Esaki, J. Appl. Cryst. 10, 1 (1977).
21. R. M. Fleming, D. B. McWhan, A. C. Gossard, W. Wiegmann, and R. A. Logan, J. Appl. Phys. 51, 357 (1980).
22. J. Hornstra and W. J. Bartels, J. Cryst. Growth, 44, 513 (1978).
23. W. H. Zachariasen, Theory of X-Ray Diffraction in Crystals, (Wiley, New York, 1945).
24. Speriosu is grateful to Drs. Lehel Zsoldos and Armin Segmüller for questioning the general validity of eq. (6) in Ref. (16).
25. V. S. Speriosu, M-A. Nicolet, S. T. Picraux, and R. M. Biefeld, Appl. Phys. Lett., MS # L-4662.
26. We thank Y.C.M. Yeh and J. L. Tandon of Applied Solar Energy Corporation for providing GaAlAs/GaAs superlattices.

27. We thank W. K. Chu of the University of North Carolina at Chapel Hill for providing AlSb/GaSb superlattices.
28. J. A. Ibers and W. C. Hamilton, Eds., International Tables for X-Ray Crystallography, Vol. IV, (Kymoch Press, Birmingham, 1974).
29. G. A. Rozgonyi, P. M. Petroff, and M. B. Panish, J. Cryst. Growth, 27, 106 (1974).
30. E. Estop, A. Izrael, and M. Sauvage, Acta Cryst., A32, 627 (1976).
31. See for example, R. F. S. Hearmon, An Introduction to Applied Anisotropic Elasticity, (Oxford Univ. Press, Oxford, 1961).
32. Marvin K. Farr, J. G. Taylor, and S. K. Sinha, Phys. Rev. B 11, 1587 (1975).

FIGURE CAPTIONS

- Figure 1(a) Measured (dashed line) and calculated (solid line) $\text{Fe K}_{\alpha 1}$ (400) rocking curves of GaAlAs/GaAs superlattice. The calculated curve corresponds to the bilayer structure of the period discussed in the text.
- Figure 1(b) $\text{Fe K}_{\alpha 1}$ (400) rocking curves of GaAlAs/GaAs superlattice. The calculated curve corresponds to $\sim 5\%$ fluctuations in layer thicknesses.
- Figure 1(c) $\text{Fe K}_{\alpha 1}$ (400) rocking curves of GaAlAs/GaAs superlattice. The calculated curve corresponds to $\sim 5\%$ fluctuations in both layer thicknesses and strains.
- Figure 1(d) $\text{Fe K}_{\alpha 1}$ (400) rocking curves of GaAlAs/GaAs superlattice. Best fit of experimental curve using the four-layer period of Table II.
- Figure 2(a) $\text{Fe K}_{\alpha 1}$ (200) rocking curves of GaAlAs/GaAs superlattice. The calculation corresponds to the bilayer period used in Fig. 1(a).
- Figure 2(b) $\text{Fe K}_{\alpha 1}$ (200) rocking curves of GaAlAs/GaAs superlattice. Best fit using the four-layer period of Table II.
- Figure 3 $\text{Fe K}_{\alpha 1}$ (400) rocking curves of AlSb/GaSb superlattice. The calculated curve is based on the bilayer period of Table III.
- Figure 4 $\text{Fe K}_{\alpha 1}$ (200) rocking curves of AlSb/GaSb

1
superlattice. The calculated curve used the period of Table III.

Figure 5 Fe $K_{\alpha 1}$ (422), $\gamma_0 > |\gamma_H|$ rocking curves of AlSb/GaSb superlattice. The calculated curve used the period of Table III.

Figure 6 Cu $K_{\alpha 1}$ (422), $\gamma_0 < |\gamma_H|$ rocking curves of AlSb/GaSb superlattice. The calculated curve used the period of Table III. The absolute reflecting power of the measured curve is underestimated, as discussed in the text.

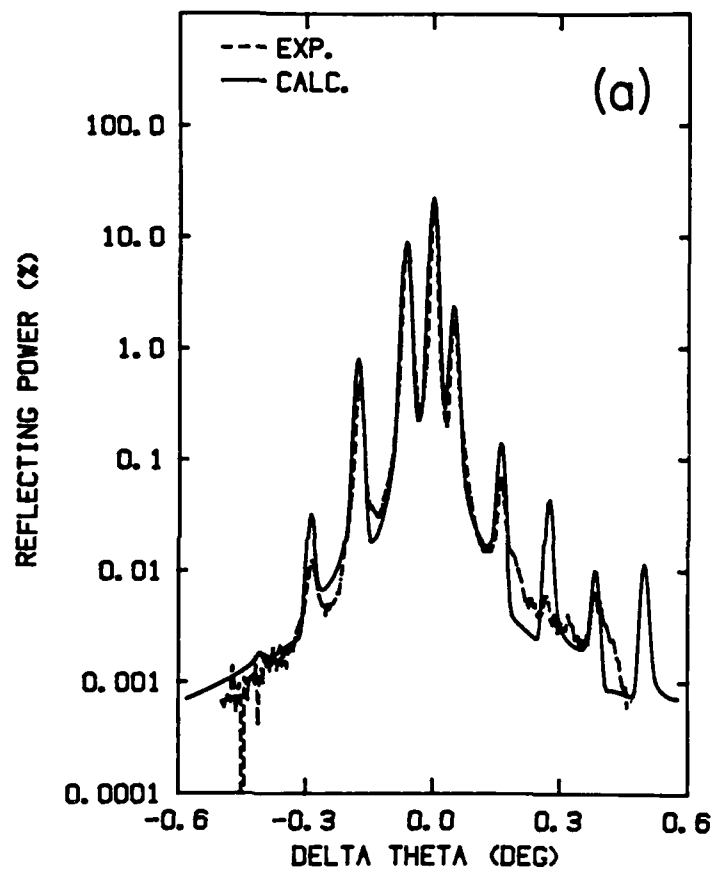


Fig.1

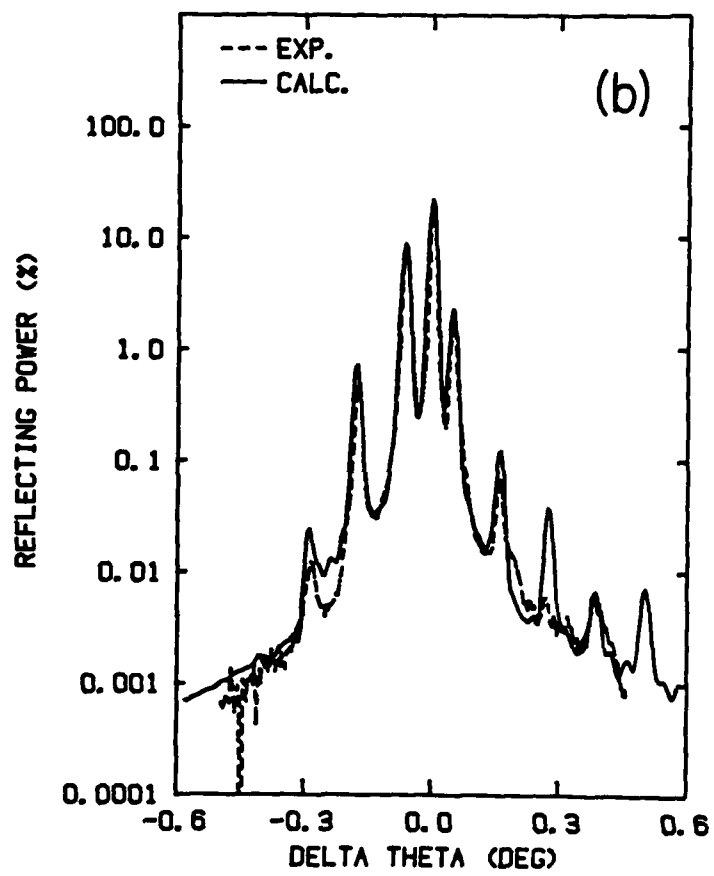


Fig.1

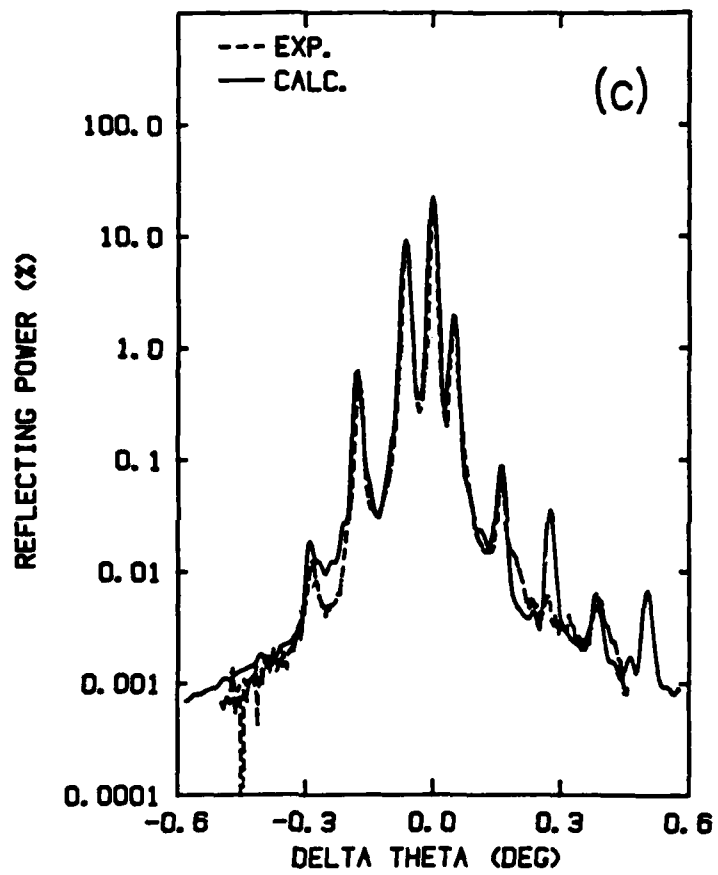


Fig.1

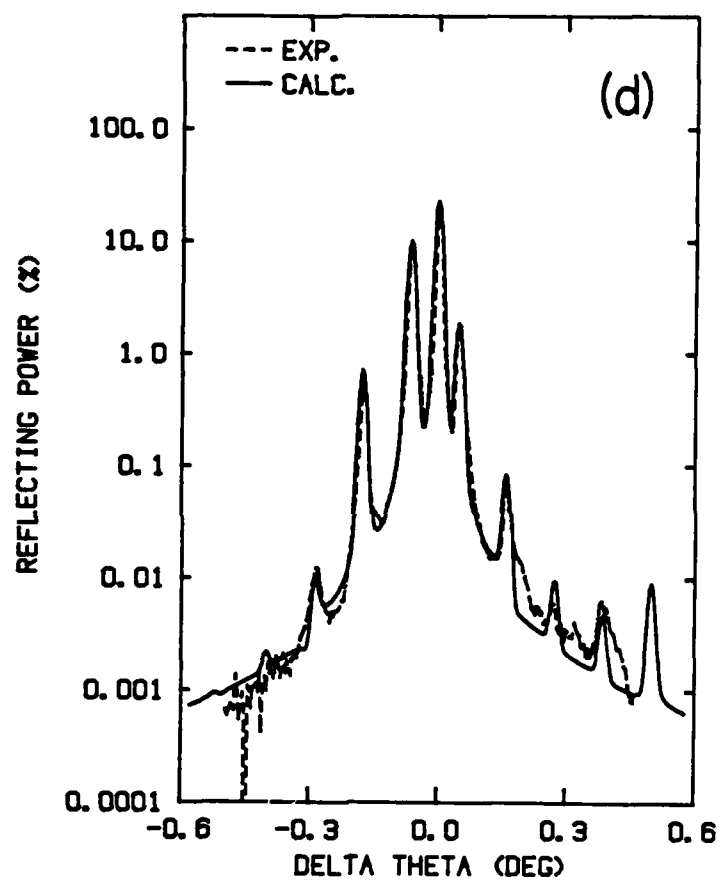


Fig.1

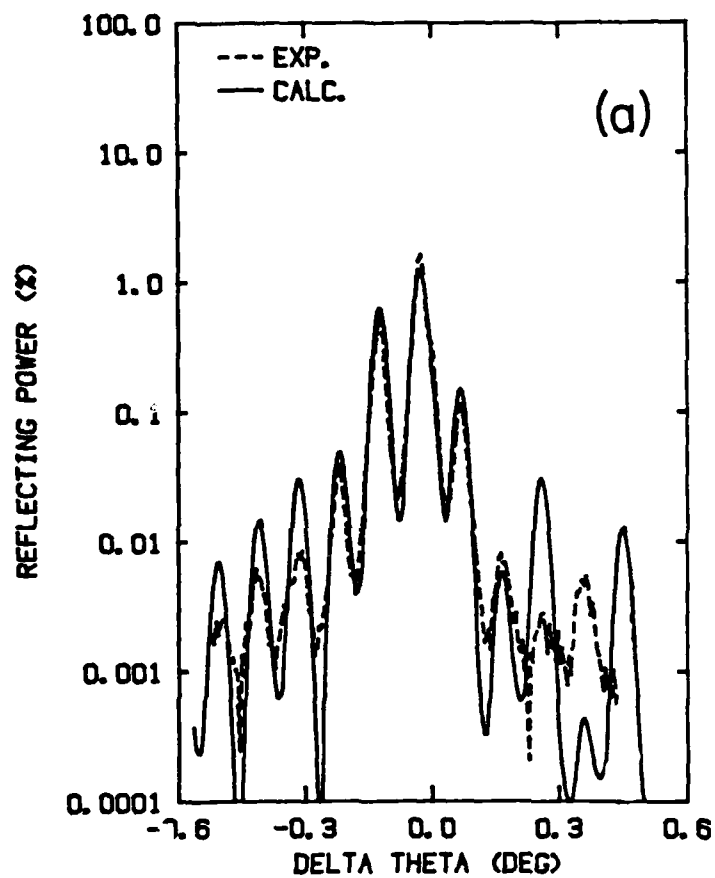


Fig.2

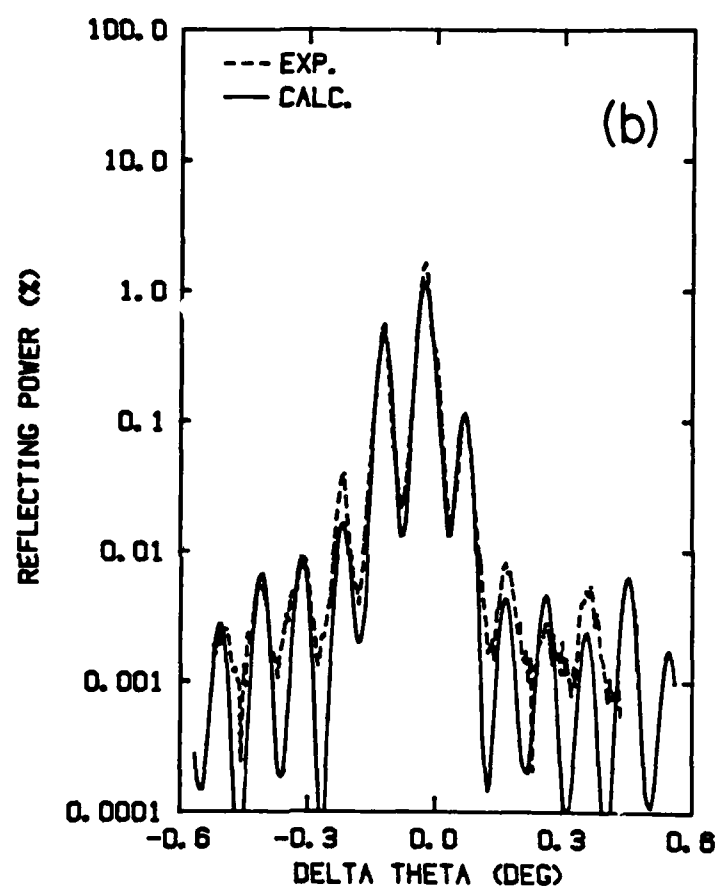


Fig.2

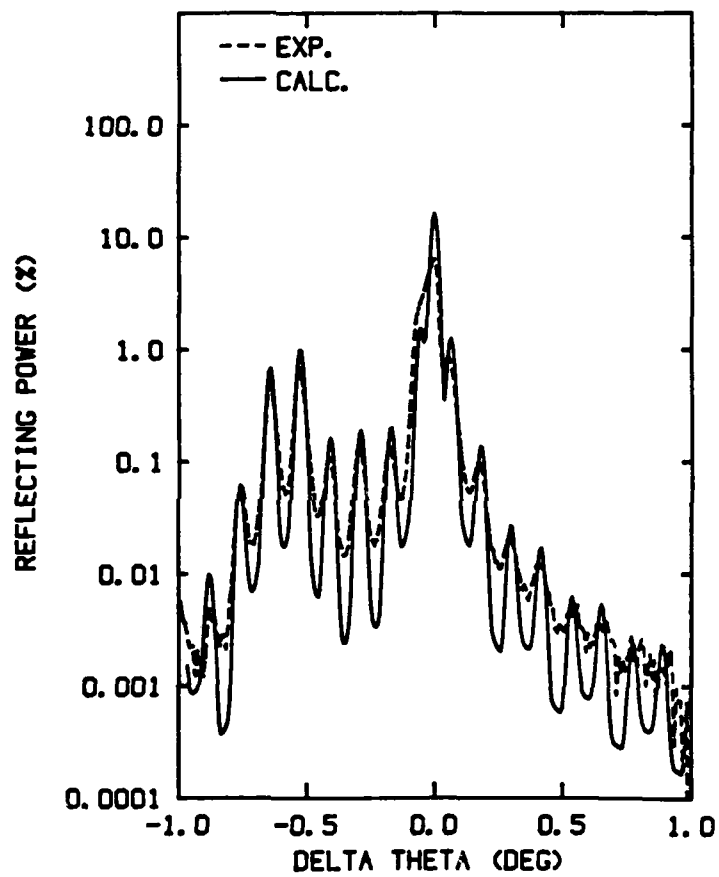


Fig.3

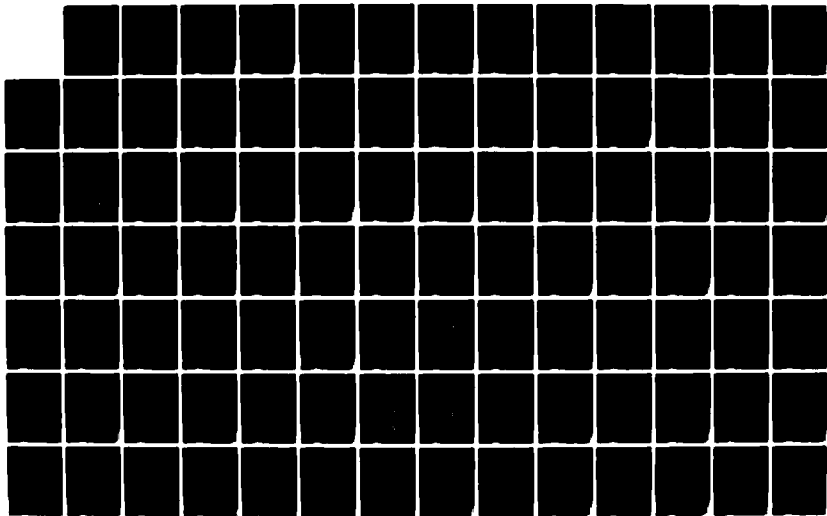
AD-A147 449

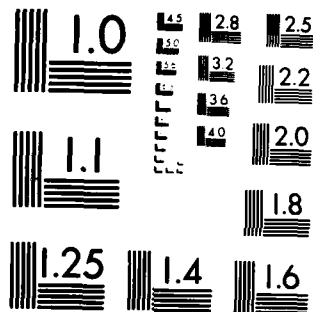
X-RAY AND BACKSCATTERING ANALYSIS OF ION IMPLANTATION
PHENOMENA IN GAAS A.; (U) CALIFORNIA INST OF TECH
PASADENA M A NICOLET ET AL. 04 AUG 84 MDA903-82-C-0348

2/3

UNCLASSIFIED

F/G 20/12 NL





MICROCOPY RESOLUTION TEST CHART
NATIONAL BUREAU OF STANDARDS-1963-A

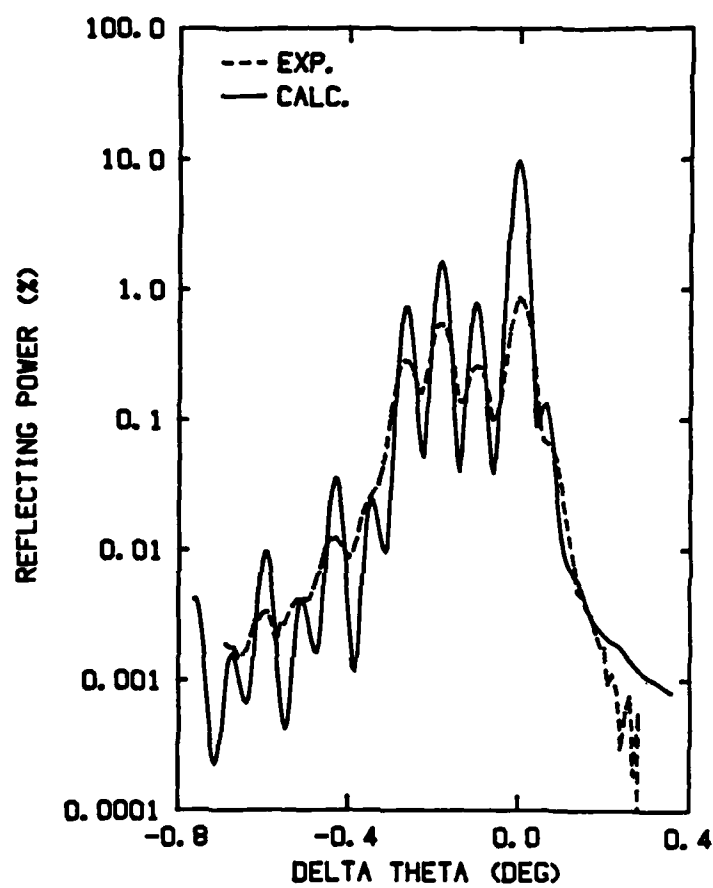


Fig.4

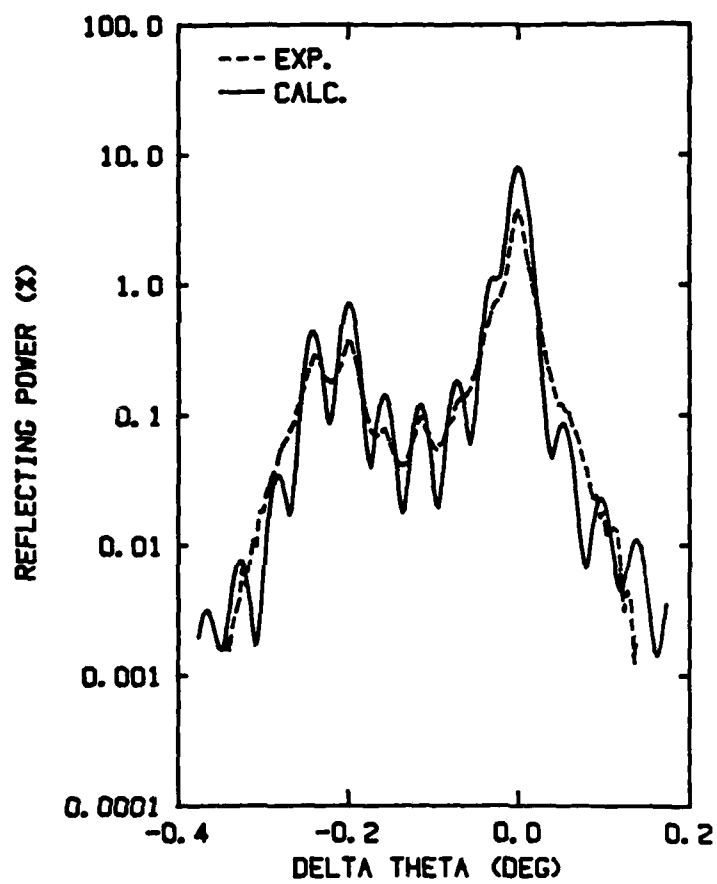


Fig.5

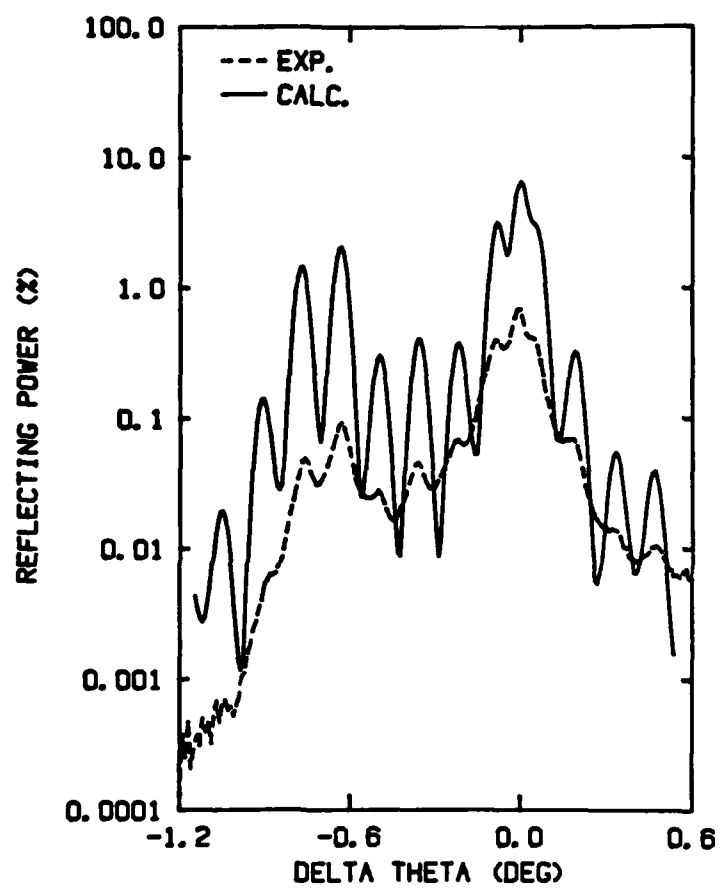


Fig.6

Depth profiles of perpendicular and parallel strain in a $\text{GaAs}_x\text{P}_{1-x}/\text{GaP}$ superlattice

V. S. Speriosu^{a)} and M.-A. Nicolet
California Institute of Technology, Pasadena, California 91125

S. T. Picraux and R. M. Biefeld
Sandia National Laboratories, Albuquerque, New Mexico 87185

(Received 6 March 1984; accepted for publication 18 May 1984)

Using double-crystal x-ray rocking curves, depth profiles of parallel and perpendicular strain were obtained in a $\text{GaAs}_{0.14}\text{P}_{0.86}/\text{GaP}$ superlattice grown on a buffer layer on (100) GaP. Combining symmetric $\text{Fe } K_{\alpha 1}$ (400) and asymmetric $\text{Cu } K_{\alpha 1}$ (422) reflections, a constant parallel strain of 0.19% relative to the substrate was found throughout the superlattice and buffer layer. Relative to the substrate, the perpendicular strain was found to be 0.26% in the buffer, and 0.80% and -0.19% in the 176-Å-thick superlattice $\text{GaAs}_x\text{P}_{1-x}$ and GaP layers, respectively. The strain profiles indicate the buffer is ~80% decoupled from the substrate by misfit dislocations near the buffer/substrate interface, and the lattice misfit in the superlattice is elastically accommodated by the epitaxial structure with a small shift in the average lattice constant relative to the equilibrium superlattice structure.

Superlattices¹ are a class of epitaxial materials grown by periodic depth modulation of the composition. When the lattice parameters of the alternating layers are unequal, the modulation of the composition results in a modulation of the lattice parameter (i.e., strain). For strained-layer superlattices (SLS's) of good quality, the misfit strain is entirely accommodated by elastic deformation in the layers. The electrical and optical properties of semiconductor SLS's depend on the state of strain as well as on the composition modulation of the layers.²

Present growth procedures frequently incorporate a buffer or graded layer between the superlattice and the substrate.³⁻⁵ Models of strain in the superlattice and buffer have evolved from measurements of dislocation densities,^{3,4,6} and by ion channeling,^{5,7} electrical,⁸ and optical⁴ property measurements. It is thought that if the buffer is sufficiently thick, the lattice mismatch between the buffer and substrate can be accommodated by misfit dislocations in the buffer layer. If a buffer composition close to the average composition of the superlattice is used, the lattice constant at the buffer surface can be set to minimize the elastic strain energy stored in the SLS. In this idealized case, the superlattice is decoupled from the substrate and the state of strain in the superlattice is determined entirely by the lattice mismatch, elastic properties, and thicknesses of the superlattice layers.

Double-crystal x-ray diffraction has also been used to obtain depth profiles of composition and superlattice strain in the direction perpendicular to the crystal surface.^{9,10} However, x-ray rocking curves are also capable of providing depth profiles of strains in directions other than perpendicular to the surface.^{11,12} In this letter we present rocking curve determinations of the depth profile of strain both perpendicular and parallel to the surface for a $\text{GaAs}_x\text{P}_{1-x}/\text{GaP}$ superlattice. The results provide the first direct determination of the three-dimensional state of the strain in SLS and buffer layers.

The superlattice was grown by metal organic chemical

vapor deposition (MOCVD) on a (100) oriented GaP substrate at 800 °C.¹³ The superlattice consists of 30 alternating layers of GaP and $\text{GaAs}_x\text{P}_{1-x}$ with x near 0.14. A $\text{GaAs}_y\text{P}_{1-y}$ ($y \sim 0.07$) buffer layer was grown between the substrate and superlattice. For directions perpendicular and parallel to the (100) surface we define the strain in the layers relative to the substrate by

$$\epsilon^i = (a_i^f - a_i)/a_i, \quad (1)$$

where i corresponds to \parallel or \perp , and a_i^f and a_i refer to the film and substrate lattice parameters, respectively. This definition of strain differs from the standard definition in elasticity theory where strain is defined relative to the lattice parameter of the free film rather than the substrate. From the equilibrium lattice parameter of the film, it is a simple matter to convert x-ray strain given by Eq. (1) to the strain of elasticity theory.

Double-crystal x-ray rocking curves were obtained using the $\text{Fe } K_{\alpha 1}$ (400) and $\text{Cu } K_{\alpha 1}$ (422) reflections. The symmetric (400) reflection is sensitive to ϵ^{\parallel} only, while the asymmetric (422) reflection measures both ϵ^{\parallel} and ϵ^{\perp} . For the (422) reflection with the incident beam at glancing angle $\theta_{\text{inc}} = 79^\circ$, the sensitivity to ϵ^{\perp} is five times greater than that to ϵ^{\parallel} . The x-ray beam was first collimated and rendered nearly monochromatic by the (400) reflection in (100) GaAs for the $\text{Fe } K_{\alpha 1}$ (400) reflection and by the (333) reflection in (111) Si for the $\text{Cu } K_{\alpha 1}$ (422) reflection. The divergence of the beam incident on the sample was less than 20 arcs. The spot size at the sample was limited by a set of slits to 0.5×1 mm or less. The incident beam intensity was 10^4 – 10^5 counts/s, depending on the reflection and spot size. Rocking curves (reflecting power versus angle) were measured with a microprocessor-controlled diffractometer. A detailed discussion of the application of x-ray analysis to superlattices will be given elsewhere.¹⁴

Theoretical rocking curves were obtained using a kinematical model of diffraction in epitaxial layers with diffraction in the substrate treated using dynamical theory.¹¹ The structure factor and normal absorption coefficient were calculated from the approximate composition and tabulated

^{a)} Present address: IBM, Research Division, 5600 Cottle Road, San Jose, California.

atomic scattering values.¹⁵ Although the structure factor of GaP is different from that of $\text{GaAs}_{0.14}\text{P}_{0.86}$, the average composition was used for the superlattice layers. While the modulation of the structure factor does in general affect the rocking curve, in the present case its influence is much lower than that of the strain modulation.¹⁴ Rocking curves were calculated using the nominal number of superlattice periods (15) and assuming that each period consists of layers A and B, each with its own thickness and ϵ^{\perp} and ϵ^{\parallel} values. The presence of a buffer layer of arbitrary thickness and strain gradients was also allowed. The strain distribution was varied through a systematic trial-and-error procedure¹¹ until a good fit to the experimental curves was obtained. Good agreement between measured and calculated curves determines the average superlattice periodicity and strain, as well as the strain in the buffer layer, to a precision of about $\pm 2\%$.¹¹ The amplitude of the superlattice strain modulation and the relative layer thickness should be accurate to within 5%.

Figure 1 shows experimental (dashed line) and calculated (solid line) rocking curves. The angle $\Delta\theta$ is shown relative to the Bragg angle of the substrate peak. The abscissa is shown at significantly higher magnification for Fig. 1(b) than 1(a), because of the narrower intrinsic diffraction widths and satellite structure for the (422) reflection. The calculated curves are the plane wave, planar structure solutions convolved with Gaussians with standard deviations of 45 and 20 arcs for Figs. 1(a) and 1(b), respectively. Although in Fig. 1(b) the predicted narrow oscillations for the (422) reflections were not resolved experimentally, the envelopes of the curves are in agreement. The broadening of the narrow oscillations implies small undulations in atomic planes and/or fluctuations in the local value of strain. Although lateral variations in strain and undulations in crystal planes affect the results of Fig. 1(b) much more than Fig. 1(a), both rocking curves imply undulations of less than 1 arcmin.

Final results for the depth profile of the strain corresponding to the rocking curves of Fig. 1 are given in Table I. The $\text{Fe } K_{\alpha 1}$ (400) reflection determined the values of the perpendicular strain and layer thickness for the buffer and su-

TABLE I. Profiles of perpendicular and parallel strain in buffer and superlattice. Strain is defined with respect to the substrate [see Eq. (1)].

| | Thickness (Å) | ϵ^{\perp} (%) | ϵ^{\parallel} (%) |
|---|---------------------|---------------------------|-------------------------------|
| Superlattice ^a | | | |
| GaAs _{0.14} P _{0.86} layers | 176 | 0.80 | 0.19 |
| GaP layers | 176 | -0.19 | 0.19 |
| Buffer | 10 000 ^b | 0.26 | 0.19 |

^a Number of periods = 15.

^b Value assuming same structure factor as for SLS. Angle lap and chemical strain results suggest a thicker buffer layer ($\sim 1.7 \mu\text{m}$) suggesting a lowering of the structure factor for the buffer layer possibly due to point defects.

perlattice. The ϵ^{\perp} values in the $\text{GaAs}_{0.14}\text{P}_{0.86}$ and GaP layers were found to be uniform throughout the SLS. The ϵ^{\perp} in the buffer is also uniform throughout most of the buffer layer thickness, with the transition region (where ϵ^{\perp} drops to zero at the interface with the substrate) confined to less than 10% of the buffer layer thickness. The values of ϵ^{\perp} obtained with the $\text{Fe } K_{\alpha 1}$ (400) rocking curve were used together with the $\text{Cu } K_{\alpha 1}$ (422) rocking curve to obtain the depth profile of ϵ^{\parallel} . The large ϵ^{\parallel} indicates that, to a significant extent, the buffer and superlattice are crystallographically decoupled from the underlying substrate. The uniformity of ϵ^{\parallel} versus depth suggests that the decoupling has occurred by misfit dislocations originating in a narrow region ($< 0.1 \mu\text{m}$) of the buffer near the substrate consistent with previous studies.⁶ From the measured parallel strain of 0.19% we may estimate, for example, $\sim 5 \times 10^4$ misfit dislocations of type $b = 1/2$ (011) along a unit length of line in the plane of growth, or a total of $\sim 10^5/\text{cm}^2$ in the transition region near the buffer/substrate interface.

If the buffer layer was totally decoupled from the substrate then the ϵ^{\perp} and ϵ^{\parallel} values would be equal to each other and would correspond to the equilibrium lattice constant as defined by Eq. (1). For the case of (100) oriented layers and isotropic in-plane strain, the perpendicular and parallel strains are related by

$$\epsilon^{\perp} = (1 + 2C_{12}/C_{11})(a_0 - a_{\text{GaP}})/a_{\text{GaP}} - \epsilon^{\parallel} 2C_{12}/C_{11}, \quad (2)$$

where the layer ϵ^{\perp} , ϵ^{\parallel} are referenced to the GaP substrate [Eq. (1)], C_{11} and C_{12} are the elastic constants¹⁶ and a_0 the unstrained lattice constant of the layer. For the $\text{GaAs}_{0.14}\text{P}_{0.86}$ buffer layer we obtain $a_0 = 5.463 \text{ Å}$; which from Eq. (1) corresponds to $\epsilon^{\perp} = \epsilon^{\parallel} = 0.23\%$. Thus the buffer layer contains a small residual coherency strain of $\Delta\epsilon^{\parallel} = (0.23 - 0.19) = 0.04\%$. Also by Vegard's law for alloyed semiconductors we may infer a composition $y = 0.061 \pm 0.003$, which is close to the nominal value of 0.07. From the ϵ^{\perp} and ϵ^{\parallel} values in the SLS we may similarly determine an equilibrium lattice parameter $a_0 = 5.4560 \text{ Å}$ for the $\text{GaAs}_{0.14}\text{P}_{0.86}$ layers, which corresponds to $x = 0.14 \pm 0.01$; independent Rutherford backscattering measurements gave a consistent value of $x = 0.16 \pm 0.02$. One can verify this procedure by applying it to the superlattice GaP layers for which the relaxed unit cell should be identical to the substrate. For the GaP layers, Eq. (2) yields $a_0 = 5.4504 \text{ Å}$ compared to the bulk value of 5.4512 Å . The difference corresponds to an error of -3×10^{-4} , which is

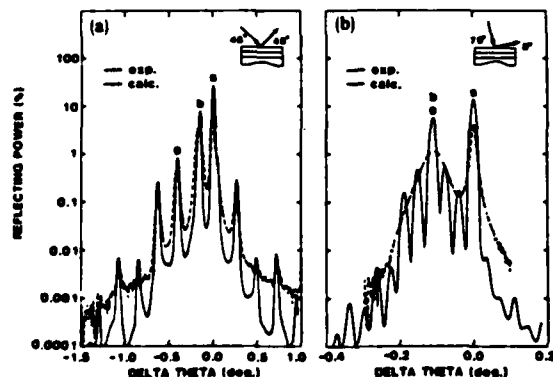


FIG. 1. Measured (dashed line) and calculated (solid line) rocking curves corresponding to the (a) $\text{Fe } K_{\alpha 1}$ (400) reflection and (b) $\text{Cu } K_{\alpha 1}$ (422), $\theta_{\text{inc}} = 79^\circ$. The substrate, buffer and zero order superlattice peaks are indicated by s, b, and 0, respectively; in (a) the superlattice + 1 order peak falls under the buffer peak.

probably due to a misorientation of $\sim 1^\circ$ in the $\langle 100 \rangle$ axis of the substrate.

The equilibrium value for the in-plane lattice constant of the SLS can be calculated under the conditions of the superlattice floating free of the buffer and substrate.² This corresponds to the minimum stored energy in the superlattice, and using the above composition values we obtain an equilibrium $\epsilon^H = 0.25\%$. This in-plane strain is larger than the observed ϵ^H of 0.19% and indicates that a small, cumulative component of compressive stress is stored in the SLS. This offset is produced by the slightly lower than ideal lattice constant at the buffer surface, and arises from the residual coherency strain in the buffer and the slightly lower ($y = 0.061$ vs 0.07) than optimal As concentration in the buffer layer. We suggest that such effects may be important factors in the stability of SLS structures under the growth of thick layers or in subsequent device applications.

In summary, we have used x-ray rocking curves to measure the depth profiles of perpendicular and parallel strain in a $\text{GaAs}_x\text{P}_{1-x}/\text{GaP}$ superlattice. The technique is simple, rapid, nondestructive and unmatched in its ability to obtain strain profiles with high precision. The nonzero parallel strain in buffer and superlattice layers provides direct evidence for the hypothesis that the epitaxial structure is crystallographically decoupled from the underlying substrate. The strain decoupling occurs in a narrow region at the buffer/substrate interface. The combined values of parallel and perpendicular strains provide a detailed description of the state of elastic strain of the structure. A discussion of the degree of decoupling for different buffer layer conditions, as well as comparisons with other techniques, will be given later in a detailed report. We may conclude that the x-ray rock-

ing curve method is a powerful tool to determine the complete state of strain of strained-layer superlattices.

The work of the Caltech group was supported by the Defense Advanced Research Projects Agency (MDA 903-82-C-0348) (S. Roosild) and the work of the Sandia National Laboratories group was supported by the U.S. Department of Energy under contract number DE-AC04-76DP00789.

¹L. Esaki and L. L. Chang, *Phys. Rev. Lett.* **33**, 495 (1974).

²G. C. Osbourn, *J. Appl. Phys.* **53**, 1586 (1982).

³J. W. Matthews and A. E. Blakeslee, *J. Cryst. Growth* **32**, 265 (1976).

⁴M. D. Camras, J. M. Brown, N. Holonyak, Jr., M. A. Nixon, R. W. Karkis, M. J. Ludowise, W. T. Dietze, and C. R. Lewis, *J. Appl. Phys.* **54**, 6183 (1983).

⁵S. T. Picraux, L. R. Dawson, G. C. Osbourn, R. M. Biefeld, and W.-K. Chu, *Appl. Phys. Lett.* **43**, 1020 (1983).

⁶G. H. Olsen, M. S. Abrahams, C. J. Buicocchi, and T. J. Zamerowski, *J. Appl. Phys.* **46**, 1643 (1975).

⁷W.-K. Chu, C. K. Pan, and C.-A. Chang, *Phys. Rev. B* **28**, 4033 (1983).

⁸I. J. Fritz, L. R. Dawson, and T. E. Zipperian, *Appl. Phys. Lett.* **43**, 846 (1983).

⁹Armin Segmüller, P. Krishna, and L. Esaki, *J. Appl. Cryst.* **10**, 1 (1977).

¹⁰R. M. Fleming, D. B. McWhan, A. C. Gossard, W. Wiegmann, and R. A. Logan, *J. Appl. Phys.* **51**, 357 (1980).

¹¹V. S. Speriosu, *J. Appl. Phys.* **52**, 6094 (1981).

¹²V. S. Speriosu, and C. H. Wiltz, *J. Appl. Phys.* **54**, 3325 (1983).

¹³R. M. Biefeld, G. C. Osbourn, P. L. Gourley, and I. J. Fritz, *J. Electron. Mater.* **12**, 903 (1983).

¹⁴V. S. Speriosu, B. M. Paine, and T. Vreeland, Jr., *J. Appl. Phys.* (in press).

¹⁵J. A. Ibers and W. C. Hamilton, eds., *International Tables for X-Ray crystallography* (Kymoch, Birmingham, 1974), Vol. IV.

¹⁶J. Hornstra and W. J. Bartels, *J. Cryst. Growth* **44**, 513 (1978). Note misprint in Table I; $C_{12} = 6.253 \times 10^{11}$ dyn/cm² for GaP.

INTERFACIAL STRAIN IN $\text{Al}_x\text{Ga}_{1-x}\text{As}$ LAYERS ON GaAs

V. S. Speriosu and M-A. Nicolet
California Institute of Technology
Pasadena, California 91125

J. L. Tandon and Y. C. M. Yeh
Applied Solar Energy Corporation
City of Industry, California 91749

Abstract

Detailed analysis of x-ray rocking curves was used to determine the depth profile of strain and composition in a 2500 Å thick layer of $\text{Al}_x\text{Ga}_{1-x}\text{As}$ grown by metalorganic chemical vapor deposition on <100> GaAs. The x-value and layer thickness were in good agreement with the values expected from growth parameters. The presence of a transition region, 280 Å thick, was detected by the rocking curve. In this region, the Al concentration varies smoothly from 0 to 0.87. Measurement and control of the sharpness of such interfaces has important implications for heterojunction devices.

In epitaxially grown layers where the composition is modulated, one expects the existence of interfacial transition regions with smoothly varying composition. It is difficult to predict from first principles or growth conditions the thickness of such a region. Measurement of transition regions is also difficult. The x-ray rocking curve has been shown⁽¹⁻³⁾ to be a highly sensitive tool for measuring strains due to composition variations. More recently the technique has also been used to obtain detailed strain profiles in epitaxial structures⁽³⁻⁵⁾. In this letter, we report rocking curve measurements which demonstrate that the technique can probe transition regions with thicknesses above $\sim 50 \text{ \AA}$.

The $\text{Al}_x\text{Ga}_{1-x}\text{As}$ layers used in this study were grown by metalorganic chemical vapor deposition (MOCVD) on GaAs substrates oriented 2 to 3° off $\langle 100 \rangle$ axis. The layers were grown in a computer-controlled reactor at $\sim 730^\circ\text{C}$. The trimethylaluminum and trimethylgallium ratios to arsene were adjusted to obtain a growth rate of $\sim 550 \text{ \AA/min}$. From the growth parameters, the expected Al concentration was ~ 0.88 and the layer thicknesses $\sim 2200 \text{ \AA}$. Bragg case double-crystal x-ray rocking curves were obtained with the $\text{Fe K}_{\alpha 1}$ (400) reflection. The x-ray beam was collimated and rendered nearly monochromatic by (400) reflection in $\langle 100 \rangle$ GaAs. The incident beam divergence was below 20 arcsec . The spot size was limited to $\sim 2 \text{ mm} \times 1 \text{ mm}$. Experimental rocking curves were fitted using the method of Ref. (4). For the calculated curves, a structure factor and absorption coefficient in the epitaxial layer corresponding to 0.88 Al was used. The

strain profiles obtained are in the direction perpendicular to the surface and with respect to the GaAs substrate.

Figure 1(a) shows experimental (dashed line) and calculated (solid line) rocking curves of a representative sample. The angle $\Delta\theta$ is plotted relative to the Bragg angle of the substrate peak which has a maximum reflecting power of $\sim 50\%$. The oscillatory structure at $\Delta\theta < 0$ is due to the epitaxial layer. The calculated curve is obtained from the strain profile of Fig. 1(b). The strain $\epsilon^\perp = 0.231\%$ and the thickness $T = 2520 \text{ \AA}$ produce a reasonably good fit to the experimental curve (Fig. 1(a)). However, there remains a discrepancy between measured and calculated amplitudes of the subsidiary oscillations, especially for $-0.1 < \Delta\theta < -0.03^\circ$. This discrepancy can only be removed (Fig. 2(a)) by a strain profile which includes a transition region, as shown in Fig. 2(b). The thickness (280 \AA) of this region and its strain profile are determined by matching the experimental curve.

An increase of 140 \AA in the thickness of the transition region (Fig. 3(b)) results in a distinctly poorer fit (Fig. 3(a)). Comparison of Figs. 1 through 3 clearly demonstrates the sensitivity of the technique in detecting the transition region and also in determining its thickness. The thickness is 280 \AA to an accuracy better than 50 \AA . Although the strain is expected to vary smoothly, its profile in this region is represented by two discrete, equally spaced steps since the resolution does not permit finer detail. Due to the very low absorption of x rays in thin layers, the calculated curve is insensitive to mirror

reflections of the strain profile. Thus the transition region could be at the air-film interface. In addition, because of the small thickness of the transition region compared to that of the film, the possibility of thinner transition regions on both sides of the film with total thickness of 280 \AA cannot be ruled out. This ambiguity can be resolved by etching a few hundred \AA off the surface and remeasuring. Independently, the growth conditions suggest that there is only one transition region located at the layer/substrate interface.

From Fig. 2(b), the total thickness of the epitaxial layer is $2520 \pm 50 \text{ \AA}$. Using bulk AlAs and GaAs lattice parameters and elastic constants of GaAs⁽⁶⁾, a strain $\epsilon^{\perp} = 0.231\%$ corresponds to an Al concentration $x = 0.87$, in good agreement with the expected value (0.88). Since the strain is uniquely related to the concentration of Al, a strain profile corresponds to a profile of Al concentration. Thus the concentration of Al varies smoothly from 0 to 0.87 over a 280 \AA thick transition region at the layer/substrate interface.

In conclusion, the x-ray rocking curve technique is an excellent tool for the characterization of interfacial transition regions. For the epitaxial $\text{Al}_x\text{Ga}_{1-x}\text{As}$ layer, 2520 \AA thick, considered in this letter, the thickness of the transition region has been measured with an accuracy better than 50 \AA .

Acknowledgments

We would like to thank D. A. Smith and A. Mehta at Applied Solar Energy Corporation for their assistance in sample preparation. The work at Caltech was financially supported by the Defense Advanced Research Projects Agency [MDA903-82-C-0348], (S. Roosild).

References

⁺ Present Address: IBM, Research Laboratory, 5600 Cottle Road,
San Jose, California 95193.

1. W. J. Bartels and W. Nijman, J. Cryst. Growth, 44, 518 (1978).
2. W. J. Bartels and H. Veenliet, Inst. Phys. Conf. Ser. No. 45: Chapter 3, 229 (1979).
3. V. S. Speriosu and H. L. Glass, U.S.-France Seminar on Topography, Snowmass, Colorado (1983).
4. V. S. Speriosu, J. Appl. Phys. 52, 6094 (1981).
5. V. S. Speriosu and C. H. Wilts, J. Appl. Phys. 54, 3325 (1983).
6. J. Hornstra and W. J. Bartels, J. Cryst. Growth, 44, 513 (1978).

Figure Captions

Figure 1 (a) Measured (dashed line) and calculated (solid line) $\text{Fe K}_{\alpha 1}$ (400) x-ray rocking curves of a $\text{Al}_x\text{Ga}_{1-x}\text{As/GaAs}$ sample. The calculated curve corresponds to the flat strain profile shown in (b).

Figure 2 (a) Measured (dashed line) and calculated (solid line) $\text{Fe K}_{\alpha 1}$ (400) x-ray rocking curves of the same sample as in Fig. 1. The calculated curve in this case includes a 280 \AA thick transition region with strain profile as shown in (b).

Figure 3 (a) Measured (dashed line) and calculated (solid line) $\text{Fe K}_{\alpha 1}$ (400) x-ray rocking curves of the same sample as in Fig. 1. The calculated curve corresponds to the strain profile in (b) with a 420 \AA transition region.

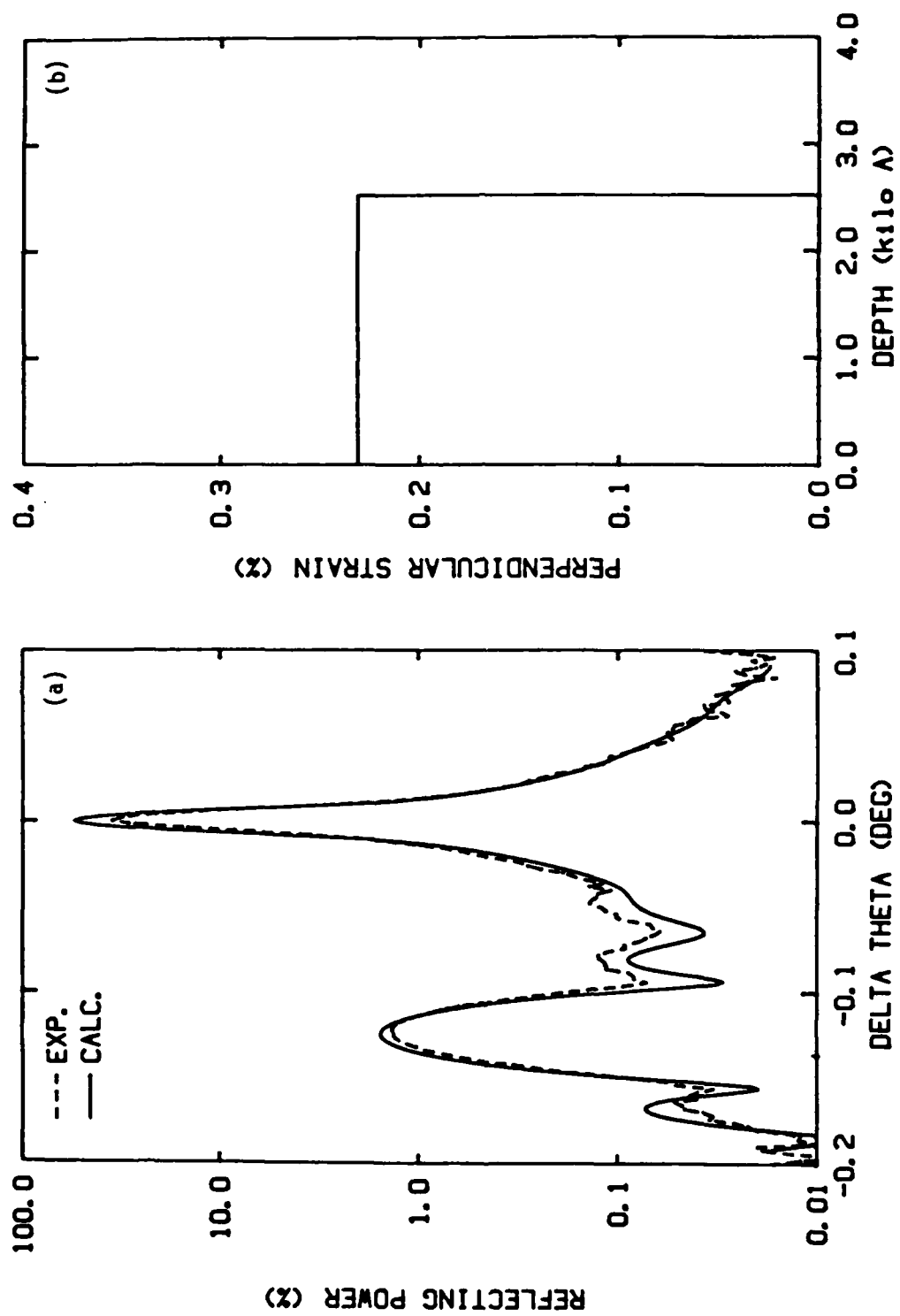


Fig. 1

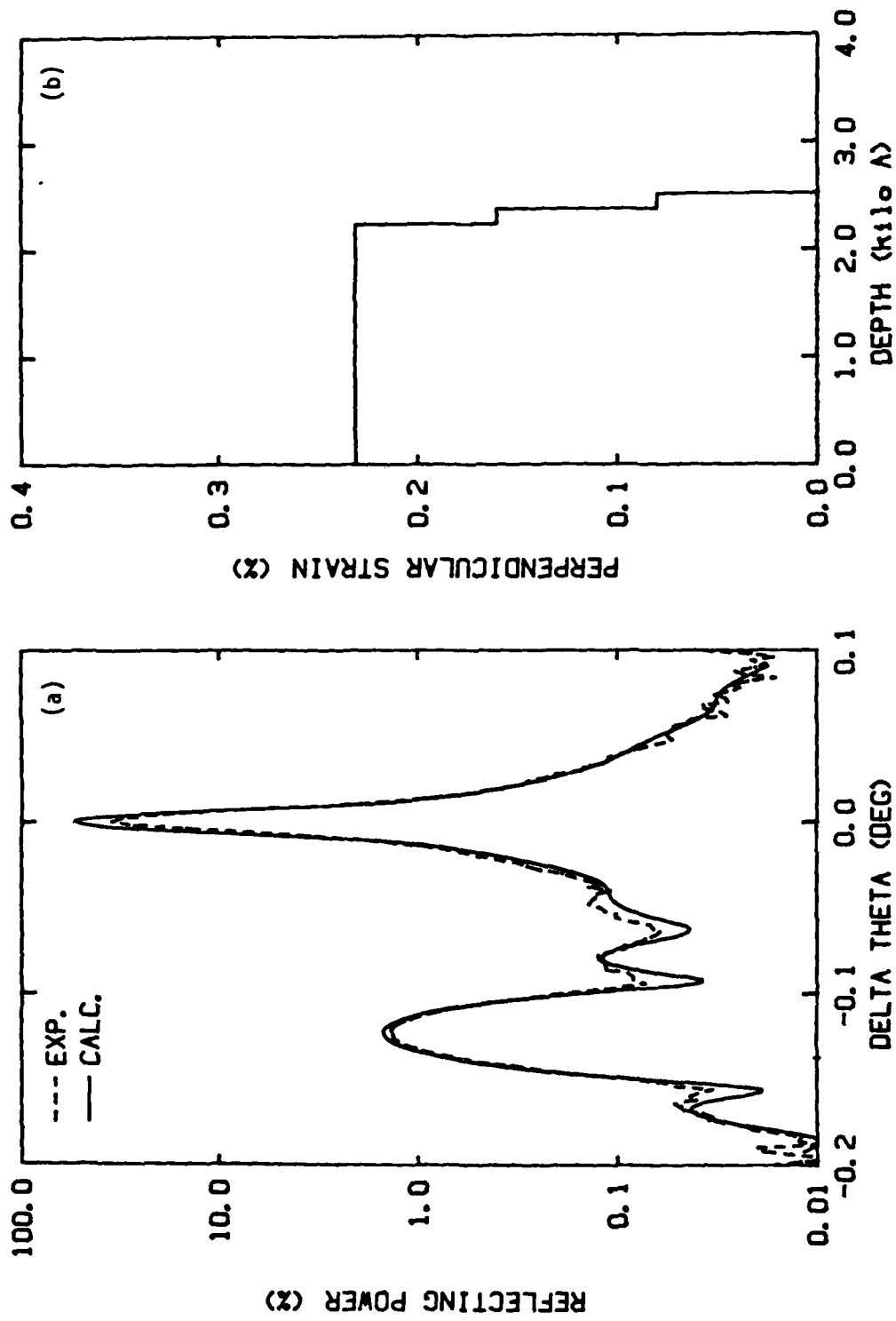


Fig.2

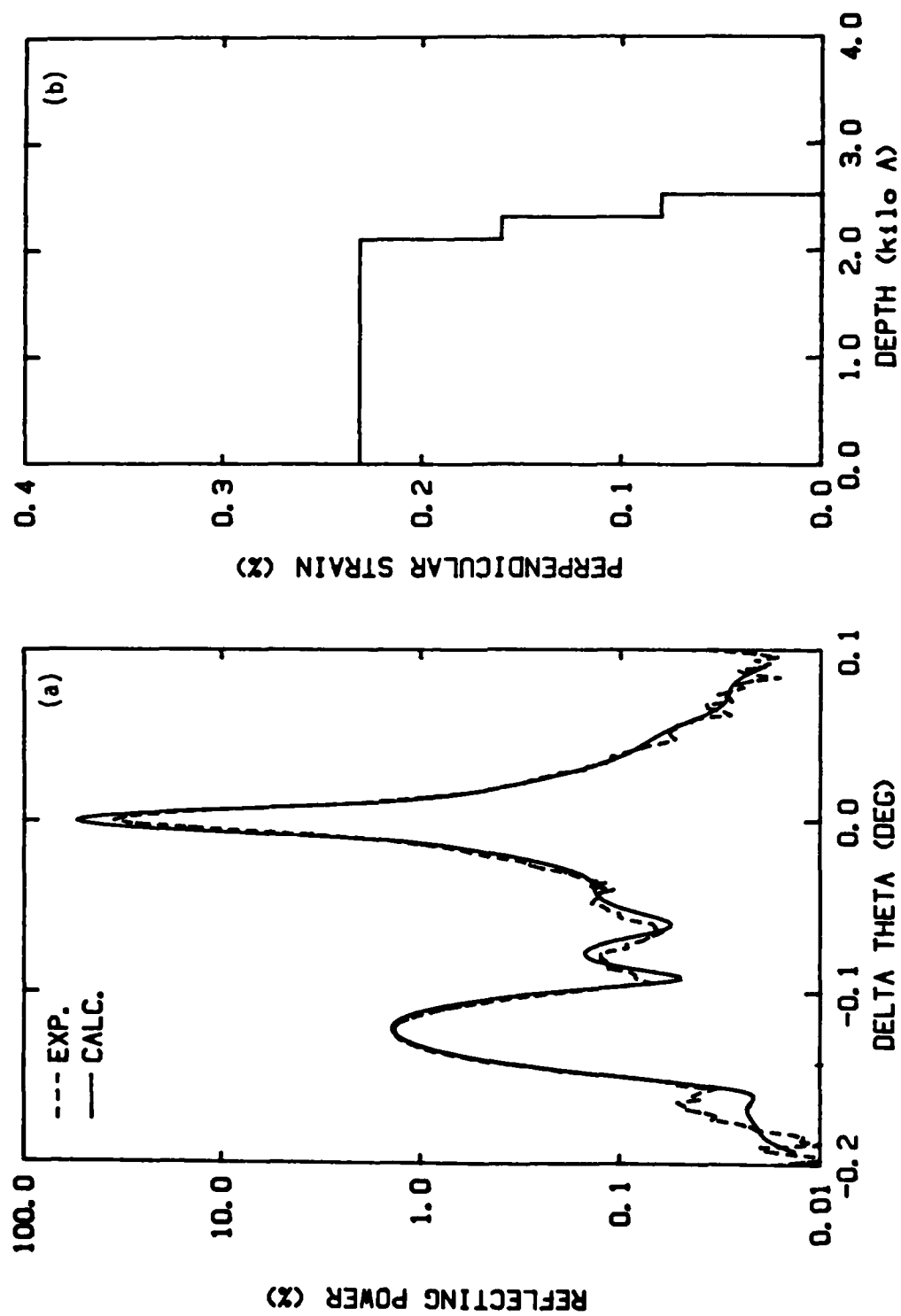


Fig.3

ANALYSES OF METALORGANIC CHEMICAL VAPOR DEPOSITION-GROWN

$\text{Al}_x\text{Ga}_{1-x}\text{As}/\text{GaAs}$ STRAINED SUPERLATTICE STRUCTURES BY
BACKSCATTERING SPECTROMETRY AND X-RAY ROCKING CURVES

A. H. Hamdi, V. S. Speriosu^{a)}, and M-A. Nicolet
California Institute of Technology
Pasadena, California 91125

J. L. Tandon and Y. C. M. Yeh
Applied Solar Energy Corporation
City of Industry, California 91749

ABSTRACT

Backscattering spectrometry with channeling and x-ray rocking curves have been employed to analyze metalorganic chemical vapor deposition-grown $\text{Al}_x\text{Ga}_{1-x}\text{As}/\text{GaAs}$ strained superlattice structures in significant detail. Both techniques complement each other in the precise determination of composition, thickness and strain in the individual layers of the superlattices. In addition, the sensitivity of the two techniques allows quantitative measurements of transition regions at the interfaces of various layers. Such fine probing into thin layered superlattice structures provides essential feedback in controlling their growth.

PACS numbers: 68.55 + b, 61.10, 81.15. Gh, 72.80.Ey

In the past decade, strained thin layer $\text{Al}_x\text{Ga}_{1-x}\text{As}/\text{GaAs}$ superlattice (SLS) structures have received considerable attention because of their unique electrical and optical properties⁽¹⁾. Modern developments in Molecular Beam Epitaxy (MBE) and Metalorganic Chemical Vapor Deposition (MOCVD) have made the growth of these structures possible with a claimed individual layer thickness of as low as $\sim 60 \text{ \AA}$ ⁽²⁾. However, to control the growth of these structures, accurate quantitative measurements of their composition, thickness and uniformity are mandatory. Analytical techniques that have been used mainly to characterize SLS structures, e.g. Auger Electron Spectroscopy (AES), Secondary Ion Mass Spectrometry (SIMS), Transmission Electron Microscopy (TEM), are all destructive and have not been able to provide precise details sufficiently. In addition, AES and SIMS require standards for absolute determination of composition and have limited depth resolution.

In this letter, Backscattering Spectrometry (BS) with channeling and x-ray rocking curves have been employed to analyze MOCVD grown $\text{Al}_x\text{Ga}_{1-x}\text{As}/\text{GaAs}$ SLS structures. The two techniques are essentially non-destructive, self-calibrating, and together provide the precise determination of composition, strain, thickness, crystal quality and uniformity of the SLS structure.

The $\text{Al}_x\text{Ga}_{1-x}\text{As}/\text{GaAs}$ SLS structures used in this study were grown in a computer-controlled large-capacity MOCVD reactor. The reactor is production-compatible with a handling capacity of 90, 2 cm x 4 cm wafers at a time. Two sets of SLS structures were grown on semi-insulating GaAs wafers oriented $\sim 2^\circ$ off $\langle 100 \rangle$

axis. Individual layers of $\text{Al}_x\text{Ga}_{1-x}\text{As}$ and GaAs were grown at $\sim 730^\circ\text{C}$ by switching on and off the Al source (trimethyl-aluminum) and modulating the mole fraction of the Ga source (trimethyl-gallium). Table I gives the time cycles involved in the growth of one period of the two SLS structures, along with the expected thicknesses calculated from growth rates determined from measurements made on thicker ($\sim 2000 \text{ \AA}$) layers. These two SLS sets represent typical samples expected to be grown in a real production-type large-scale MOCVD reactor with a reasonable growth rate ($\sim 7.5 \text{ \AA/sec}$).

BS measurements were made by a 2 MeV $^4\text{He}^+$ beam tilted at an angle of 80° with respect to the sample's surface normal, to obtain high depth resolution⁽³⁾. Channeling was carried out along $\langle 100 \rangle$ axis. Bragg case, double-crystal, x-ray rocking curves were obtained with the Fe $K_{\alpha 1}$ (200) reflection. The x-ray beam was collimated and rendered nearly monochromatic by (400) reflection in $\langle 100 \rangle$ GaAs. Experimental rocking curves were fitted using a kinematical model of x-ray diffraction in thin epitaxial layers⁽⁴⁾.

Backscattering and channeling spectra obtained from SLS1 (see Table I) and virgin GaAs samples are shown in Fig. 1. The oscillatory behavior in the random spectrum is due to modulation in the Ga concentration in the alternating layers of $\text{Al}_x\text{Ga}_{1-x}\text{As}$ and GaAs. The spectrum resolves only the first four periods of the sample. A 80° tilt angle was used for this measurement to enhance the depth resolution near the surface. Also, resolving deep layers becomes difficult due to the interfering signals from

Al. Compared with the random spectrum from the virgin GaAs sample, the random spectrum from the SLS1 sample has a lower yield. This implies that in the growth of the SLS1 structure, pure GaAs layers were not achieved (the energy resolution of the measurement system used in 5 channels, which is enough to resolve at least the first GaAs peak in the SLS1 spectrum). Corresponding measurements carried out at a 45° tilted angle, where the analyzing beam probed to a greater depth into the samples, showed that both the virgin and the SLS1 samples had identical substrate yields. It is also interesting to observe a nonsymmetry in the signals of the individual periods. This reflects the existence of uneven composition transition regions at the two interfaces in a period of SLS1 structure. However, excellent crystalline quality of the SLS1 sample was verified by channeling along the $\langle 100 \rangle$ direction. The measured minimum yield of $\sim 5\%$ is comparable to that of the virgin GaAs sample.

The measured (dashed line) and calculated (solid line) x-ray rocking curves obtained from the SLS1 sample are shown in Fig. 2. The angle $\Delta\theta$ is plotted relative to the Bragg angle of the substrate peak. The reflecting power is normalized with respect to the intensity of the incoming x-ray beam. Several peaks in the rocking curves are observed which are due to the periodicity in the sample. The substrate peak is at $\Delta\theta = 0$. The major peak P_0 (which overlaps with the substrate peak in this case) measures the average strain in the SLS structure. The magnitude of the average strain was determined using Fe $K_{\alpha 1}$ (400) reflection in another measurement where P_0 could well be separated from the

substrate peak. The separation between the subsidiary peaks (P_1 , P_{-1} , etc.) in Fig. 2 corresponds to the average period thickness of the SLS structure. Details of the interpretation of the rocking curves for SLS structures are given in Ref. (5). The calculated curve was fitted to the experimental curve using a kinematical model of x-ray diffraction in thin epitaxial layers⁽⁴⁾. In the fitting, normal absorption coefficient and structure factor values were calculated from the tabulated atomic scattering factors⁽⁶⁾. Best fitting was accomplished by incorporating nonsymmetric transition regions at the two interfaces of the one period in the SLS structure, without feedback from the BS data. The strain distribution as a function of thickness in one period of SLS structure which provided the best fit to the experimental curve is given in Fig. 3. Since a one-to-one correlation exists between strain and Al concentration in $\text{Al}_x\text{Ga}_{1-x}\text{As}/\text{GaAs}$ structures⁽⁷⁾, an analysis of the rocking curve quantitatively determines the variation of Al concentration in the period. The result of this calculation is also reported in Fig. 3 (right-hand scale), and confirms the BS observations that Al undergoes uneven composition transition within one period. The sensitivity of the fitted rocking curve is such that the mismatch between the higher order peaks in the measured and the calculated curves in Fig. 2 suggests a nonuniformity in the thickness of the various periods of $< 50 \text{ \AA}$.

The skewed strain (Al concentration) distribution determined by x-ray rocking curves in the period of SLS1 sample is compared with expected sharp distribution in Fig. 3. The average measured

thickness of the period is $410 \pm 15 \text{ \AA}^{(8)}$ when compared with expected thickness of 120 \AA . The steps in the strain distribution are only suggestive of the true strain curve which one should expect to be continuous, as shown in Fig. 3 by the dotted curve. Qualitative features of this continuous strain (composition) curve are also evident from the BS measurements (see Fig. 1).

The skewed strain curve provides insight into the growth of $\text{Al}_x\text{Ga}_{1-x}\text{As}$ and GaAs layers within the period of the SLS1 sample. The relatively sharp rise during the growth of the $\text{Al}_x\text{Ga}_{1-x}\text{As}$ layer is explained by a rapid injection of Al and Ga source gases into the reactor (see Table I). On the other hand, upon shutting off the gas supply, the residual gases in the reactor must be pumped out, which is slow and accounts for the extended tail in the Al composition and the strain curve. The non-zero strain beyond the tail suggests again that the growth of the pure GaAs layer was not achieved, as indicated by BS measurements (Fig. 1). Measurements conducted on the SLS2 samples (see Table I) revealed similar skewness in the strain (composition) distribution, confirming that the thickness of the transition regions were related to the reactor growth parameters.

In conclusion, the combined use of BS with channeling and x-ray rocking curves has provided detailed information about the depth distribution of composition, thickness, strain, crystal quality, and uniformity of $\text{Al}_x\text{Ga}_{1-x}\text{As/GaAs}$ SLS structures. Precise information such obtained proves useful in giving feedback in the controlled growth of these structures.

ACKNOWLEDGMENTS

We would like to thank D. A. Smith, A. Mehta, and J. Wendt at Applied Solar Energy Corporation for their assistance in the preparation of samples. A. H. Hamdi extends his thanks to IBM for a research fellowship.

REFERENCES

1. G. A. Rozgonyi, P. M. Petroff, and M. B. Panish, J. Crystal Growth, 27, 106 (1974).
2. R. D. Dupuis, P. D. Dapkus, C. M. Garner, C. Y. Su, and W. E. Spicer, Appl. Phys. Lett. 34, 335 (1979).
3. W. K. Chu, J. W. Mayer, and M-A. Nicolet, Backscattering Spectrometry, (Academic Press, New York, 1979).
4. V. S. Speriosu, J. Appl. Phys. 52 , 6094 (1981).
5. V. S. Speriosu and T. Vreeland, Jr., (to be published in J. Appl. Phys.).
6. J. A. Ibers and W. C. Hamilton, eds., International Tables for X-Ray Crystals, Vol. 4, (Kymoch Press, Birmingham, 1974).
7. M. C. Rowland and D. A. Smith, J. Cryst. Growth, 33, 143 (1977).
8. Thickness measurements by BS technique are in excellent agreement with the x-ray rocking curve measurements.

TABLE I. Growth Parameters for SLS1 and SLS2 Samples.

| | Time Schedule for Growth of One Period (sec) | | | Expected Period Thick- ness (Å) |
|----------------------|--|------------------------|--|---|
| | TMA ON (MF=2.06x10 ⁻⁴) TMG ON (MF=1.44x10 ⁻⁵) | TMA OFF TMG OFF | TMA OFF TMG ON (MF=1.15x10 ⁻⁴) | |
| SLS1 (10 Periods) | 7 | 20 | 9 | 120 |
| SLS2 (15 Periods) | 24 | 20 | 30 | 400 |

REMARKS: MF = Mole fraction
TMA = Trimethyl-aluminum
TMG = Trimethyl-gallium

FIGURE CAPTIONS

Figure 1 Random (80° tilted) and $\langle 100 \rangle$ channeled Backscattering spectra obtained from SLS1 and virgin GaAs samples. The lower yield of the random SLS1 spectrum, when compared with the random virgin GaAs spectrum, implies that pure GaAs layers were not achieved during the growth of the SLS1 structure.

Figure 2 Measured (dashed line) and calculated (solid line) x-ray rocking curves obtained from the SLS1 sample with $\text{Fe K}_{\alpha 1}$ (200) reflection.

Figure 3 Depth distributions of perpendicular strain and Al concentration in one period of the SLS1 sample. The expected distribution was estimated from growth rates determined by ' α -step'-stylus type measurements performed on $\sim 2000 \text{ \AA}$ thick layers. See text for the explanation of measured and real distributions.

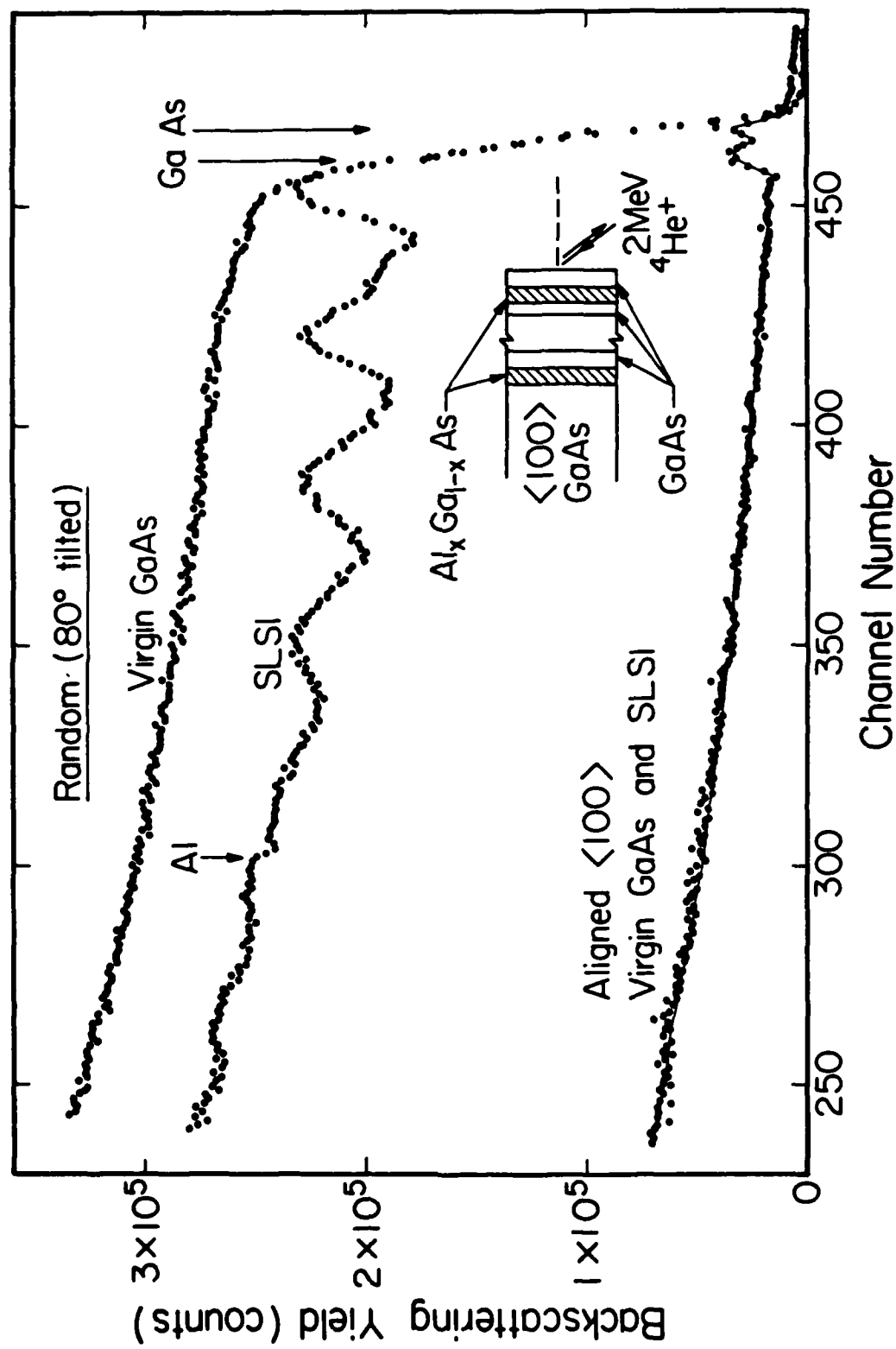


Fig.1

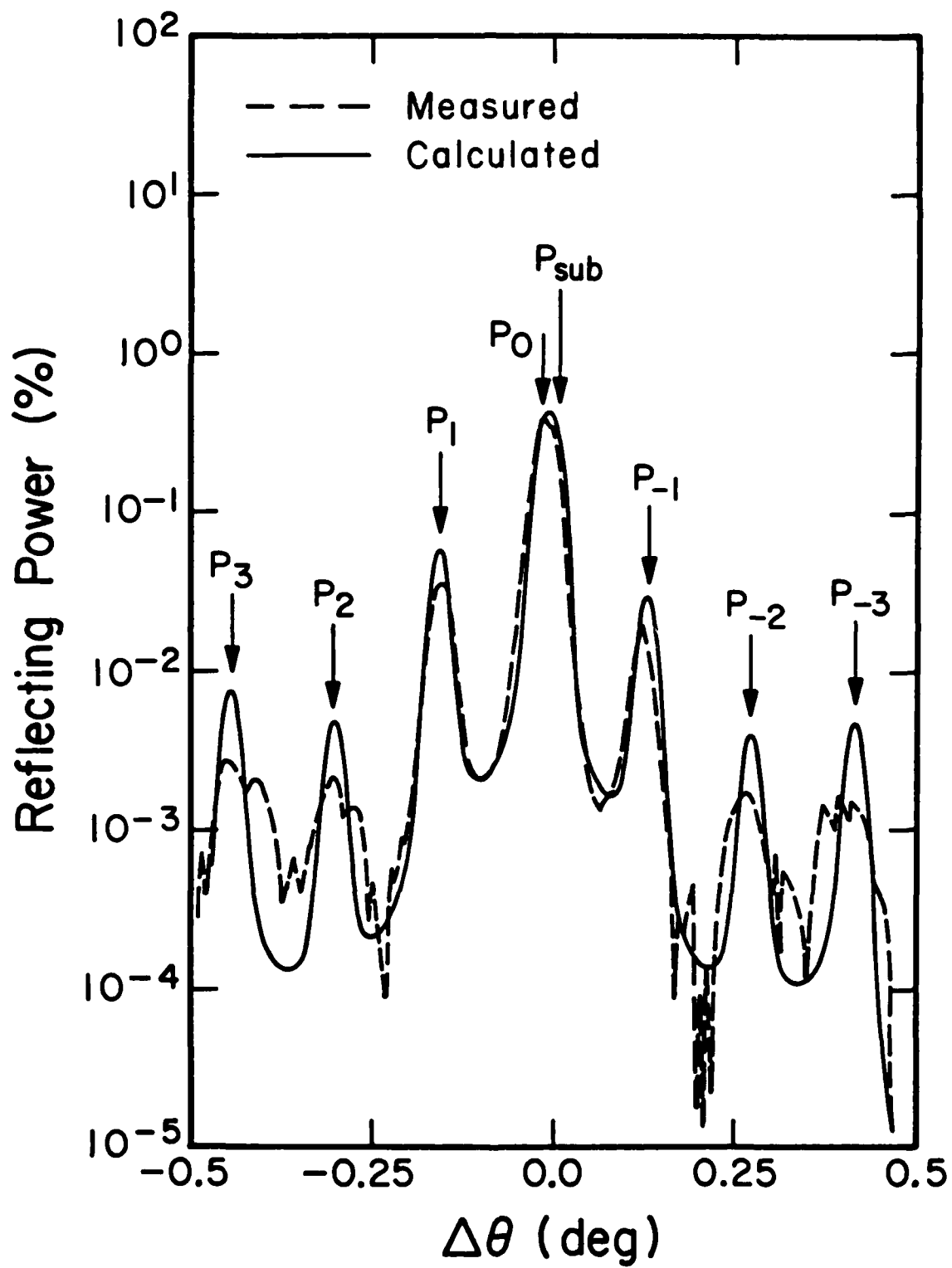


Fig.2

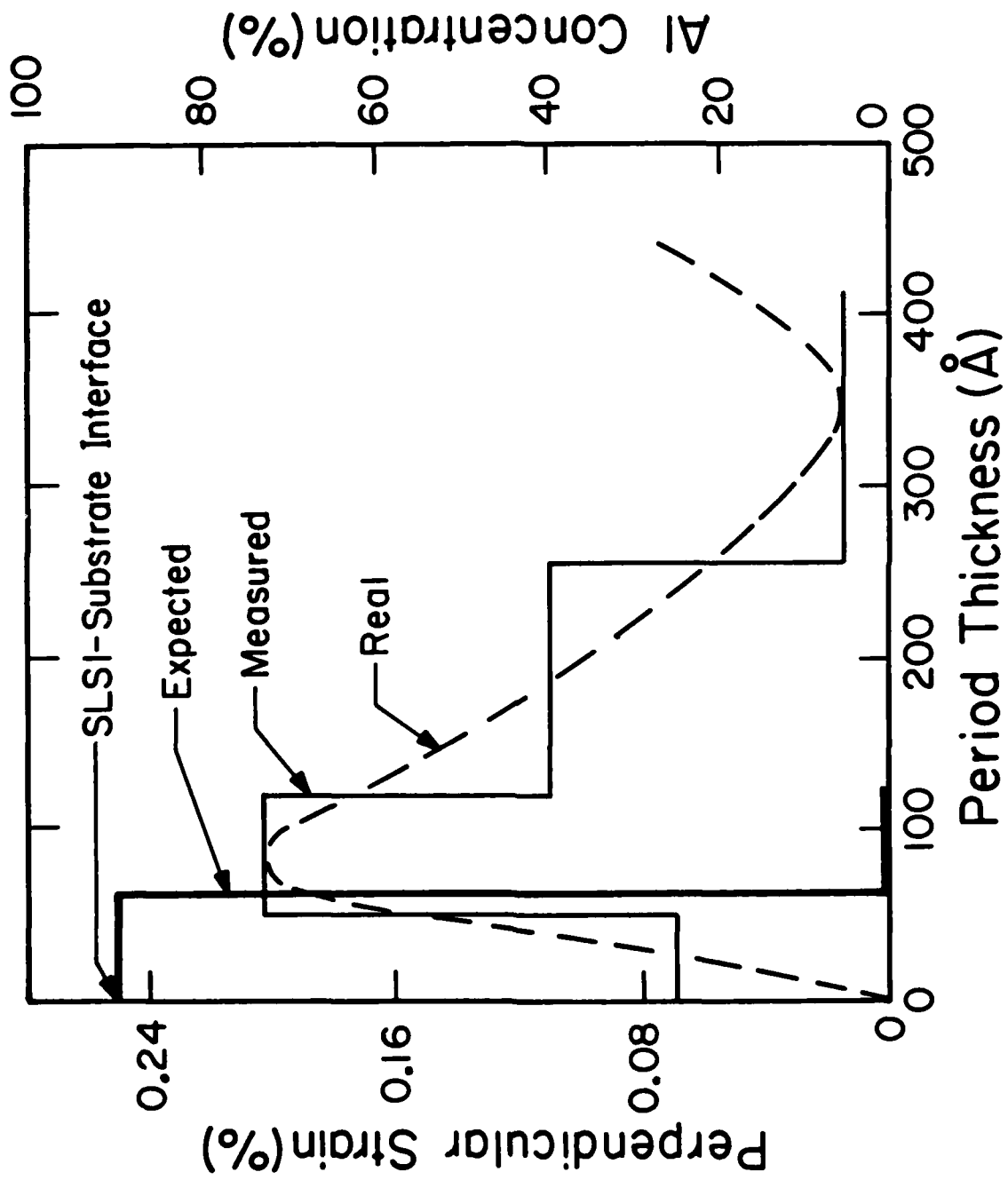


Fig. 3

Submitted to Phy. Rev. (B) 6/84

A STRUCTURE STUDY OF GaSb/AlSb STRAINED LAYER SUPERLATTICE

C. K. Pan,* D. C. Zheng,** T. G. Finstad and W. K. Chu
Department of Physics and Astronomy
The University of North Carolina
Chapel Hill, North Carolina 27514

V. S. Speriosu and M.-A. Nicolet
California Institute of Technology
Pasadena, California 91125

J. H. Barrett
Solid State Division
Oak Ridge National Laboratory
Oak Ridge, Tennessee 37830

ABSTRACT

Due to the lattice mismatch between GaSb and AlSb, a superlattice consisting of alternating layers of these materials will be strained. We have carried out ion channeling measurements by backscattering of 1.76 MeV He ions and present an experimental procedure and data analysis technique to measure the difference in strain between the two individual layers of the superlattice. A computer simulation of channeling in the superlattice has been made. The results are in excellent agreement with the channeling measurement. X-ray rocking curve analysis yields detailed profiles of strains in directions perpendicular and parallel to the surface. The X-ray value for the strain present at an unirradiated spot on the crystal is in excellent agreement with the value calculated by elasticity theory. In the bombarded region the values of strain are less than the value calculated by elasticity theory. It appears that bombardment by the He ions reduced the strain by 50% and created lateral inhomogeneities in the crystal structure.

*Permanent address: Jiangxi Engineering College, Jiangxi, China.
**Permanent address: Jiangxi Education College, Jiangxi, China.

I. INTRODUCTION

Superlattices fabricated by epitaxial growth of alternating layers of two different semiconductors constitute a group of materials with unique electrical and optical properties. The introduction of lattice mismatched superlattices¹ has broadened this group of materials. Under certain circumstances the lattice mismatch in these systems will be accommodated by an approximately uniform strain.¹⁻³ This makes it possible to use a larger variety of semiconductor materials in the alternating layers. Besides, the strain in each individual layer can be used to modify the intrinsic physical properties and the structures are also of interest for zone folding experiments. It is well known that there exists some maximum thickness of a lattice mismatched epitaxial overlayer above which dislocations develop and the strain is less than for thinner layers. In equilibrium this can be predicted; however, it is not yet clear where these limits will be for the different specific growth conditions used to fabricate various superlattices. Further it is not clear how stable these structures will be. For these reasons strain measurements on superlattices are an important task in the characterization of these materials.

Ion beam channeling and X-ray diffraction have proven to be valuable tools for characterizing strained layer superlattices. X-ray diffraction has provided detailed depth profiles of perpendicular strain in AlAs/GaAs superlattices.^{4,5} The first investigation of strained superlattices with the backscattering channeling method was carried out on a GaSb/InAs superlattice structure.^{6,7} Recently various different methods for the characterization and measurement of the strain in superlattices have been developed.⁸⁻¹¹

We have previously reported upon the channeling measurement of strain in a GaSb/AlSb superlattice.⁸ The measurement was based upon the fact that for a

superlattice grown along the [100] direction the "angle for best channeling" along the [110] direction will be different for the individual layers in the superlattice. The angle difference for best channeling of first and second layer was measured to be $0.17 \pm 0.03^\circ$. If the lattice mismatch is completely accommodated by strain in the layers, one can calculate the magnitude of the angle between [110] axes of two layers from elastic constants and lattice parameters of the individual layers. We named that a "kink angle".

In this paper, we will elaborate on the channeling measurements briefly reported earlier,⁸ and also include X-ray rocking curve analysis and computer simulations of the same GaSb/AlSb superlattice sample. A comparison between the results and an evaluation of the methods used will be given.

II. EXPERIMENTAL PROCEDURES

In this section we will describe the sample preparation, details of the ion channeling measurements and details of the X-ray measurements.

The layered structure of the sample used in this investigation is given in Fig. 1. The sample was a GaSb/AlSb (30 nm/30 nm) periodic structure with a total of 10 periods. The films were grown by Molecular-Beam Epitaxy. A 2 μ m thick GaSb buffer layer was first grown on a GaSb [100] substrate to smooth the surface. Details of the growth procedure have been given elsewhere.¹²

Figure 2 shows a schematic model of a strained-layer superlattice. The GaSb layer is unstrained due to its conformity with the substrate. When layers with different lattice constants are grown on top of each other and the interface atoms are in registry with each other, the lattice constant perpendicular to the growth direction will be different for the two layers. When the growth direction is along the [100] direction, this will cause the [110] crystallographic direction to be different for the two layers. A "kink angle" is developed.

Ion backscattering and channeling is well described by several authors.^{13,14} In this investigation, backscattering of 1.76 MeV $^4\text{He}^+$ ions with a scattering angle of 162° was used. Figure 3 shows schematically the situation when the sample is aligned so that the beam is along the $[110]$ direction. As shown in the figure, the $[110]$ axis is kinked at each interface of the superlattice. The channeling measurements in this work consist of collecting backscattering spectra for several incident directions separated by small angles all lying in a plane containing the $[110]$ axis.

For aligning the crystal with one of the $\langle 110 \rangle$ axes we use a two axis goniometer with a rotational axis designated ϕ and tilt angle designated θ . The axis of rotation is perpendicular to the surface and the tilt axis is in the surface plane and perpendicular to the beam direction. Figure 4 shows part of a polar diagram of crystallographic axes and planes in a coordinate system tied to the experimentally recorded tilt and rotation angles.

The major crystallographic planes shown in Fig. 4 are first found from monitoring "dips" in the backscattering intensity when the sample is rotated and the surface normal is tilted several degrees away from the beam direction. The minima found in this way are then plotted in a polar diagram where the coordinate system is defined by the tilt angle θ and the rotation angle ϕ . A $\langle 100 \rangle$ axis is then found by setting the goniometer to the intersection of lines through these points followed by a fine tuning. Then a $\langle 110 \rangle$ axis is found by "bobsleighing" along a $\{100\}$ plane until the minimum is found close to a $\langle 110 \rangle$ direction. This corresponds to the minimum scattering intensity averaged over several superlattice periods. The actual angular scan is then performed by varying both θ and ϕ for each step in the scan so that the angular scan plane does not coincide with any major crystallographic planes. The chosen scan direction in our experiments made an angle of 14° to a $\{100\}$

plane. The exact angle in the crystal between the $\langle 100 \rangle$ and $\langle 110 \rangle$ directions cannot be precisely determined in our measurements since small inaccuracies in the experimental setup could influence this. However, the precision in measuring small differences between angles is very good ($\pm 0.02^\circ$). Details on the channeling data reduction procedures will be given in section IV.

The same samples used in the channeling measurements were also characterized by x-ray rocking curve analysis. Details about experimental procedure to characterize the depth distribution of strain in strained layer superlattices have previously been described.^{4,5,15-17} In this investigation a double crystal diffractometer with $\text{Fe}(\text{K}\alpha_1)$ radiation was used. A $[100]$ GaAs crystal was used as the first crystal with (400) reflections for both sample and first crystal. The experimental data are analyzed by comparison with computer calculated reflection intensities.¹⁵ The computer program assumes a certain strain distribution with depth and scattered x-ray intensities are modeled by kinematical theory which is a good approximation under the present circumstances. A detailed discussion of x-ray analysis of superlattices and additional information on measurements of the present samples is given elsewhere.¹⁸

III. STRAIN CALCULATIONS

In this section we present the values for the expected lattice constant in the superlattice structure under study and also the expected values for the angle between the $[110]$ directions of each of the layers in the superlattice based on elasticity theory of layered structures.

GaSb and AlSb which contribute the individual layers in the superlattice both have the Zinc blende crystal structure and their lattice constants are only slightly different from each other. In Fig. 2, a_1 and a_2 are the bulk

lattice constants for GaSb and AlSb respectively. a_2 is slightly larger than a_1 . The lattice mismatch f defined by

$$f = \frac{2(a_2 - a_1)}{(a_2 + a_1)} \quad (1)$$

is 0.65%.

When a thin layer is grown on the substrate, atoms will register at the atoms of the substrate. The lattice constant a_{\parallel} in the growth plane (Fig. 2) will then conform to that of the substrate. As the substrate is much thicker than the layers in the superlattice, the changes in the lattice constant of the substrate will be insignificant. Thus, the AlSb layers in the superlattice will register with a parallel lattice constant close to that of the bulk (i.e. $a_{\parallel} = a_1$). The lattice constant perpendicular to the plane a_{\perp} can be calculated from the Poisson Effect.

$$\begin{aligned} a_{\perp}^{(1)} - a_1 &= -2 \left(\frac{C_{12}}{C_{11}} \right)_{\text{GaSb}} (a_{\parallel} - a_1) \\ a_{\perp}^{(2)} - a_2 &= -2 \left(\frac{C_{12}}{C_{11}} \right)_{\text{AlSb}} (a_{\parallel} - a_2) \end{aligned} \quad (2)$$

where, $a_{\perp}^{(1)}$ and $a_{\perp}^{(2)}$ are the lattice constants perpendicular to the plane for GaSb and AlSb respectively. C_{11} and C_{12} are the elastic stiffnesses corresponding to stress along the growth direction and to a direction in the growth plane respectively.

In our case, the GaSb layer can be practically unstrained since a_{\parallel} is very close to a_1 .

The [110] axis of the strained layers are changed while no change occurs in the unstrained layers with respect to the [110] axis of the substrate. The

angle $\Delta\theta$ between the $[110]$ axis of the two different layers can be calculated from

$$\Delta\theta = \theta_2 - \theta_1 = \arctan \frac{a_1^{(2)}}{a_1} - \arctan \frac{a_1^{(1)}}{a_1} \quad (3)$$

$\Delta\theta$ is the "kink angle" which is a way to express the strain of the system, and θ_2 and θ_1 are defined in Fig. 2.

A tabulation of calculated values of the "kink angles" for the superlattice under study is shown in Table 1, for two different values of the lattice constant of GaSb cited in the literature. We expect the lattice parameter of Ref. 19 to be a more accurate one which is in agreement with the published value of the National Bureau of Standards (NBS). A similar calculation assuming that both layers of the superlattice are strained, as would have been the case if the growth had started out with an infinitesimally thin substrate or with a buffer layer decoupling the superlattice layer from the substrate completely, do not make any significant difference in the value of the calculated "kink" angle $\Delta\theta$. Experimental measurement of the "kink angle" is given in the next section.

IV. CHANNELING MEASUREMENTS

Fig. 5 shows some typical experimental backscattering spectra from the GaSb/AlSb superlattice. The oscillations seen in the scattering yield in the spectra are due to the variation in composition with depth. The spectrum labelled "[100] Aligned" was obtained with the analysis beam incident along the $[100]$ direction of the superlattice. The one labelled "[110] Aligned" was obtained by the analysis beam incident along with the average $[110]$ direction of the superlattice layers. They indicate that the dechanneling is higher

along the [110] direction than the [100] direction as is normally observed in strained layer superlattices.⁸⁻¹⁰ The spectrum labelled "Random" was obtained with the incident beam direction making an angle of 3° with the [110] axis and 10° {110} plane. For the measurements of the "kink angle" we collected a large number of individual spectra all with the beam direction laying in a plane that makes an angle of 14° with a {100} plane as indicated in Fig. 4. The angular difference between the analysis direction for consecutive spectra was 0.05° or 0.1°. Figure 5 shows three out of a total of fifty two of these spectra. Since the energy scale in Figure 5 can be converted to a depth scale, the above mentioned data set allow us to plot the yield at different depths as function of tilt angle from the [110] axis of the first layer. In Fig. 5, the energy intervals corresponding to the individual GaSb (layer 1,3,5) and AlSb (layer 2,4,6) have been indicated for the Sb part of the spectrum (1.4-1.6) MeV and for the superimposed contribution from Ga and Sb (below 1.4 MeV). The energy positions for each individual layer has been assumed to be identical for a random direction and an aligned direction, neglecting differences in stopping cross section and energy straggling for the random and aligned cases. For the purpose of converting the energy scale to a depth scale this is a reasonable approximation.

Figure 6 shows angular yield curves extracted from experimental measurements, such as Fig. 5, at four different depths. The yields have been normalized to the random yield. From each of these curves we find an angular position termed the direction or angle for "best channeling" for a given depth. It is defined as the midposition between the intercept of half heights of the left and right hand portion of the angular yield curve respectively. This parameter serves to quantify the observed effect.⁸ It is interesting to note that the direction for "best channeling" shifts back and forth from layer

to layer in the superlattice. We attribute the observed periodic changes in the angular yield curves to the periodic changes of the [110] direction in the superlattice structure.

Figure 7 shows the angular position of the best channeling direction as a function of depth. The depth corresponding to the individual layers are also indicated in the figure. The error bars are typical for all the datapoints. Datapoints of layers deeper than the fourth layer are somewhat doubtful since they have been extracted from portions of the spectrum where the Ga signal from one depth overlaps the Sb signal from another depth. One can see from Fig. 7 that the damping of the oscillations is quite clear. We attribute this to the fact that the channeling behavior of ions in a given layer will always be influenced by the previous history of the ion trajectory. After passing through many layers, the flux distributions become more uniform and the direction for best channeling will tend to be a direction between the two different [110] directions for the two layers. The observed differences between the best channeling direction for the first two layers is $0.17^\circ \pm 0.03^\circ$. These findings will be compared with the computer simulation and the x-ray rocking curve measurements.

V. COMPUTER SIMULATIONS

Computer simulations by Monte Carlo method of the channeling of ions in the crystal can be used to infer more precise information from measurements. A description of such computer simulation has been given previously^{2,21} and applied to the analysis of experiments on superlattices of InAs/GaSb.^{6,7} Only one modification has been added to that program for the present purposes; this modification is for the purpose of keeping separate records of ion encounters with the group III and group V atoms in each layer. This feature turns out to

be important in reproducing the correct shapes for the shoulders in angular scans such as observed in Fig. 6.

Fig. 8 shows the contour diagram of a Monte Carlo simulation run on GaSb/AlSb. The contour levels over the depth--incident angle plane are of scattering probabilities. The "kink angle" for Fig. 8 was chosen to be 0.37° for the simulation. It is quite evident that the contours of Fig. 8 is asymmetric with respect to the angle of incidence. Fig. 9 shows the contour diagram of a simulation assuming zero "kink angle". It is seen that the major asymmetry due to "kink angle" is not apparent. Minor asymmetry due to ions incident close to group III vs group V can be seen. The simulation scanning profiles shown in Fig. 10 were extracted from the data of the contour diagram at different depths given in Fig. 8. One can see that the angle for best channeling as previously defined oscillates with depth is in good agreement with our experiments (see Fig. 7). We have varied the "kink angle" for different simulation runs but kept all other parameters constant. Fig. 11 shows the angle difference $\Delta\psi$ between the "direction for best channeling" of the first and second superlattice layer as a function of assumed "kink angles" $\Delta\theta$. It is noted that the angle difference between first and second layer is always somewhat smaller than the assumed "kink angle". One can use Fig. 11 to extract the "kink angle" from the channeling measurements. The experimental measured value for $\Delta\psi$ was 0.17 degree. From Fig. 11 this corresponds to a "kink angle" of 0.27 ± 0.03 degree. The actual shape of the shoulders in the simulation scanning profiles (Fig. 10) closely resemble the experimental ones (Fig. 6). However, the width of the angular scan profiles are somewhat broader than the actual experimental ones. This might be due to neglecting surface oxides or beam divergence or improper values of thermal vibration in the simulation. The main difference between the simulated and experimental scan profiles are the flatter bottom of the former. This is typical of computer simulated scan properties.

VI. X-RAY ROCKING CURVE MEASUREMENTS

The X-ray measurements were performed on the same sample as the channeling measurements. A large difference in structure was found between data taken on the RBS spot, i.e. the spot bombarded by the He beam during the channeling measurements, and data taken a few mm away. Figure 12 shows the experimental (dashed) and calculated (solid) Fe $K_{\alpha 1}$ (400) rocking curves for an unirradiated spot away from where the channeling measurements were taken. Since there is no phase detection, a direct inversion of an experimental rocking curve into a strain profile is not possible. Instead a strain versus depth profile is first assumed and a computer program then calculates the expected X-ray intensity variations. When a good fit is obtained, it is assumed that the correct strain profile has been found. It should be mentioned that the calculations are very sensitive to small differences in assumed strain profiles (~1%). The strain is defined here with respect to the lattice constant a_1 of the substrate

$$\begin{aligned}
 \text{parallel strains} \quad \epsilon_1^{(1)} &= \frac{a_1^{(1)} - a_1}{a_1} \\
 \epsilon_1^{(2)} &= \frac{a_1^{(2)} - a_1}{a_1} \\
 \text{perpendicular strain} \quad \epsilon_1^{(1)} &= \frac{a_1^{(1)} - a_1}{a_1} \\
 \epsilon_1^{(2)} &= \frac{a_1^{(2)} - a_1}{a_1}
 \end{aligned} \tag{4}$$

where the numbers (1) and (2) stand for GaSb and AlSb separately. The best fit was constructed from a profile using 10 periods of GaSb (30 nm)/AlSb (30 nm) with a perpendicular strain of 1.25% and -0.03% in the AlSb and GaSb

layers respectively. Symmetric reflections, such as (400), are sensitive only to perpendicular strain. Asymmetric reflections are sensitive to ϵ_{\perp} and ϵ_{\parallel} and combination until symmetric reflections produces values for both. Using Fe K $_{\alpha 1}$ (422) reflections, a uniform $\epsilon_{\parallel} = (+ 0.03 \pm 0.02\%)$ was measured throughout the superlattice.¹⁸

Since the cross section of the x-ray beam can be confined by slits to less than 1 mm² we can analyze different areas of the surface. In particular we were able to perform the analysis on the same spot where the channeling measurement had been carried out since this RBS spot is clearly visible probably due to cracking of diffusion pump oil by the He beam during the channeling analysis. The experimental rocking curve on the RBS spot is shown in Fig. 13. The structure of the experimental rocking curve indicates that the strain in AlSb layer is about half of what it is for the unirradiated spot. The reduction in the intensities of peaks located away from zero angle is due to broadening caused by lateral nonuniformities in the sample. The X-ray rocking curve data and channeling data are summarized in Table 2. The value of strain in GaSb layers is so small that it can be considered to be zero in the theoretical calculation like we did previously.

VII. DISCUSSION

We have studied GaSb/AlSb superlattice structures by combination of channeling scans and computer simulations and X-ray rocking curve measurements.

The value of "kink angle" detected by X-ray on a unirradiated spot is in good agreement with elasticity calculation. However on the spot used for channeling measurements the value of "kink angle" detected by X-ray is different from the value obtained by channeling scans combining with computer

simulation. It is reasonable to assume that the He bombardment has caused the structural changes in the superlattice. We should mention that in the present case much of the bombardment was done on the sample during test runs and the alignment procedures of crystal before the channeling scans. And also a lot of runs on the same sample were taken after channeling scans and before X-ray measurements. The results reveal that the strain in the superlattice is slowly released during MeV ion bombardment. It would be necessary to ascertain the critical dose below which channeling can measure the actual strain in certain superlattice without perturbing it. The mechanism for this is not clear. The initial mechanism could be direct knock on (nuclear stopping) to create Frenkel pairs or the effect of ionization in the breaking of bonds. The generation of vacancies could facilitate intermixing of the individual layers although no evidence for this has been observed by us. Our observation on the change of strain also raises the questions about how stable this strained layer superlattices are. There have been several reports on degradation of strained superlattice lasers. M. J. Ludowise, et al.²² reported upon continuous (CS) 300K laser operation of $\text{GaAs}/\text{In}_x\text{Ga}_{1-x}\text{As}$ ($x \sim 0.2$) super layer with a strain of 0.7% and of $\text{GaAs}_{1-x}\text{P}_x/\text{GaAs}$ ($x \sim 0.25$) laser with a strain of 0.45%. The superlattice with lowest stress had the lowest failure rate.

VIII. CONCLUSIONS

From our channeling and x-diffraction measurement on strained layer superlattices of AlSb/GaSb we can state that

1. X-ray rocking curve analysis is a very powerful method for characterizing the strain in superlattices as a function of depth since it determines the geometry of the distortion (parallel, perpendicular, negative or positive strain).

2. Backscattering and channeling measurements in combination with computer simulation are sensitive to relative changes in the channel direction, changes which can be caused by a variety of distortions and yield lower limit for the "kink angle", which is a way to express the strain in the superlattices.
3. He ion beam bombardment at extended doses relieves portion of the strain of the AlSb/GaSb strained superlattice. This limits the beam dose that can be used in making ion backscattering measurements without perturbing the specimen. On the other hand, this ion beam perturbation might be utilized to modulate strain in superlattices in a controllable manner onto unmasked area. This has potential processing application on integrated optics involving superlattices layered structures.

Table 1

Lattice Constant and "kink angle" Calculation

| | | |
|-------------------------------------|--------------------|-------------------|
| $a_1(\text{GaSb})$ | 6.095 Å (Ref. 19)* | 6.118 Å (Ref. 20) |
| $a_2(\text{AlSb})$ | 6.135 Å (Ref. 19) | 6.135 Å |
| $a_1(\text{GaSb})$ | 6.095 Å | 6.118 Å |
| $a_1^{(1)}(\text{GaSb})$ | 6.095 Å | 6.118 Å |
| $a_1^{(2)}(\text{AlSb})$ | 6.175 Å | 6.152 Å |
| $\Delta\theta(\text{"kink angle"})$ | 0.374° | 0.159° |

*Lattice parameter of Ref. 19 is believed to be more accurate.

Table 2

Experimental Results

| | x-ray (on unirradiated spot) | x-ray (on RBS spot) | RBS |
|-----------------------|---------------------------------|------------------------|-----------------------------|
| $\epsilon_1^{(1)}(z)$ | -0.03 | ~0 | (0) |
| $\epsilon_1^{(2)}(z)$ | 1.25 | ~0.6 | 0.95 |
| $\epsilon_1^{(1)}(z)$ | 0.03 | ~0 | (0) |
| $\epsilon_1^{(2)}(z)$ | 0.03 | ~0 | (0) |
| $\Delta\theta$ | $0.365^\circ \pm 0.004^\circ$ | $\sim 0.17^\circ$ | $0.27^\circ \pm 0.03^\circ$ |

ACKNOWLEDGEMENT

The authors would like to thank S. T. Picraux for valuable discussions regarding channeling and elasticity and E. Frey, and D. Y. Han for assistance on the data reduction. Superlattice samples used in this work is identical to that used in Ref. 8. We acknowledge C.-A. Chang of IBM for making such a sample available to us. Part of the work is supported by MCNC. At the California Institute of Technology, authors (VSS and M-AN) would like to acknowledge the support of the Defense Advanced Research Projects Agency Contract [MDA 903-82-C-0348] (S. Roosild).

References

1. G. C. Osbourn, J. Appl. Phys. 53, 1586 (1982).
2. J. H. Barrett, Phys. Rev. B28, 2328 (1983).
3. J. W. Mathews and A. E. Blakeslee, J. Vac. Sci. Technol. 14, 989 (1977).
4. A. Segmüller, P. Krishna and L. Esaki, J. Appl. Cryst. 10, 1 (1977).
5. R. M. Fleming, D. B. Mewhan, A. C. Gossard, W. Wiegmann, and R. A. Logan, J. Appl. Phys. 51, 357 (1980).
6. F. W. Saris, W. K. Chu, C. A. Chang, R. Ludeke, and Esaki, Appl. Phys. Lett. 37, 931 (1980).
7. W. K. Chu, F. W. Saris, C. A. Chang, R. Ludeke, and Esaki, Phys. Rev. B26, 1999 (1982).
8. W. K. Chu, C. K. Pan, and C.-A. Chang, Phys. Review B, Rapid Comm. 28, 4033 (1983).
9. S. T. Picraux, L. R. Dawson, G. C. Osbourn, and W. K. Chu, Appl. Phys. Lett. 43, 930 (1983).
10. S. T. Picraux, L. R. Dawson, G. C. Osbourn, R. M. Biefeld, and W. K. Chu, Appl. Phys. Lett. 43, 1020 (1983).
11. W. K. Chu, J. A. Ellison, S. T. Picraux, R. M. Biefeld and G. C. Osbourn, Phys. Rev. Lett. 52, 125 (1984).
12. C. A. Chang, H. Takaoka, L. L. Chang, and L. Esaki, Appl. Phys. Lett. 40, 983 (1982).
13. W. K. Chu, J. W. Mayer and M.-A Nicolet, Backscattering Spectrometry, (Academic, New York 1978).
14. L. C. Feldman, J. W. Mayer and S. T. Picraux, Materials Analysis by Ion Channeling, Academic, New York 1982.
15. V. S. Speriosu, J. Appl. Phys. 52, 6094 (1981).
16. V. S. Speriosu and C. H. Wilts, J. Appl. Phys. 54, 3325 (1983).
17. V. S. Speriosu, M.-A. Nicolet, S. T. Picraux and R. M. Biefeld (to be published Appl. Phys. Lett.).
18. V. S. Speriosu and T. Vreeland, Jr., accepted for publication in J. Appl Phys.
19. Marvin K. Farr, J. G. Traylor, and S. K. Sinha, Phys. Rev. B11, 1587 (1975).
20. D. S. Gemmel, Rev. Mod. Phys. 46, 129 (1974).

21. J. H. Barrett, Phys. Rev. B3, 1527 (1971).
22. M. J. Ludowise, W. T. Dietze, C. R. Lewis, M. D. Camres, N. Holonyak, Jr., B. K. Fuller, and M. A. Nixon, Appl. Phys. Lett. 42, 487 (1983).

Figure Captions

- Fig. 1 The configuration of a strained-layer superlattice GaSb/AlSb.
- Fig. 2 Schematic diagram of the layers of GaSb/AlSb sample. The lattice distortion of AlSb due to mismatch to substrate is shown.
- Fig. 3 The difference in channeling directions between $[110]$ directions due to the strained layers.
- Fig. 4 Polar coordinate diagram to illustrate the exact directions in the channeling experiments. The scanning direction 14° away from a $\{100\}$ plane is also shown.
- Fig. 5 Energy spectra of 1.76 MeV He^+ ions backscattered from $[100]$ GaSb/AlSb superlattices. Depth scale based on Sb signals and Ga signals are marked in the unit of number of layers (30 nm/per layer), $[100]$ aligned, $[110]$ aligned, random taken at an angle of 3° with respect to $[110]$ direction and three more spectra between the $[110]$ and random spectra are given.
- Fig. 6 Angular scan by setting an energy window from the first layer to fourth layer from 52 spectra run at 52 different angles. The center position of the angular scan changes from layer to layer indicating that the $[110]$ direction varies.
- Fig. 7 The oscillation of the angular position of minimum yield plotted as a function of depth. Both experimental results and computer simulation are shown.
- Fig. 8 Monte Carlo simulation backscattering probability contours for 1.76 MeV He ions in GaSb/AlSb. The "kink angle" assumed was 0.37° . The level of local maxima and minima are shown, and the interval between contours is 0.1.
- Fig. 9 Monte Carlo simulation backscattering probability contours for 1.76 MeV He ions in GaSb/AlSb. The "kink angle" assumed was zero. The level of local maxima and minima are shown and the interval between contours is 0.1.
- Fig. 10 Angular scan profiles abstracted from Fig. 8 the computer simulation for the first four layers of GaSb/AlSb under the same depths as that in the experiments.

Fig. 11 The angle difference ($\Delta\psi$) between "directions for best channeling" of the first and second layer plotted as a function of assumed "kink angle" $\Delta\theta$.

Fig. 12 Experimental (dash) and calculated (solid) Fe $K_{\alpha 1}$ (400) x-ray rocking curves of GaSb/AlSb superlattice on the unirradiated spot.

Fig. 13 Experimental x-ray Fe $K_{\alpha 1}$ rocking curve of GaSb/AlSb superlattice on the RBS investigated spot.

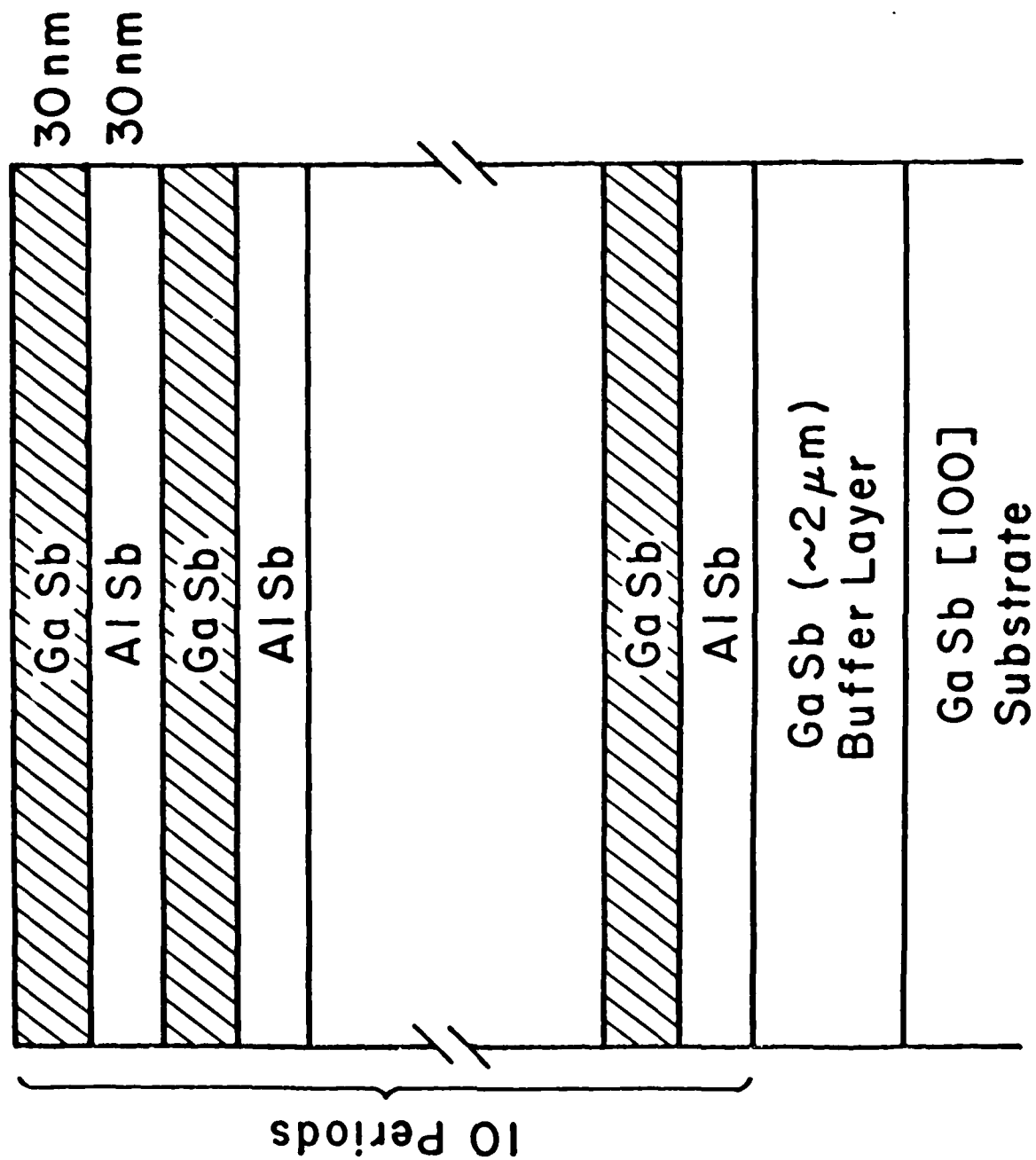
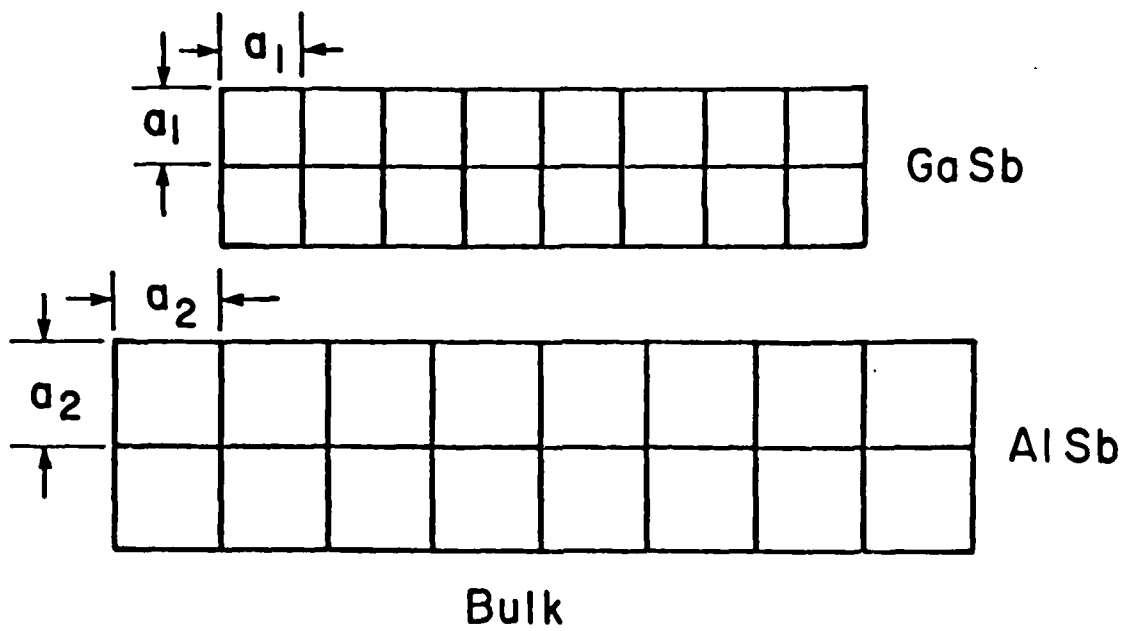


Figure 1



$$a_{\perp} > a_2 > a_{\parallel} = a$$

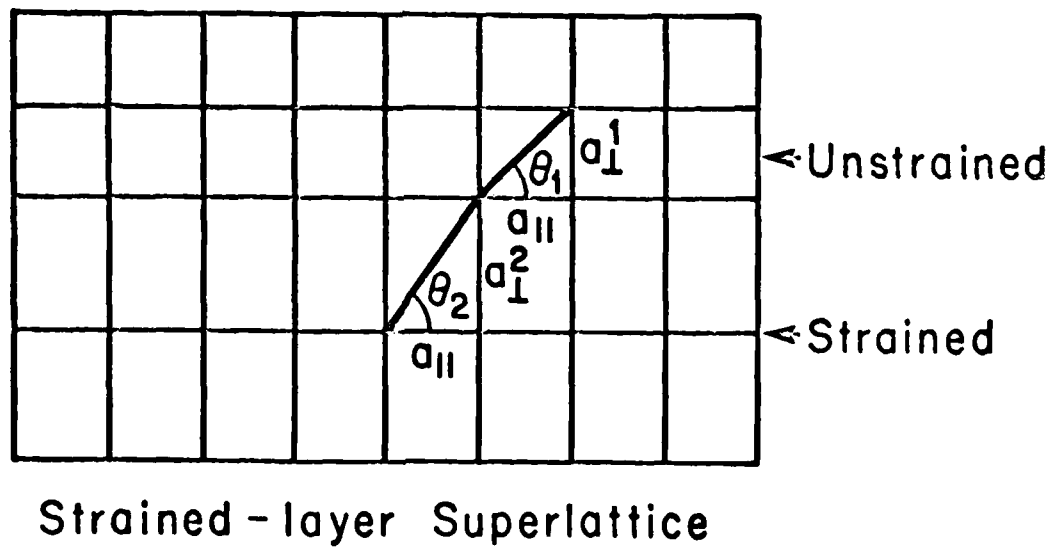


Figure 2

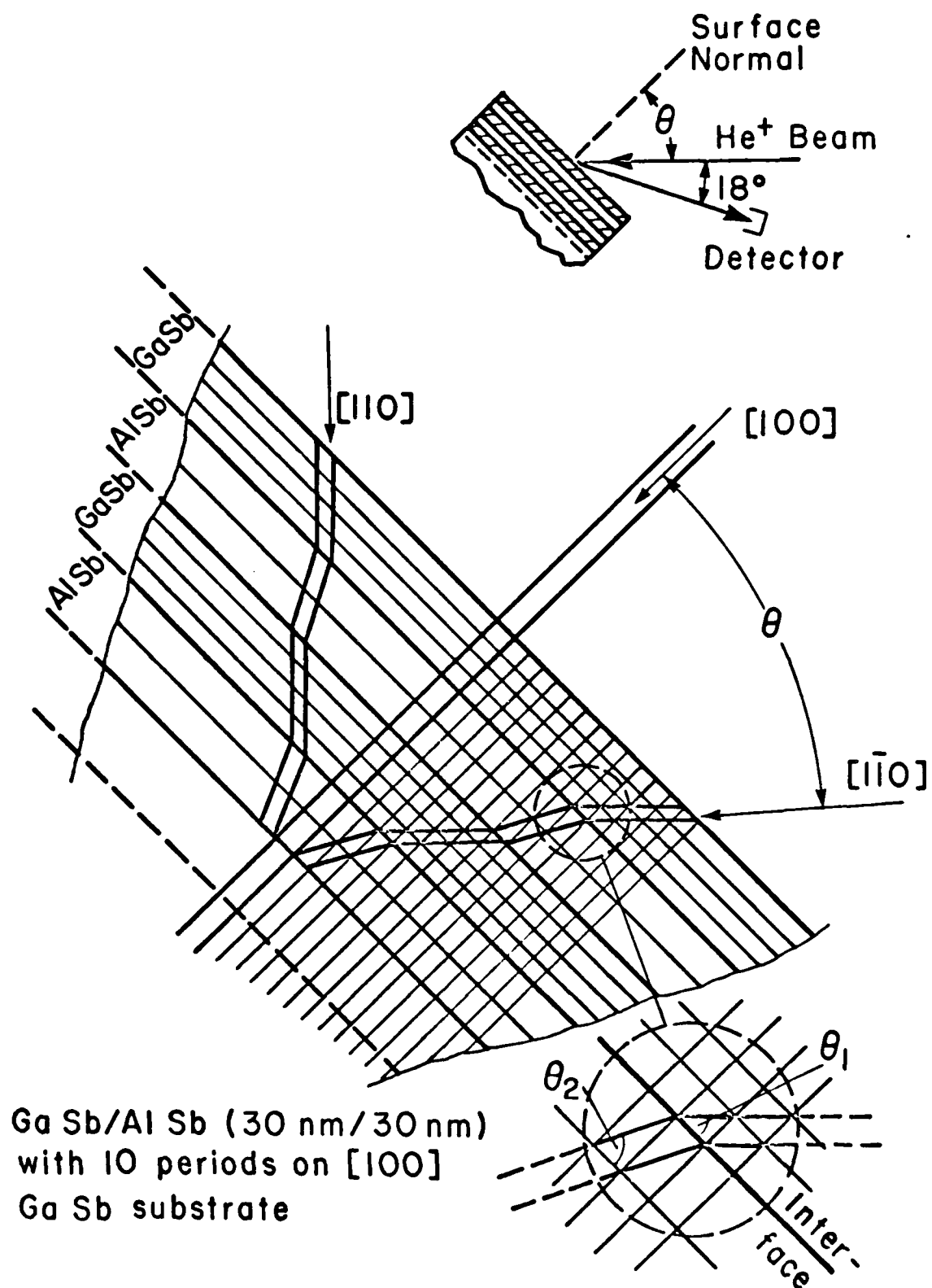
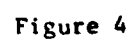


Figure 3



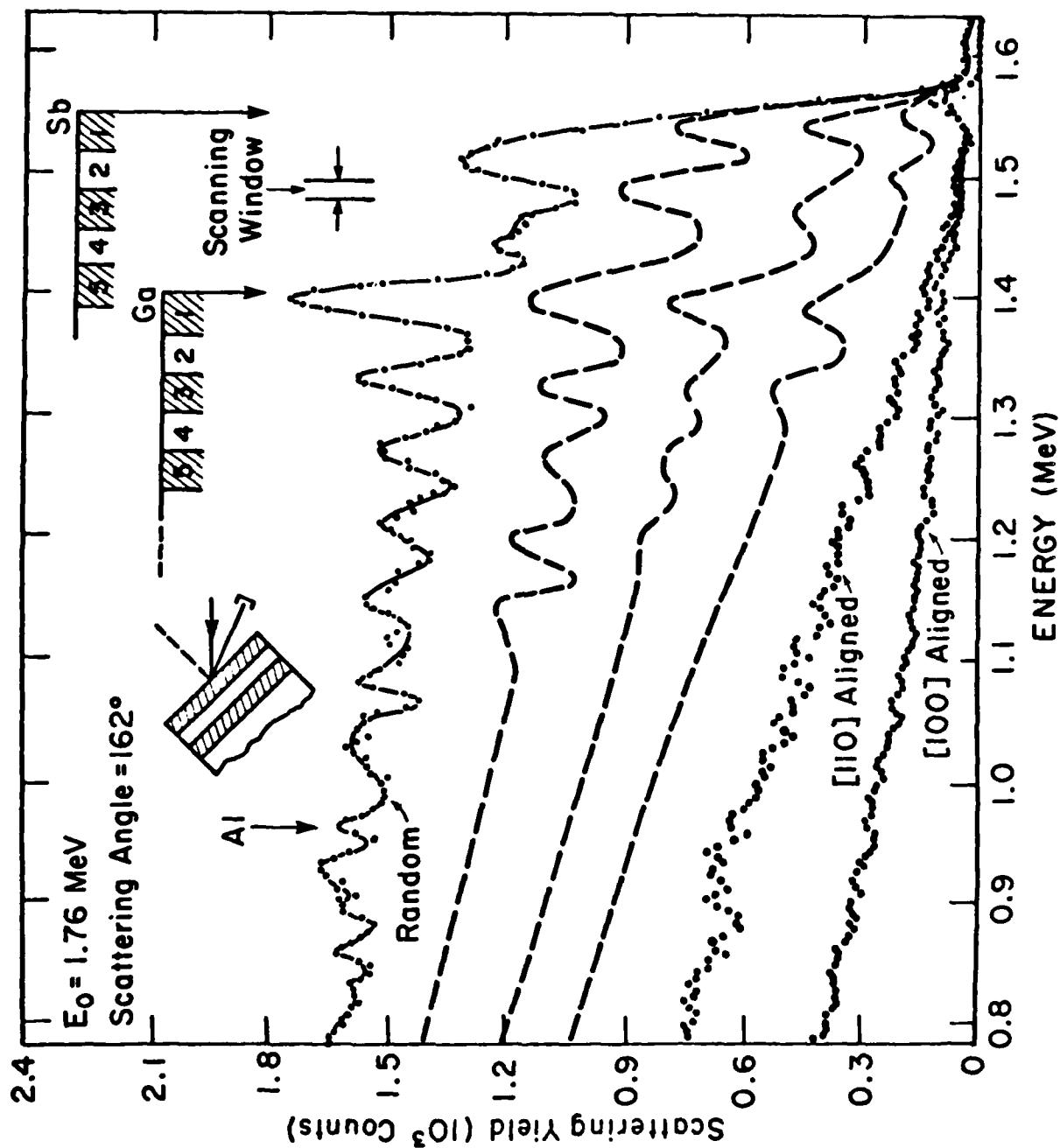


Figure 5

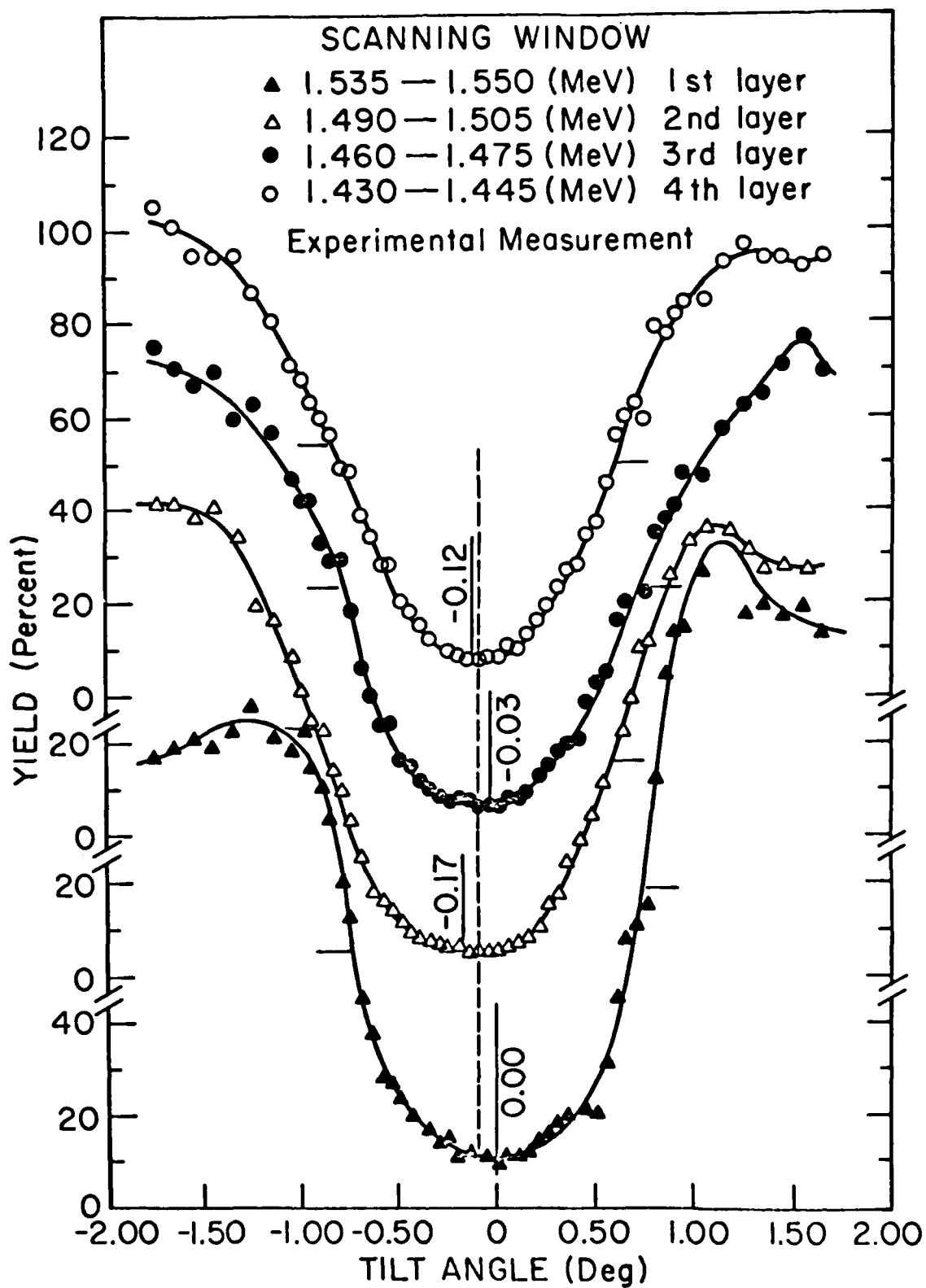


Figure 6

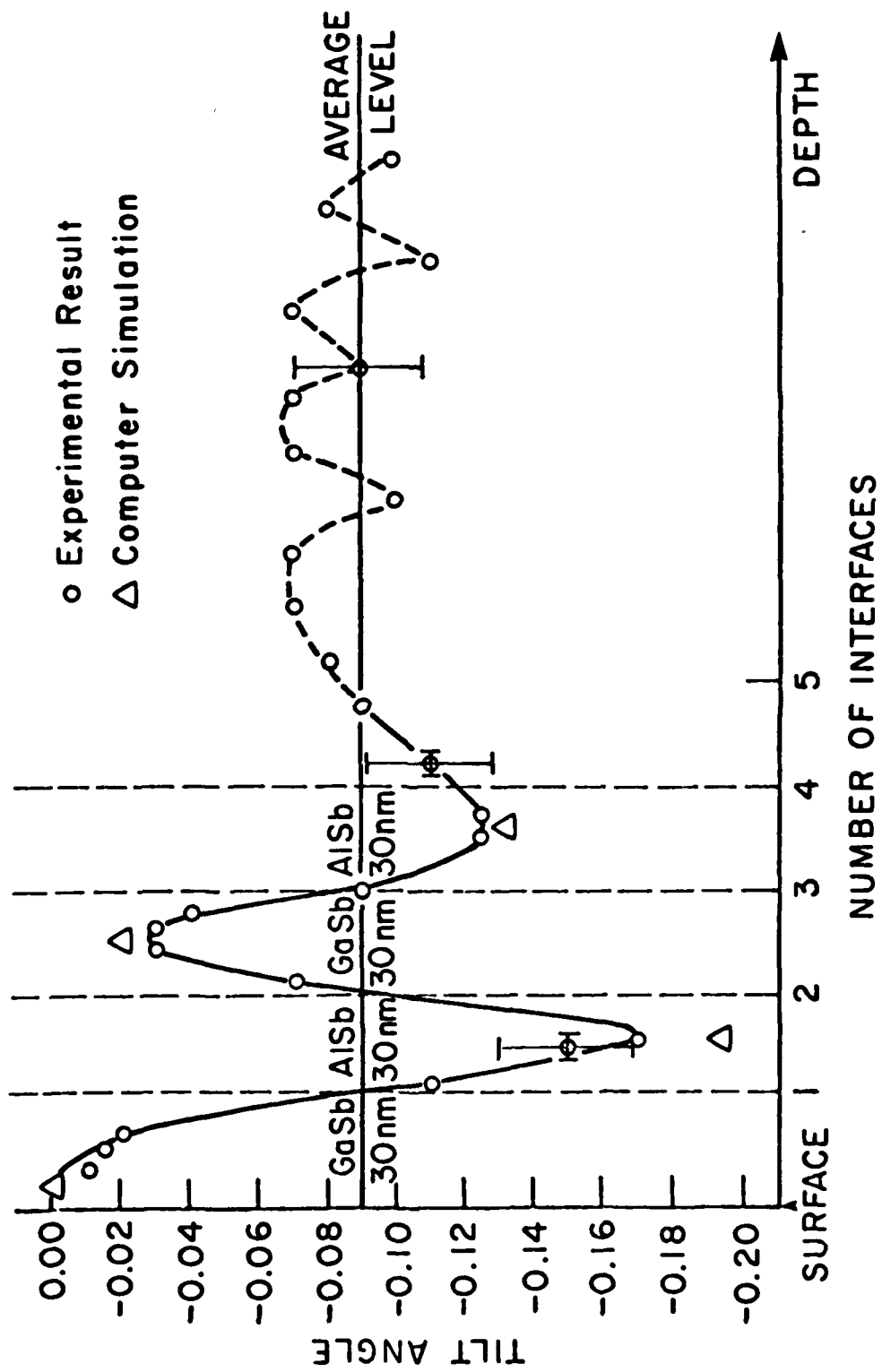


Figure 7

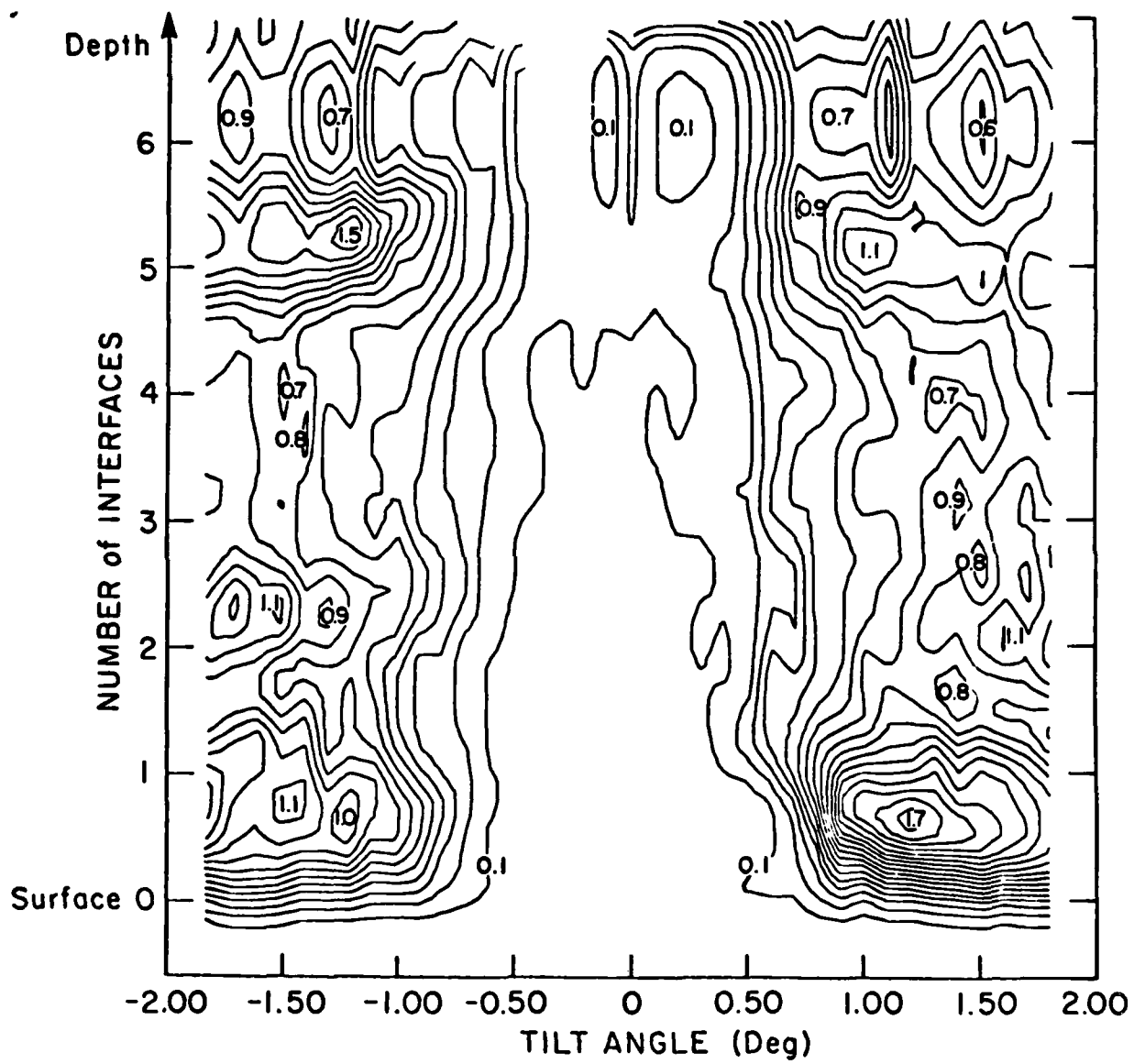


Figure 8

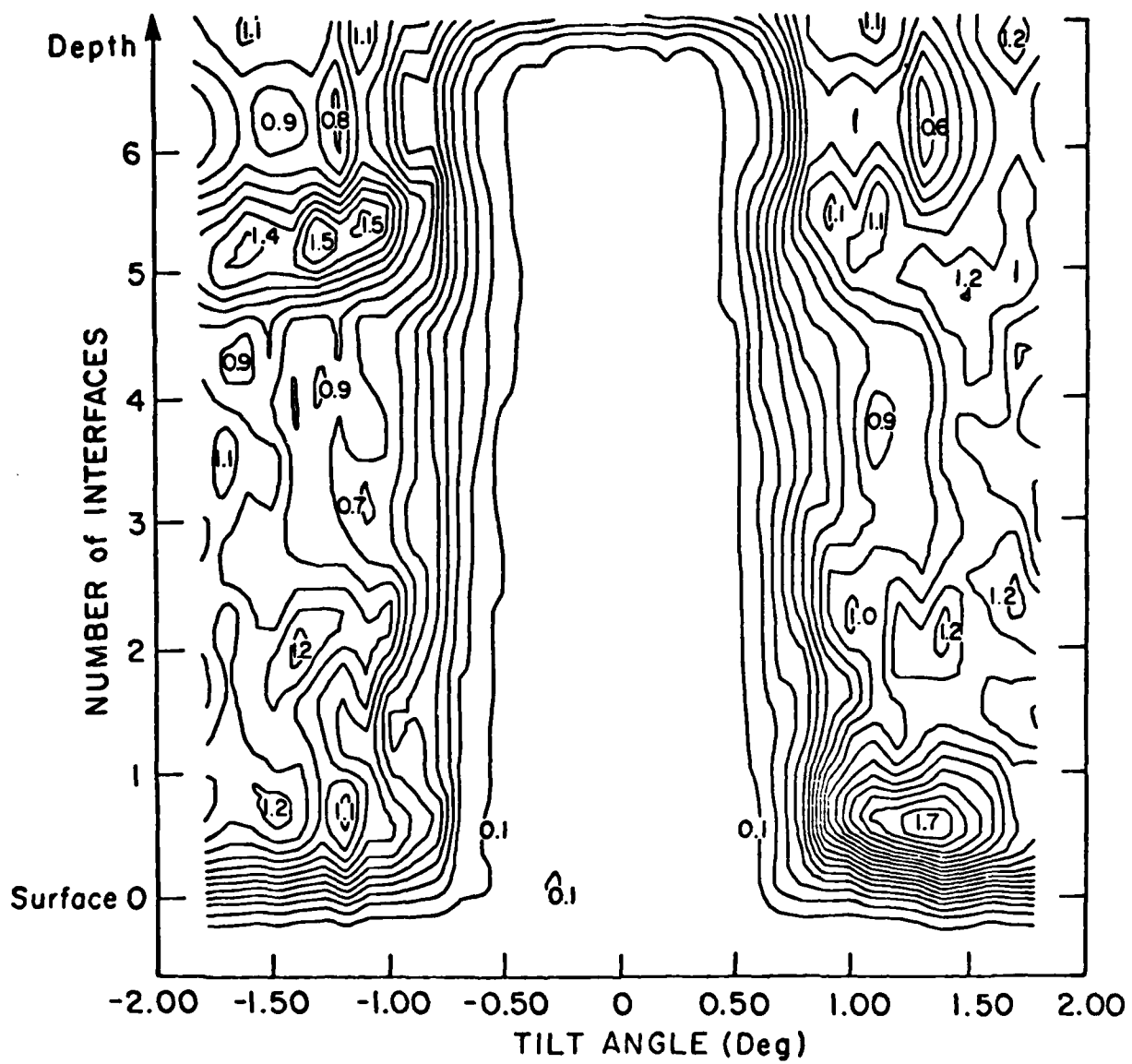


Figure 9

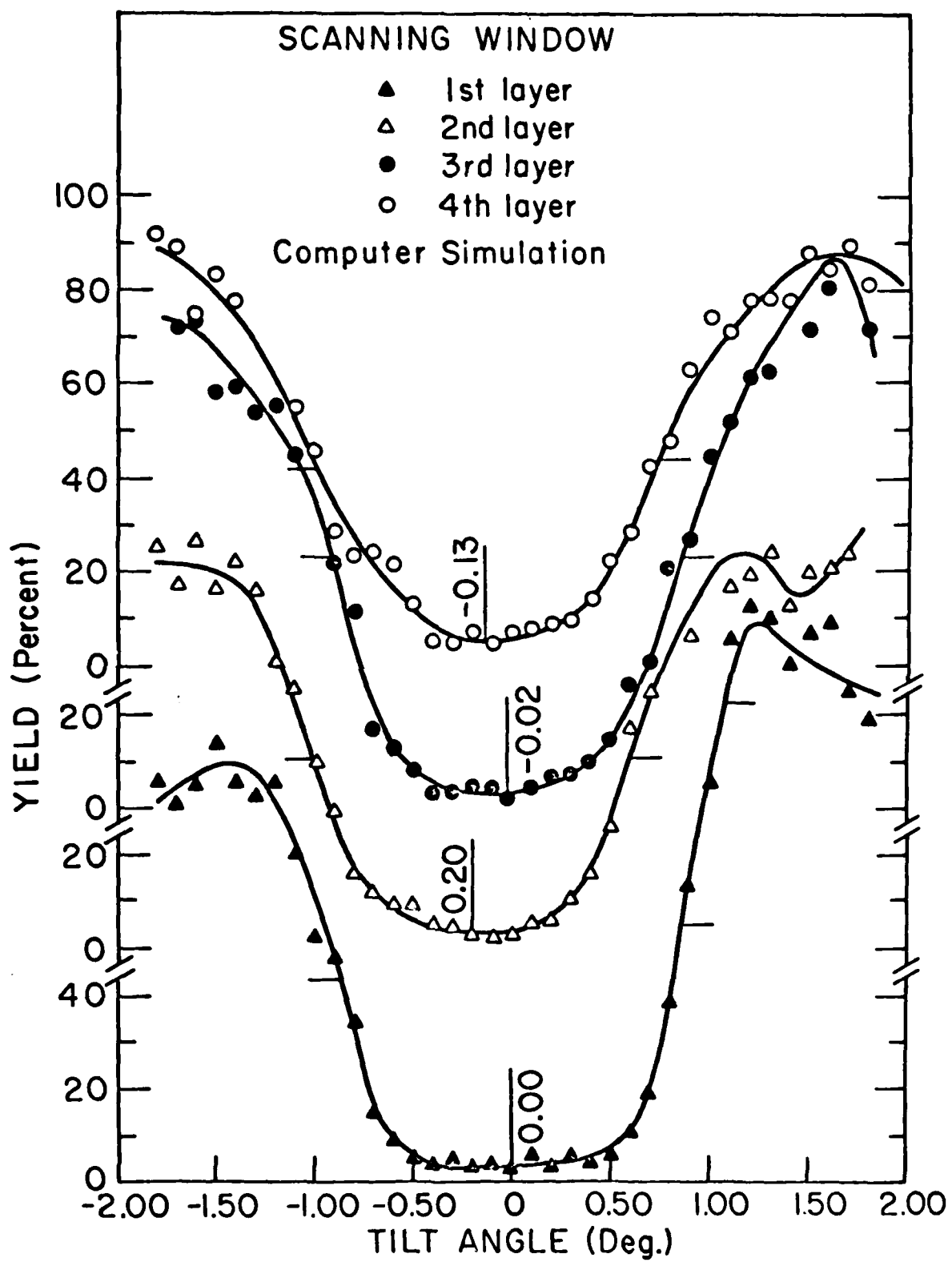


Figure 10

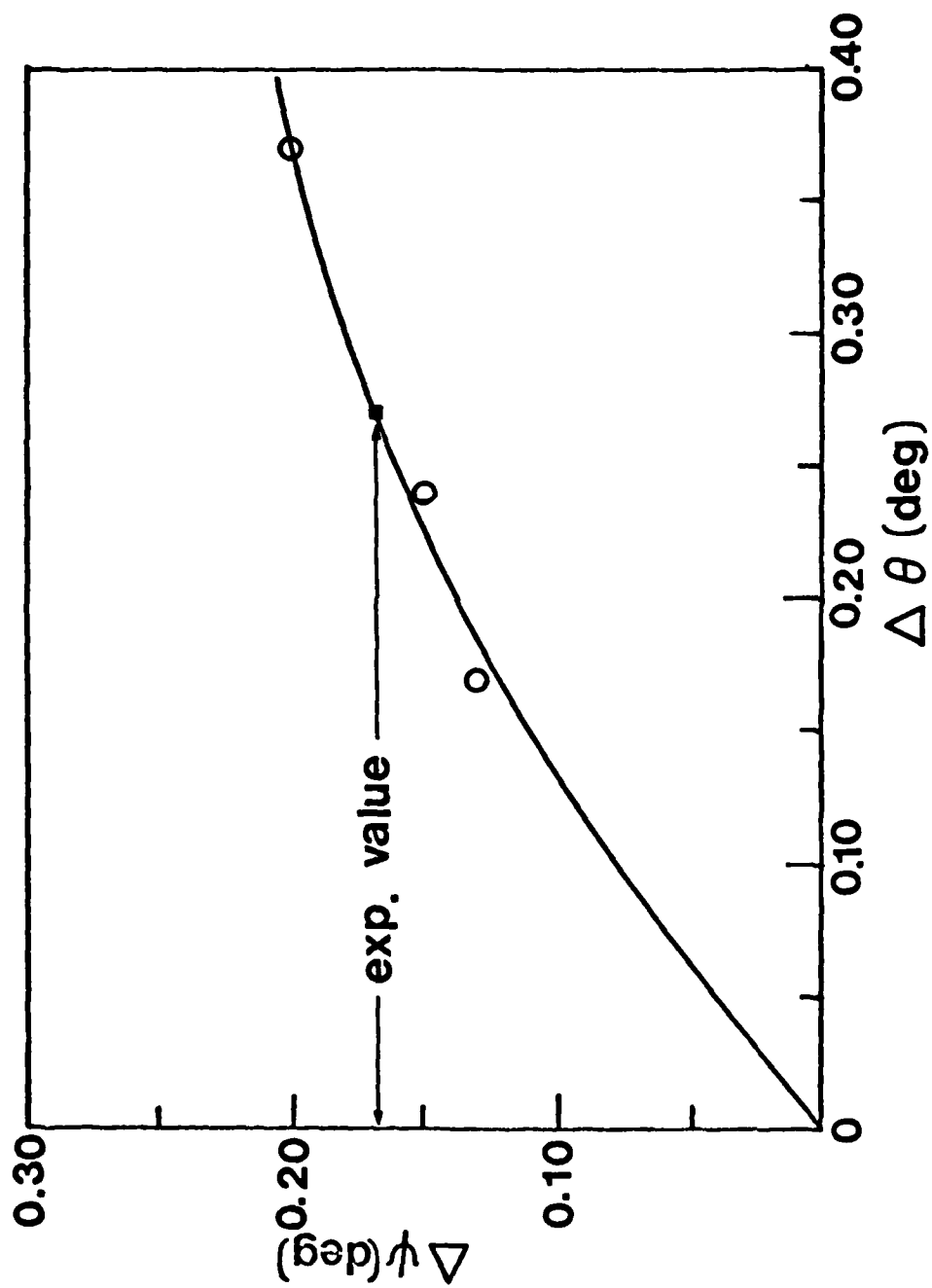


Figure 11

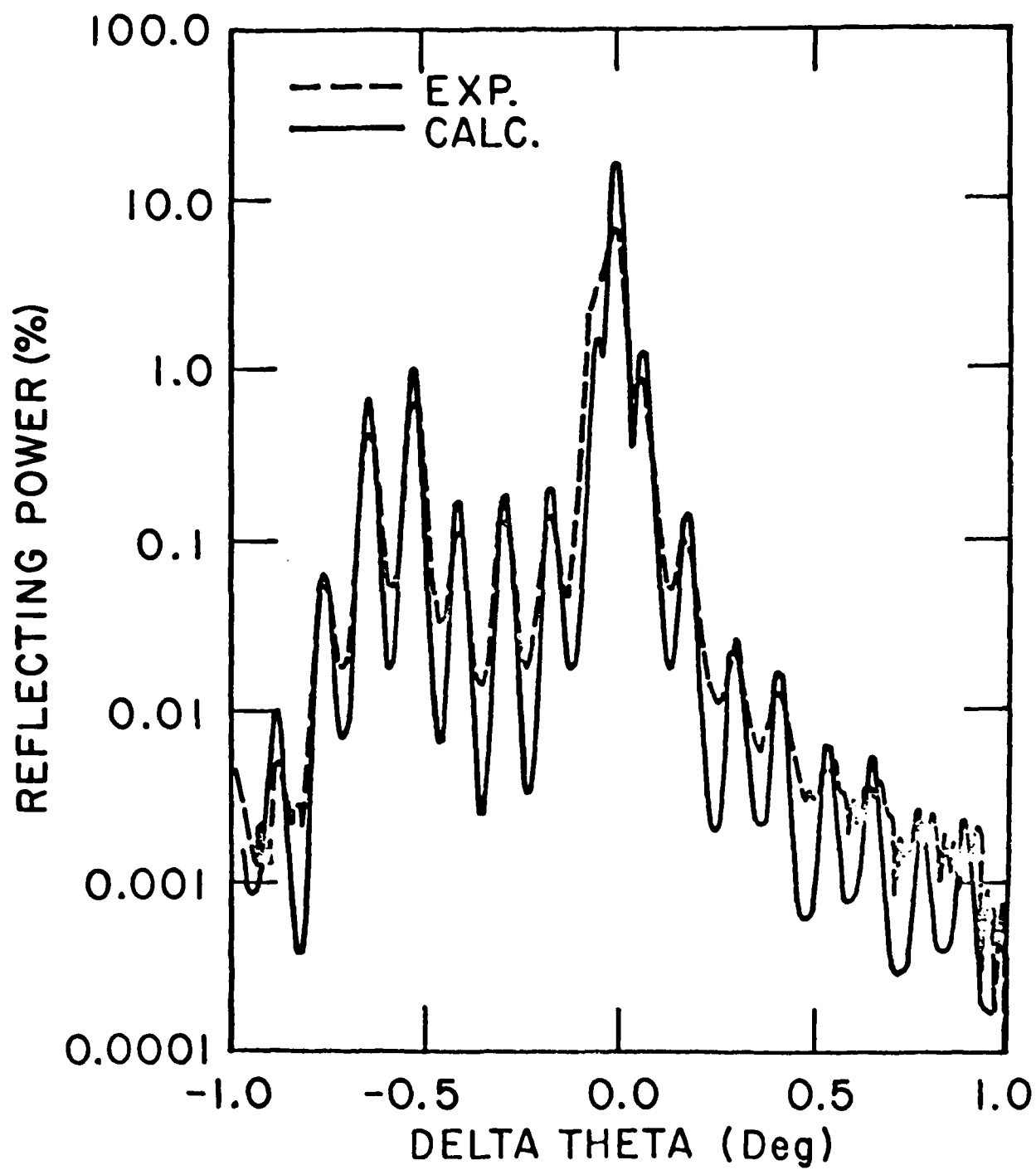


Figure 12

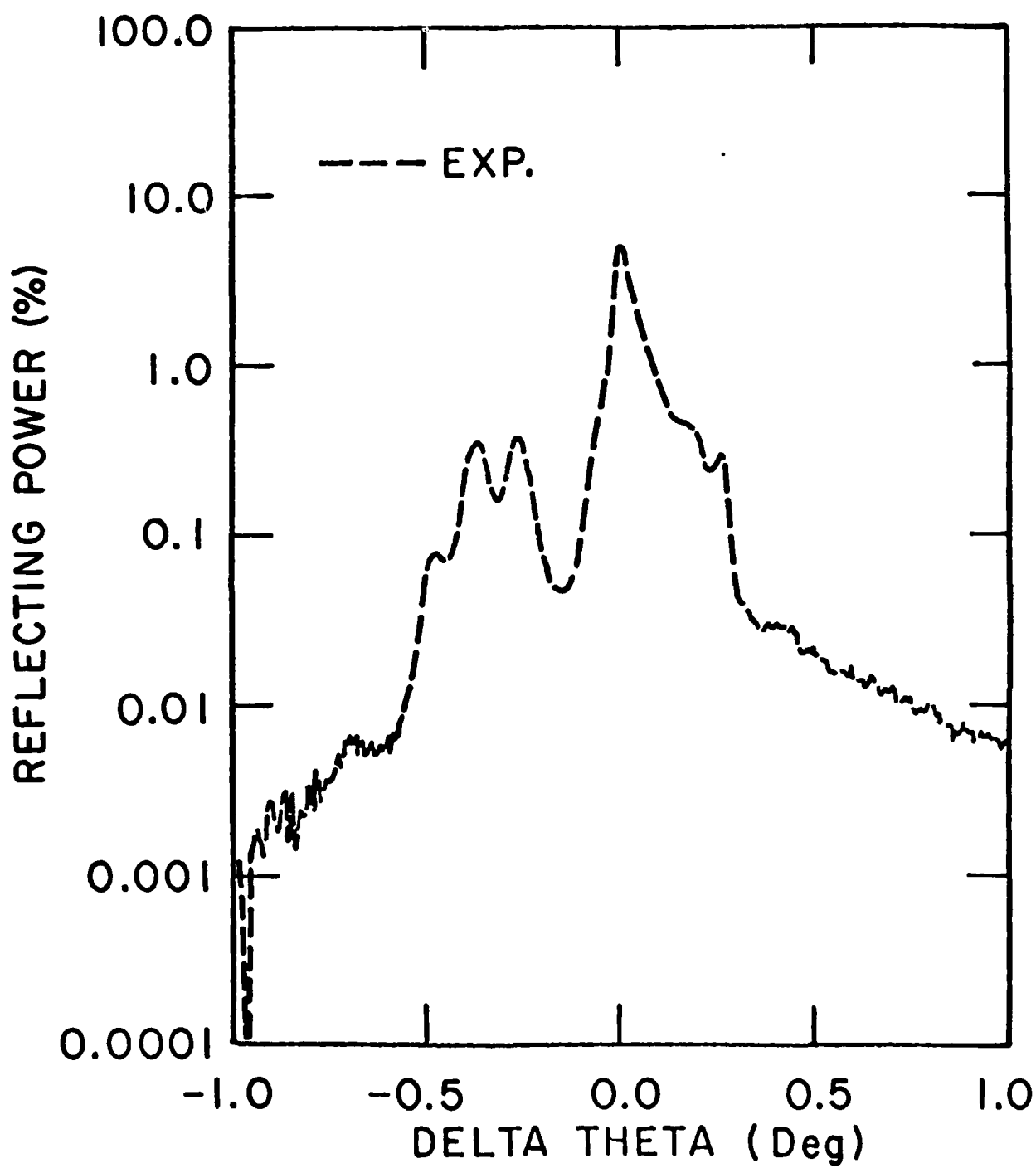


Figure 13

ANALYSIS OF Zn-DIFFUSED $\text{Al}_{0.88}\text{Ga}_{0.12}\text{As}/\text{GaAs}$ SUPERLATTICE
STRUCTURE BY X-RAY ROCKING CURVES AND BACKSCATTERING SPECTROMETRY

A. H. Hamdi⁺, J. L. Tandon^{*}, and M-A. Nicolet⁺

⁺ California Institute of Technology,

Pasadena, California 91125

^{*} Applied Solar Energy Corporation,
City of Industry, California 91744

ABSTRACT

The techniques of x-ray rocking curves and backscattering spectrometry with channeling have been used to analyze $\text{Al}_{0.88}\text{Ga}_{0.12}\text{As}/\text{GaAs}$ strained-layer-superlattices (SLS), before and after Zn diffusion. The two techniques are non-destructive, complement each other, and together serve as powerful analytical tools in providing detailed information on the depth profile of strain, composition and crystalline quality of the SLS structures. In an SLS with 10 periods, each consisting of alternating layers of GaAs (270 Å) and $\text{Al}_{0.88}\text{Ga}_{0.12}\text{As}$ (140 Å), a complete depth redistribution of strain and of Ga and Al concentrations was observed after Zn diffusion at 600°C for 1 h. The resultant single layer possessed good crystalline quality and uniform composition ($\text{Al}_{0.3}\text{Ga}_{0.7}\text{As}$). The strain in this layer was measured to be constant, equal to the depth-average strain before Zn diffusion.

1. INTRODUCTION

The disordering of AlAs/GaAs strained-layer-superlattice (SLS) structures upon Zn diffusion has been investigated recently by several groups [1,2]. Dramatic intermixing of Ga and Al in these structures has been observed and attributed to the fast diffusion of Zn at temperatures as low as 550°C [3]. Several mechanisms have also been proposed to explain this phenomena [4,5]. The remarkable feature of disordering is that it is accomplished at a temperature much lower than the growth temperature of the SLS (620-750°C), and only during Zn diffusion.

In this paper the nondestructive, self-calibrative techniques of x-ray rocking curves and backscattering spectrometry with channeling have been used to obtain quantitative information on Zn diffused $\text{Al}_{0.88}\text{Ga}_{0.12}\text{As}/\text{GaAs}$ SLS structures. Measurements of strain, composition and crystalline quality as a function of depth obtained using these two techniques provide further detailed insight into the phenomena.

2. EXPERIMENTAL

$\text{Al}_{0.88}\text{Ga}_{0.12}\text{As}/\text{GaAs}$ SLS structures were grown in a computer-controlled metal organic chemical vapor deposition (MOCVD) reactor. Alternating layers of $\text{Al}_{0.88}\text{Ga}_{0.12}\text{As}$ and GaAs, 10 each, were grown at 730°C by switching on and off the Al source (trimethyl-aluminum) and modulating the mole fraction of Ga source (trimethyl-gallium) [6]. The substrates used were

semi-insulating GaAs wafers, oriented 2-3° off <100> axis. Zinc diffusion was carried out in an evacuated ($\sim 10^{-5}$ Torr) closed quartz ampoule with a Zn_2As_3 source. The ampoule was ~ 24 cm long and had a volume of $\sim 12 \text{ cm}^3$. The SLS sample was placed on one end of the ampoule along with $\sim 1.3 \times 10^{-3} \text{ g}$ of Zn_2As_3 . The other end contained a plate of Ti. Prior to diffusion, the end of the ampoule possessing the Ti plate was heated to $\sim 900^\circ\text{C}$ for 3 h, to getter residual oxygen. The other end during this gettering step was maintained at room temperature. For Zn diffusion, the entire ampoule was heated at 600°C for 1 h. As a control, an SLS sample was also heated in a similar ampoule at the same temperature without the Zn source.

Bragg case double-crystal x-ray rocking curves were obtained on SLS samples with the $\text{Fe K}_{\alpha 1}$ (400) or (200) symmetric reflections. The x-ray beam was collimated and rendered nearly monochromatic by (400) reflection in <100> GaAs. Experimental rocking curves were fitted using a kinematical model of x-ray diffraction in thin epitaxial layers [7], while the diffraction in the substrate was treated dynamically [8]. Backscattering measurements were made by a 2.0 MeV $^4\text{He}^+$ beam. To obtain high depth resolution, the sample was tilted at an angle of 75° with respect to the sample's surface normal [9]. Channeling was carried out along <100> direction.

3. RESULTS AND DISCUSSION

3.1 X-Ray Rocking Curve Measurements

Measured (dashed line) and calculated (solid line) x-ray rocking curves obtained from the as-grown SLS sample before Zn diffusion are shown in fig. 1. The angle $\Delta\theta$ is plotted relative to the Bragg angle, θ_B , of the substrate peak which is at $\Delta\theta = 0$. The reflecting power, plotted on the vertical axis, is normalized with respect to the intensity of the incoming x-ray beam. Several peaks in the rocking curve are observed which are due to the periodicity in the structure factors and strains of the various layers in the SLS sample. The displacement of the peak P_0 from the substrate peak $P_{\text{subs.}}$, $\Delta\theta_{P_0}$, measures the average strain in a period of the SLS sample. The (400) rocking curve gives no information on parallel strain ϵ_{\parallel} , but previous work has shown [10,11,12] that it is zero for epitaxial AlAs layer, up to several microns thick, grown on GaAs. For symmetric reflections, the depth-average of perpendicular strain is given by [13]

$$\langle \epsilon_{\perp} \rangle = \frac{\epsilon_{\perp a} t_a + \epsilon_{\perp b} t_b}{t_a + t_b} = - \Delta\theta_{P_0} \cot \theta_B \quad (1)$$

where $\epsilon_{\perp a}$, $\epsilon_{\perp b}$ and t_a , t_b correspond to the perpendicular strains and thicknesses of the two layers a and b ($\text{Al}_{0.88}\text{Ga}_{0.12}\text{As}$ and GaAs) respectively, constituting the period of the SLS structure.

Experimentally, $\Delta\theta_{p_0}$ and θ_B are measured, thus $\langle \epsilon^\perp \rangle$ can be determined precisely. For symmetric reflection, as in this case, the equal separation between the peaks (P_0, P_{-1}, \dots etc.) measures the average period thickness of the SLS structure, according to the relation,

$$\Delta\theta_{p_0 - p_1} = \Delta\theta_{p_0 - p_{-1}} = \dots = \frac{\lambda}{2(t_a + t_b)\cos\theta_B} \dots \quad (2)$$

where λ is the wave length of Fe $K_{\alpha 1}$ line (1.937 Å). The calculated curve in fig. 1(a) was obtained using the strain distribution shown in fig. 1(b). In the calculation, the strain, the structure factors [14] and the thicknesses of the two layers in one period of the SLS were required. An iterative method was adopted to obtain the best fit to the measured curve. As shown in fig. 1(b), the thickness of the layers a ($\text{Al}_{0.88}\text{Ga}_{0.12}\text{As}$) and b (GaAs) are 140 ± 5 and 270 ± 10 Å, respectively. The strains in these layers are 0.25% and 0.0%, respectively. Since by Vegard's law [15], a one to one correlation exists between strain and the Al concentration; the strain of 0.25% corresponds to 88% Al and of 0.0% to 0.0% Al. The remaining discrepancy between the measured and calculated curves in fig. 1(a) can be attributed to nonabrupt transition at the interfaces of the individual layers in the SLS period, and/or due to minute variations between periods. These minor discrepancies notwithstanding, the average period thickness and the number of periods (in this case, 10) of the SLS structure are accurately determined by the x-ray rocking

curve measurements.

Figure 2(a) shows x-ray rocking curve measured (dashed line) on the SLS sample after Zn diffusion. A marked decrease in the intensity of subsidiary peaks is observed, when compared with the curve in fig. 1(a). This dramatic change in the rocking curve upon Zn diffusion can only be accommodated by a constant depth strain distribution, as shown in fig. 2(b), which yields the best fitted curve (solid line) in fig. 2(a). Clearly, after Zn diffusion, the SLS structure is transformed into a uniform single $\text{Al}_x\text{Ga}_{1-x}\text{As}$ layer. The reflecting power intensity of the peak P_0 and its position in the as-grown SLS sample (fig. 1(a)) does not change after Zn diffusion (fig. 2(a)). This implies that the crystalline quality of the epitaxial layer and its average perpendicular strain are conserved after Zn diffusion. From fig. 2(b), the strain is measured to be 0.085% which corresponds to 33% Al.

3.2 Backscattering and Channeling Measurements

Random and $\langle 100 \rangle$ channeled backscattering spectra obtained from the SLS samples before and after Zn diffusion are shown in fig. 3. The oscillations in the random spectrum of the as-grown sample are due to modulating Ga concentration in the layers constituting the SLS. The number of periods (≈ 10) can clearly be counted. The average period thickness was calculated to be 410 \AA , using standard stopping power values of He in the layers of SLS [9]. This thickness value is in excellent agreement with the value calculated by rocking curve measurements (see fig. 1). The concentration of Al and Ga in the first few

layers below the surface were also estimated and found to be in good agreement with x-ray measurements.

After Zn diffusion, the oscillations in the BS spectrum of the SLS sample disappear, resulting in an average flat spectrum. This indicates a uniform distribution of Al and Ga concentrations over the entire thickness of the SLS structure, and is consistent with x-ray measurements (see fig. 2).

The BS spectra for $\langle 100 \rangle$ channeled beam incidence shown in fig. 3 before and after Zn diffusion demonstrate that the crystalline quality of the SLS structure is preserved after Zn diffusion. This result further confirms the observations made from x-ray measurements. A small peak in the spectrum obtained after Zn diffusion is observed at an energy corresponding to Al at the surface. This Al signal may be due to surface oxidation of Al. The slightly higher minimum yield measured in the Zn diffused case, when compared to the as-grown case, may again be due to the aluminum oxide layer formed on the surface of the sample.

It should be pointed out that the structure of the SLS sample was stable upon similar heat treatment without Zn diffusion. Both x-ray rocking curve and backscattering measurements confirmed this. The redistribution of Al and Ga concentrations is thus a consequence of Zn diffusion in the SLS as observed earlier [3]. Present results suggest that the depth degradation of $\text{Al}_x\text{Ga}_{1-x}\text{As}/\text{GaAs}$ SLS structures due to diffusing species (e.g. Zn) can be monitored and measured by the combined use of the two nondestructive techniques discussed in this

paper. Similar studies can easily be extended to investigate the effects of other diffusing species in $\text{Al}_x\text{Ga}_{1-x}\text{As}/\text{GaAs}$, or in other superlattices. The results also raise serious questions with regard to the doping of SLS structures.

4. CONCLUSIONS

The combined techniques of x-ray rocking curves and BS with channeling constitute a powerful analytical approach for analyzing SLS structures. The two techniques are nondestructive, self-calibrative and provide quantitative information about the depth distribution of strain, composition and crystalline quality in these structures. Changes in SLS structures induced by diffusing species can be monitored in detail by employing these two techniques, as demonstrated in this paper. Such information should prove useful in understanding redistribution mechanisms in SLS structures.

ACKNOWLEDGMENTS

The contribution of Dr. Virgil S. Speriosu (IBM, San Jose) in the use and analysis of x-ray rocking curve technique at Caltech is gratefully acknowledged. We would like to thank Y.C.M. Yeh, D. A. Smith, A. Mehta, and J. Wendt at Applied Solar Energy Corporation for the growth of SLS structures. A. H. Hamdi extends his thanks to IBM for a research fellowship. The work was supported by the Defense Advanced Research Projects Agency (S. Roosild) under Contract [MDA 903-82-C-0348] at Caltech.

REFERENCES

- [1] R. M. Fleming, D. M. McWhan, A. C. Gossard, W. Wiegmann, and R. A. Logan, J. Appl. Phys. 51 (1980) 357.
- [2] W. D. Laidig, N. Holonyak, Jr., M. D. Camras, K. Hess, J. J. Coleman, P. D. Dapkus, and J. Bardeen, Appl. Phys. Lett. 38 (1981) 776.
- [3] J. W. Lee and W. D. Laidig, J. Elect. Mater. 13 (1984) 147.
- [4] U. Gösele and F. Morehead, J. Appl. Phys. 52 (1981) 4617.
- [5] W. D. Laidig, N. Holonyak, Jr., J. J. Coleman, and P. D. Dapkus, J. Elect. Mater. 11 (1981) 1.
- [6] To be published.
- [7] V. S. Speriosu, J. Appl. Phys. 52 (1981) 6094.
- [8] W. H. Zachariasen, Theory of X-Ray Diffraction in Crystals, (Wiley, New York, 1945).
- [9] W. K. Chu, J. W. Mayer, and M-A. Nicolet, Backscattering Spectrometry, (Academic Press, New York, 1978).
- [10] G. A. Rozgonyi, P. M. Petroff, and M. B. Panish, J. Crystal Growth, 27 (1974) 106.
- [11] E. Estop, A. Izreal, and M. Sauvage, Acta. crystal, A32 (1976) 627.
- [12] W. J. Bartels and W. Nijman, J. Crystal Growth, 44 (1978) 518.
- [13] V. S. Speriosu and T. Vreeland, Jr. (to be published).
- [14] J. A. Ibers and W. C. Hamilton, eds., International Tables for X-Ray Crystallography, Vol. IV, (Kymoch Press, Birmingham, 1974).

[15] M. C. Rowland and D. A. Smith, J. Crystal Growth, 33 (1977)
143.

FIGURE CAPTIONS

Figure 1 $\text{Fe K}_{\alpha 1}$ (400) rocking curves of as-grown, $\text{Al}_{0.88}\text{Ga}_{0.12}\text{As/GaAs}$ SLS structure with 10 periods. The calculated curve was obtained by an iterative method using the depth-strain distribution shown in (b).

Figure 2 $\text{Fe K}_{\alpha 1}$ (400) rocking curves of $\text{Al}_{0.88}\text{Ga}_{0.12}\text{As/GaAs}$ SLS after Zn diffusion at 600°C for 1 h. The calculated curve (solid line) was obtained using the constant strain distribution as shown in (b). The value of 0.085% strain is equal to the depth-average value of strain before Zn diffusion. The SLS structure is thus transformed into a single $\text{Al}_{0.3}\text{Ga}_{0.7}\text{As}_5$ layer after Zn diffusion.

Figure 3 2.0 MeV $^4\text{He}^+$ backscattering spectra obtained from $\text{Al}_{0.88}\text{Ga}_{0.12}\text{As/GaAs}$ SLS samples before and after Zn diffusion. The oscillations in the as-grown sample, which are due to modulation in the Ga concentration disappear after Zn diffusion, indicating disordering of the SLS structure. The $\langle 100 \rangle$ aligned spectra of the as-grown (dotted line) and the Zn diffused (solid line) samples have comparable minimum yields of 5 and 7%, respectively, showing that the crystallinity of the SLS is retained after Zn diffusion.

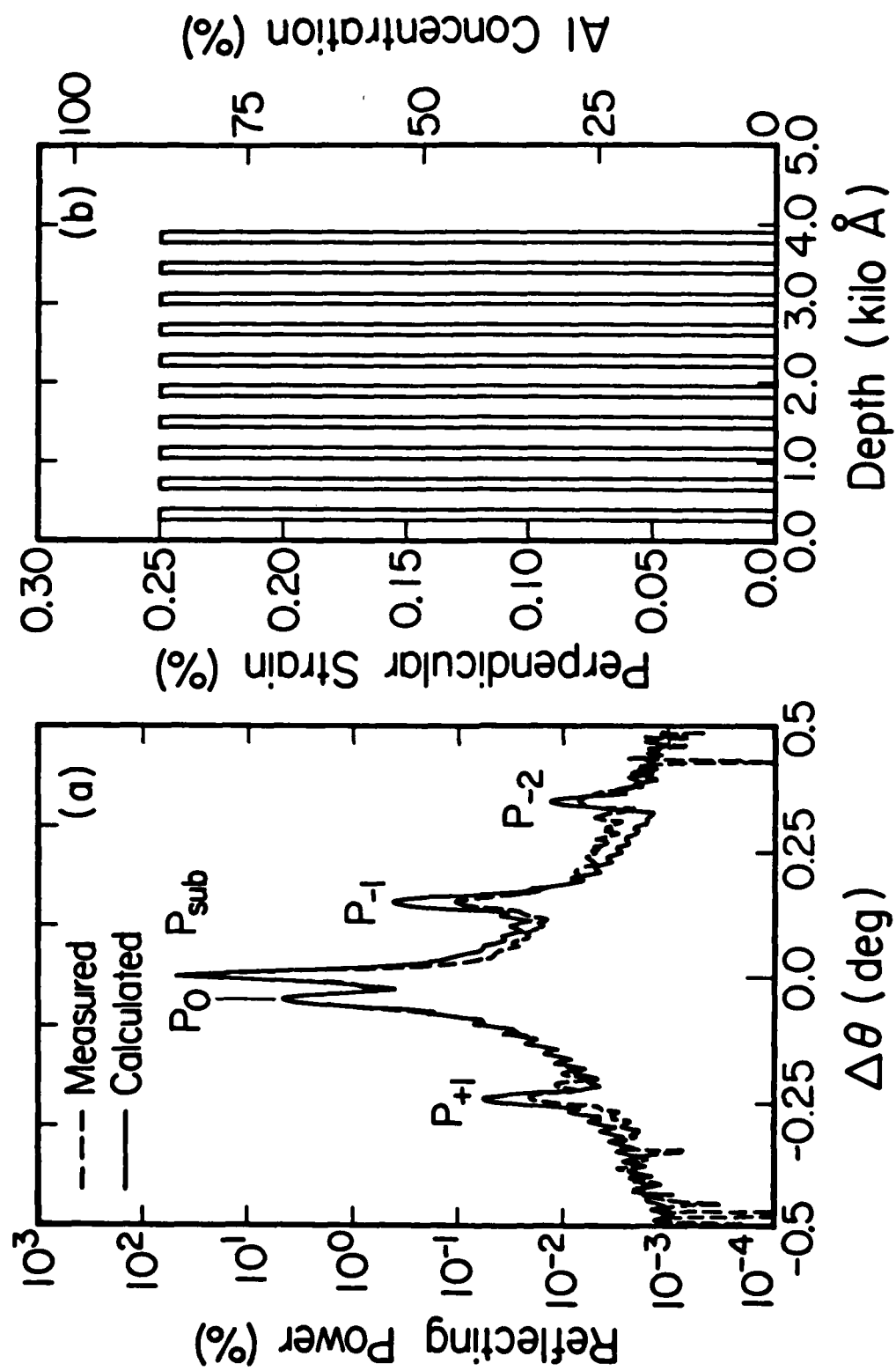


Fig.1

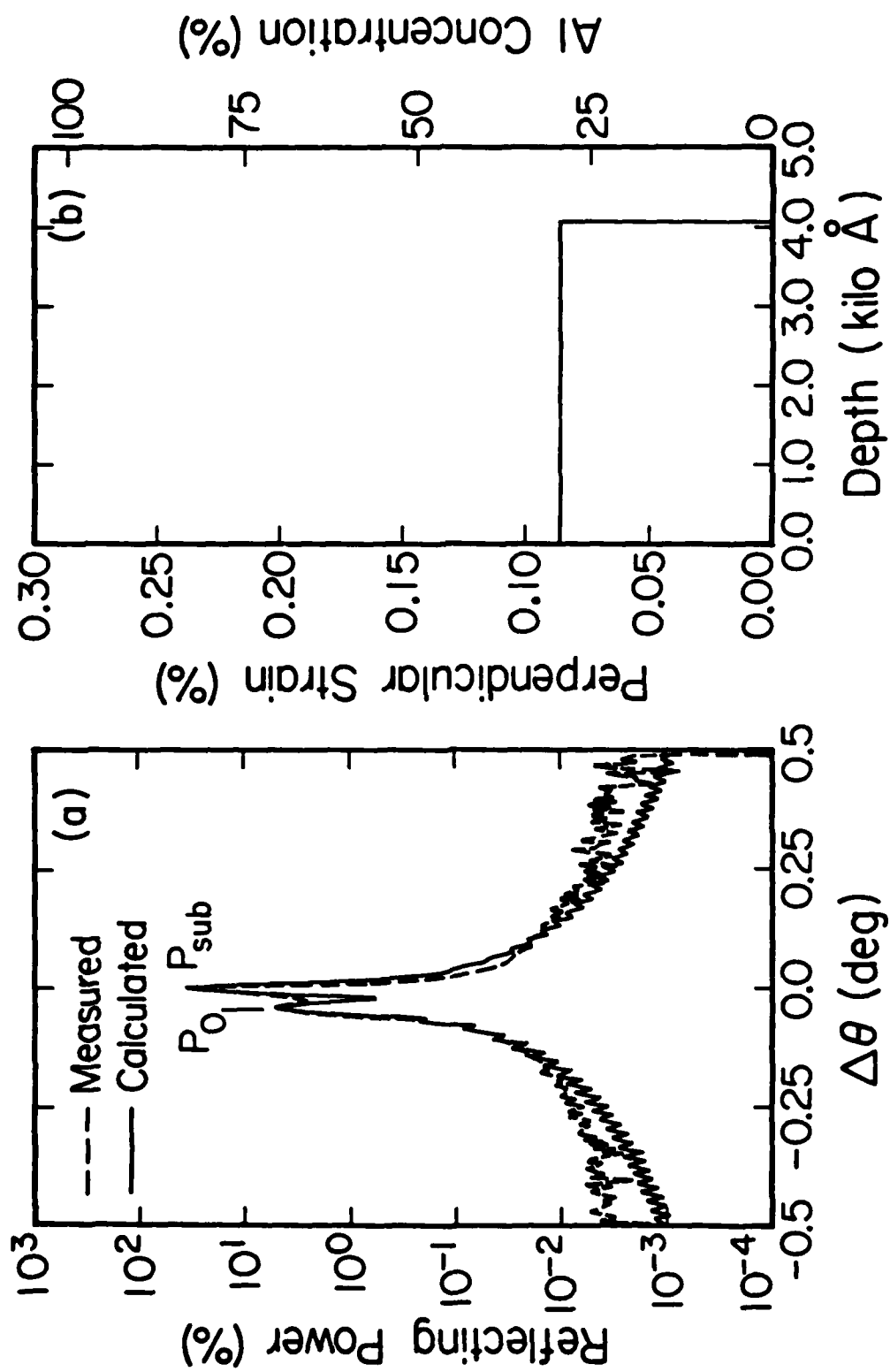


Fig.2

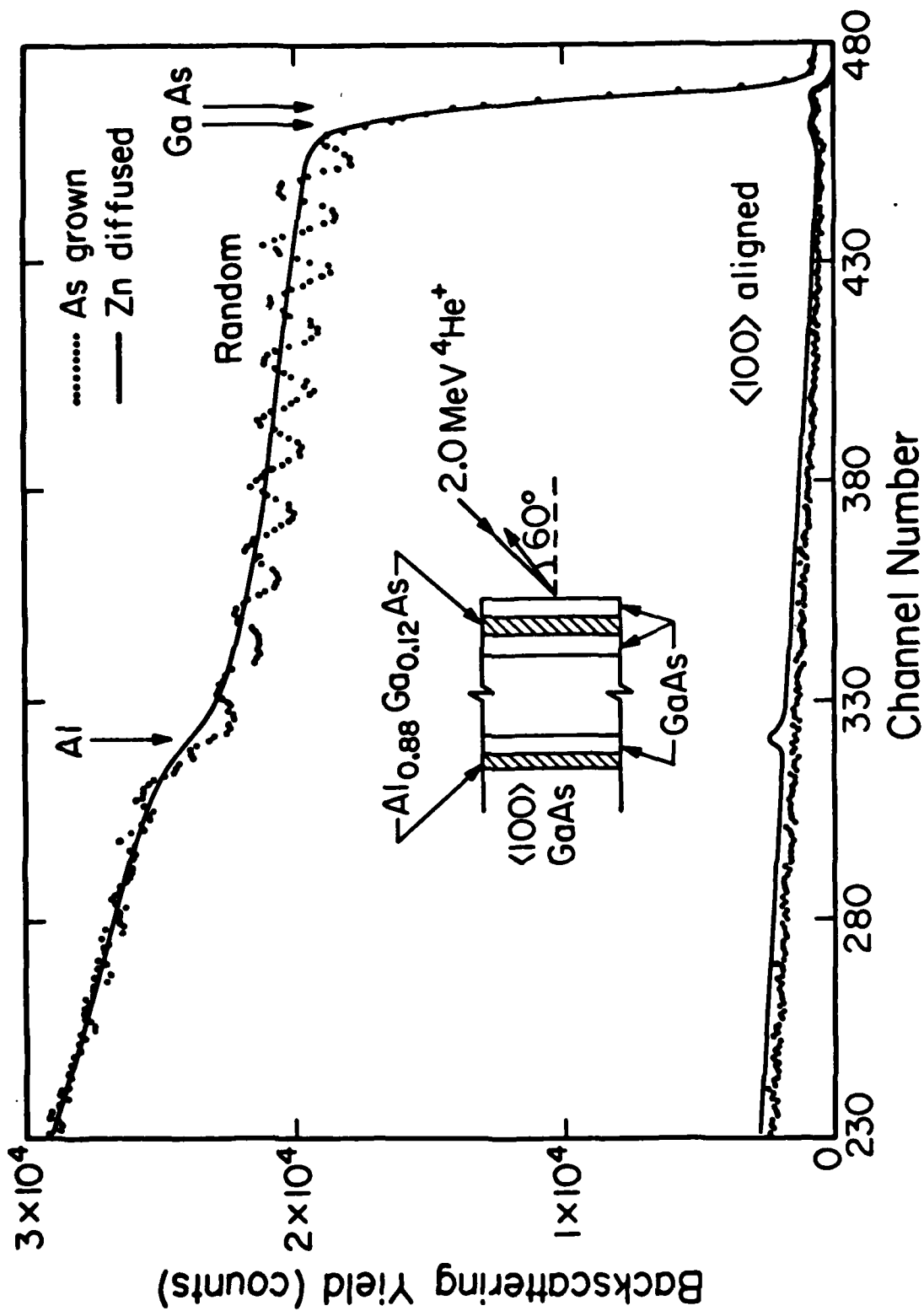


Fig. 3

COMBINED USE OF ION BACKSCATTERING AND X-RAY ROCKING
CURVES IN THE ANALYSES OF SUPERLATTICES

A. H. Hamdi, V. S. Speriosu*, J. L. Tandon**,
and M-A. Nicolet
California Institute of Technology
Pasadena, California 91125

ABSTRACT

Detailed compositional and structural analyses of superlattices have been carried out by MeV He⁺ backscattering with channeling, and with x-ray rocking curves. Through the combined use of the two techniques, depth profiles of strain, composition and crystalline quality have been determined. An example of an Al_xGa_{1-x}As/GaAs strained-layer-superlattice (SLS) is considered. The thicknesses of the individual periods in these SLS structures were accurately measured by Backscattering Spectrometry (BS). The values so obtained were used in the detailed calculations of x-ray rocking curves. An excellent agreement between measured and calculated curves was achieved. Transition regions at the interfaces of the various layers in the SLS were also detected and measured by both techniques. The two techniques complement each other and together provide powerful quantitative tools to characterize SLS structures.

* Present address: IBM, Research Laboratories, 5600 Cottle Road, San Jose, California 95193.

** Permanent address: Applied Solar Energy Corporation, City of Industry, California 91749.

I. INTRODUCTION

Modern epitaxial techniques, e.g. Metal Organic Chemical Vapor Deposition (MOCVD) and Molecular Beam Epitaxy (MBE), have made possible the growth of thin compound semiconductor superlattices. These structures, because of their unique optical and electrical properties^(1,2), open up new possibilities in the fabrication of solid-state lasers and high speed devices.⁽³⁾ Advancement in the realization of these devices demands a thorough characterization of the structure of the related materials. Analysis of such materials is also mandatory for the understanding of the physical phenomena associated with the performance of these devices.⁽⁴⁾ Material studies on SLS structures have been carried out by a variety of analytical techniques, e.g. Auger Electron Spectroscopy (AES), Secondary Ion Mass Spectrometry (SIMS)⁽⁵⁾, Transmission Electron Microscopy (TEM)⁽⁶⁾, X-Ray Diffraction⁽⁷⁾, Backscattering Spectrometry (BS) with channeling⁽⁸⁻¹¹⁾, etc.

In this paper, BS with channeling and x-ray rocking curves have been employed to analyze $\text{Al}_x\text{Ga}_{1-x}\text{As}/\text{GaAs}$ SLS structures. The combined use of the two techniques, along with the detailed interpretation of x-ray rocking curves, provides quantitative information on the depth distribution of strain, composition and crystalline quality in the SLS structures. The power and complementary nature of these two techniques in analyzing SLS structures are demonstrated.

II. EXPERIMENTAL

The $\text{Al}_x\text{Ga}_{1-x}\text{As}/\text{GaAs}$ SLS samples were grown in a large-capacity MOCVD reactor on semi-insulating GaAs wafers oriented $\sim 2^\circ$ off $\langle 100 \rangle$ axis.⁽¹²⁾ Two structures, SLS1 and SLS2 with 10 and 15 periods respectively, were grown. Each period consisted of two layers of $\text{Al}_x\text{Ga}_{1-x}\text{As}$ and GaAs. SLS1 had thinner layers than SLS2.

Backscattering (BS) measurements were made with a 2.0 MeV He^+ beam. In certain instances, to obtain high depth resolution near the surface, the samples were tilted at an angle of 80° with respect to the beam. The detector had a resolution of ~ 18 keV. Channeling measurements were carried out along $\langle 100 \rangle$ and $\langle 110 \rangle$ axes. Adjustments in the tilt and azimuthal angles were made iteratively to obtain the lowest possible minimum yields. Angular scans of yield made around the angles so determined were symmetric. X-ray rocking curve measurements were performed with a nearly monochromatic Fe $K_{\alpha 1}$ line. A computer-controlled double-crystal diffractometer was used. The beam was rendered nearly monochromatic by (400) reflection from a $\langle 100 \rangle$ GaAs crystal. The spot size of the x-ray beam was ~ 0.5 mm \times 1.0 mm. Rocking curves were obtained from symmetric (200) and (400) reflections. The measured curves were fitted using a kinematic model of x-ray diffraction in thin epitaxial layers, while the diffraction in the substrate was treated dynamically.⁽¹³⁾

III. RESULTS

A. Backscattering spectrometry measurements

The capability of the BS technique in the analysis of SLS structures is illustrated in Fig. 1. Random spectra from the SLS2 and virgin GaAs samples are compared. Three distinct regions in the BS spectra in Fig. 1, can be identified. In region I, the oscillations in the SLS2 spectrum are due to the modulated concentration of Ga in the layers consisting of the SLS structures. The number of periods (= 15) can clearly be counted. The SLS2 spectrum has a lower yield than the virgin GaAs spectrum in region I. This is because of a limited depth resolution of the system for a 25° tilted-angle geometry. Near the boundary of region II, the smearing of oscillations in region I can be explained by the interfering Al signal from the near-surface $\text{Al}_x\text{Ga}_{1-x}\text{As}$ layers. In the SLS2 spectrum, region II corresponds to the yield obtained from the GaAs substrate below the SLS structure. This yield is higher than the yield from the virgin GaAs sample because of the added Al signals. The modulated Al signal from the SLS structure cannot be clearly detected in this region because of the high GaAs background level and the limited sensitivity of the BS technique to light elements in a heavy matrix (Al in GaAs in this case). BS yield from the SLS2 and the virgin GaAs samples are nearly identical in region III. This agreement is accidental, which may be due to the difference in charge collection during acquiring the two spectra. Calculations

of the BS yield in region III using tabulated stopping cross-section and energy loss values⁽¹⁴⁾ showed that the yield for the virgin GaAs should be $\sim 10\%$ higher than that for the SLS2 sample.

To analyze the surface layers of the SLS2 sample in further detail, a high resolution BS spectrum was obtained with a tilted angle of 80° . This is shown in Fig. 2, along with the reference virgin GaAs spectrum. The BS yields from both the SLS2 and the virgin samples are identical at the surface, indicating the existence of a pure GaAs layer at the surface of SLS2. This result could not be ascertained from the spectrum in Fig. 1 because of limited resolution. The progressively lower yields of the GaAs layers below the surface of the SLS2 sample, when compared with the reference virgin GaAs sample (Fig. 2), are mainly due to the difference in the stopping powers of the He^+ beam in the two cases. In the high resolution spectrum of the SLS2 sample, uneven transition regions at the interfaces of the GaAs and $\text{Al}_x\text{Ga}_{1-x}\text{As}$ layers can also be detected. Details of these regions with respect to their thicknesses and compositional variations will be discussed later.

Channeling measurements along $\langle 100 \rangle$ and $\langle 110 \rangle$ axes (not shown) were also carried out. The minimum yields of the SLS samples are similar to those of virgin GaAs, which confirms the high crystalline quality of the SLS structures. Angular scans made across the $\langle 110 \rangle$ axis with energy windows placed in the near-surface GaAs and $\text{Al}_x\text{Ga}_{1-x}\text{As}$ layers in both the SLS1 and SLS2 samples could not detect any strain in the superlattice

structures. The precision of our channeling system is good enough to measure a strain of 1.2% in the ion-implanted materials.⁽¹⁵⁾ Thus in the $\text{Al}_x\text{Ga}_{1-x}\text{As}/\text{GaAs}$ SLS structures, the expected strain should be $< 1.2\%$.

B. X-ray rocking curve measurements

X-ray rocking curve measurements were made on both SLS1 and SLS2 samples. Figure 3(a) shows measurements made (dashed line) on the SLS1 sample with (200) reflection. The reflecting power plotted on the vertical axis has been normalized with respect to the power of the incoming beam. The angle $\Delta\theta$ is measured relative to the Bragg angle ($\theta_B \simeq 20^\circ$). Several peaks ($p_0, p_1, p_{-1} \dots$ etc.) in the rocking curve are due to the periodicity in the SLS structure. The substrate peak, p_{sub} , is embedded in the major SLS peak, p_0 in this case. In the kinematical regime, the reflecting power is proportional to the square of the structure factor.⁽¹⁶⁾ Since in the (200) reflection the structure factor of GaAs is an order of magnitude lower⁽¹⁷⁾ than that of $\text{Al}_x\text{Ga}_{1-x}\text{As}$, p_{sub} is buried in p_0 . Corresponding measurements were carried out in the (400) reflection, where p_{sub} and p_0 could be well separated. The average strain, $\langle\epsilon\rangle$, in the SLS samples was measured from the (400) rocking curves (not shown), as follows

$$\langle\epsilon\rangle \equiv \frac{\epsilon_a t_a + \epsilon_b t_b}{t_a + t_b} = -\Delta\theta_0 \cot \theta_B, \quad (1)$$

where ϵ_a , ϵ_b and t_a , t_b are the strains and the thicknesses respectively of the two layers: a, $(Al_xGa_{1-x}As)$ and b, $(GaAs)$, consisting of one period of the SLS sample; $\Delta\theta_0$ = angular difference between the peaks, p_0 and p_{sub} ; and θ_B is the Bragg angle of the substrate. Equation (1) is rigorously valid for perfectly periodic superlattice with two layers in each period.

The rocking curve measured in the (200) reflection provides a higher sensitivity to the thickness and composition variation in the periods of the SLS sample, when compared to the measurements in the (400) reflection.⁽¹⁸⁾ The (200) reflection case is thus considered here. Referring back to Fig. 3(a), the angular separations between subsidiary peaks ($\Delta\theta_{p_0-p_1}$, $\Delta\theta_{p_0-p_{-1}}$, ...etc.) are all equal and are related, for symmetric reflections, to the average thickness of the period of the superlattice, according to the relation

$$\Delta\theta_p = \Delta\theta_{p_0-p_1} = \Delta\theta_{p_0-p_{-1}} = \dots = \frac{\lambda}{2t \cos\theta_B}, \quad (2)$$

where λ is the wavelength of the x-rays, and t is the average thickness of one period. The measured curve in Fig. 3(a) (dashed line) was fitted with a calculated curve (solid line) using a kinematic model of x-ray diffraction in thin epitaxial layers. An iterative approach was adopted in the fitting, keeping the measured average strain (eq. 1) and the measured average thickness (eq. 2) values constant. Good fitting (note the logarithmic ordinate) was only obtained by accommodating

transition regions at the interfaces of GaAs and $\text{Al}_x\text{Ga}_{1-x}\text{As}$ layers. The average depth strain profile for this fitting is shown in Fig. 3(b). The Al concentration is also plotted in Fig. 3(b), since by Vegard's law⁽¹⁹⁾, perpendicular strain is linearly proportional to the Al concentration in the $\text{Al}_x\text{Ga}_{1-x}\text{As}$ layers. Another important inference from Fig. 3(b) is that in the growth of the SLS1 sample, pure GaAs layers were not achieved.

IV. DISCUSSION

Figures 1 through 3 provide insight into the structural properties of $\text{Al}_x\text{Ga}_{1-x}\text{As}/\text{GaAs}$ SLS samples. In particular, the combined use of the two techniques (BS and x-ray rocking curves) give information on the depth distribution of strain, composition, and crystalline quality. In this section, we demonstrate the complementary aspects of the two techniques in providing further details.

A. Individual period thickness determination

The ability of BS to determine the thicknesses of multilayered thin films is well established.⁽¹⁴⁾ The thicknesses of the periods of the SLS1 and SLS2 samples were determined from the stopping power data⁽¹⁴⁾ of He^+ in GaAs and $\text{Al}_x\text{Ga}_{1-x}\text{As}$ layers. For these calculations, the nominal value of $x = 0.88$ in the $\text{Al}_x\text{Ga}_{1-x}\text{As}$ layers was assumed as estimated from growth parameters. This value of x was later verified by BS and x-ray

measurements (see Figs. 2 and 3). For individual period thickness calculations, the energy loss between the two adjacent peaks in the BS spectrum (see Fig. 1) was used. The average period thickness was also estimated by dividing the total thicknesses of the SLS samples by their respective number of periods. For the total thickness calculations, the energy loss between regions I and II in Fig. 1 was used. The individual period thicknesses in SLS1 and SLS2 samples are plotted in Fig. 4, along with the average period thicknesses. The average thickness measurements made by BS agreed very well with those obtained by the x-ray rocking curves. Variations in the individual period thicknesses of the SLS samples are noticeable from Fig. 4, which may be related to the growth parameters. The relatively strong deviation from the average period thickness near the substrate interface may be due to the uncertainty in estimating the peaks in SLS BS spectra (see Fig. 1) due to the interfering Al signals.

The individual period thicknesses obtained by BS measurements, as described above, were then used to recalculate the x-ray rocking curve of the SLS1 sample. In this calculation, the parameters used were similar to those in Fig. 3(b), except that the thicknesses of the individual periods were now varied according to the BS results of Fig. 4, while keeping the sum of the products of strains and thicknesses in each period constant (see eq. (1)). The calculated rocking curve so obtained is compared with the measured curve in Fig. 5(a). The corresponding depth strain profile is shown in Fig. 5(b). As can be observed, better agreement between calculated and measured curves is

achieved in Fig. 5(a) when compared with Fig. 3(a), especially for higher order peaks. Notice here that BS and x-ray rocking curves techniques provide details on the structure of the SLS samples that nicely complement each other. The variation in the period thicknesses of the SLS samples can thus be claimed as real with good confidence.

B. Transition regions

In the analyses of the SLS1 and SLS2 samples, the transition regions between the $\text{Al}_x\text{Ga}_{1-x}\text{As}$ and GaAs sublayers are detected by both BS and x-ray rocking curves (see Figs. 2 and 3). The aluminum concentration and strain profile as a function of depth in the first period below the surface of the SLS2 sample is shown in Fig. 6. The profile derived from x-ray rocking curves was obtained in a fashion as is described in Fig. 3(b). The steps in this profile are merely representative of the real distribution, which should be continuous.⁽²⁰⁾ The Al concentration profile, measured by BS and plotted in Fig. 6, was obtained from Fig. 2. The Al concentration, (x) , was calculated from the heights $H_{\text{Al}_x\text{Ga}_{1-x}\text{As}}^{\text{GaAs}}$ and $H_{\text{GaAs}}^{\text{GaAs}}$ as defined in Fig. 2, using the relation:

$$\frac{H_{\text{GaAs}}^{\text{GaAs}}}{H_{\text{Al}_x\text{Ga}_{1-x}\text{As}}^{\text{Al}_x\text{Ga}_{1-x}\text{As}}} = \frac{\gamma_{\text{Ga}} + \gamma_{\text{As}}}{(1-x)\gamma'_{\text{Ga}} + \gamma'_{\text{As}}}, \quad (3)$$

where $H_{\text{GaAs}}^{\text{GaAs}}$ and $H_{\text{Al}_x\text{Ga}_{1-x}\text{As}}^{\text{Al}_x\text{Ga}_{1-x}\text{As}}$ are the total BS yields from Ga and As in pure GaAs and $\text{Al}_x\text{Ga}_{1-x}\text{As}$ respectively. γ_{Ga} , γ_{As} and γ'_{Ga} ,

σ_{As} are the ratios of the scattering to the stopping cross section parameters of He^+ from Ga, As in GaAs and $Al_xGa_{1-x}As$ respectively⁽¹⁴⁾. The accuracy in the composition measurement is within $\pm 1\%$. Excellent agreement in the transition regions as determined by BS and x-ray rocking curves is observed. The complementary nature of the two techniques is again exemplified. The nonsymmetric and nonabrupt profile within a period of the SLS is real and related to the growth process⁽²⁰⁾.

V. CONCLUSIONS

The combined use and power of BS and x-ray rocking curves in analyzing $Al_xGa_{1-x}As/GaAs$ SLS structures have been demonstrated. The two techniques complement each other in providing detailed information on the depth distribution of strain, composition and crystalline quality, in these structures. Such detailed information has not been accessible by previously used techniques. The analyses carried out in this paper can be easily extended to a variety of other strained-layer-superlattice structures. The quantitative information thus obtained should prove useful not only to the growers of SLS, but also in exploring their future uses in device structures.

ACKNOWLEDGMENTS

We would like to thank Y. C. M. Yeh, D. A. Smith, A. Mehta, and J. Wendt at Applied Solar Energy Corporation (ASEC) for the growth of SLS structures. Encouragement provided by K. S. Ling and P. A. Iles at ASEC is appreciated. A. H. Hamdi extends his thanks to IBM to a research fellowship. The work was supported by the Defense Advanced Research Projects Agency (S. Roosild) under contract [MDA 903-82-C-0348] at Caltech.

REFERENCES

1. J. N. Schulman and T. C. McGill, Phys. Rev. B 23, 4149 (1981).
2. L. Esaki and L. L. Chang, Phys. Rev. Lett. 33, 495 (1974).
3. W. D. Laidig, N. Holonyak, Jr., M. D. Camras, K. Hess, J. J. Coleman, P. D. Dapkus, and J. Bardeen, Appl. Phys. Lett. 38, 776 (1981).
4. G. C. Osbourn, J. Appl. Phys. 53, 1586 (1982).
5. J. W. Lee and W. D. Laidig, J. Electron. Mater. 13, 147 (1984).
6. C. M. Serrano and Chin-An Chang, Appl. Phys. Lett. 39, 808 (1981).
7. A. Segmüller, P. Krishna, and L. Esaki, J. Appl. Cryst. 10, 1 (1977).
8. W. K. Chu, F. W. Saris, C.-A. Chang, R. Ludeke, and L. Esaki, Phys. Rev. B, 26, 1999 (1982).
9. S. T. Picraux, L. R. Dawson, G. C. Osbourn, R. M. Biefeld, and W. K. Chu, Appl. Phys. Lett. 43, 1020 (1983).
10. W. K. Chu, C. K. Pan, and C.-A. Chang, Phys. Rev. B 28, 4033 (1983).
11. W. K. Chu, T. A. Ellison, S. T. Picraux, R. M. Biefeld, and G. C. Osbourn, Phys. Rev. Lett. 52, 125 (1984).
12. J. L. Tandon and Y. C. M. Yeh, (to be published).
13. V. S. Speriosu, J. Appl. Phys. 52, 6094 (1981).
14. W. K. Chu, J. W. Mayer, and M-A. Nicolet, Backscattering Spectrometry (Academic Press, New York, 1978).

15. B. M. Paine, V. S. Speriosu, L. S. Wieluński, H. L. Glass, and M-A. Nicolet, Nucl. Instrum. Meth. 191, 80 (1981).
16. W. H. Zachariasen, Theory of X-Ray Diffraction in Crystals (Wiley, New York, 1945).
17. The structure factors of $\text{Al}_{0.88}\text{Ga}_{0.12}\text{As}$ (= 61.1) and GaAs (= 6.4) were calculated from tables of atomic scattering factors for x-rays; J. A. Ibers and W. C. Hamilton, International Tables for X-Ray Crystallography, Vol. IV, (Kymoch Press, Birmingham, 1974).
18. V. S. Speriosu and T. Vreeland, Jr., (to be published in J. Appl. Phys).
19. W. J. Bartels and W. Nigman, J. Cryst. Growth, 44, 518 (1978).
20. A. H. Hamdi, (to be published).

FIGURE CAPTIONS

Figure 1 BS spectra of 2 MeV He^+ obtained for random incidence on SLS2, 15 periods (dotted lines), and virgin GaAs samples (solid lines). The SLS spectrum contains 15 maxima and minima, in region I, which indicates the number of the $\text{Al}_x\text{Ga}_{1-x}\text{As}/\text{GaAs}$ periods.

Figure 2 High resolution (80° tilted) BS spectra for random incidence on SLS2 and virgin GaAs samples. Near the surface, the yield from the SLS2 sample reaches the yield from the virgin GaAs sample, which implies that the surface layer in the SLS2 sample is pure GaAs.

Figure 3 (a) Plots of $\text{Fe K}_{\alpha 1}$ (200) reflection x-ray rocking curves from sample SLS1. The dashed line is measured. The solid line is calculated by using the strain depth profile in (b).

Figure 4 The individual and average period thicknesses of SLS1 (10 periods) and SLS2 (15 periods) derived from BS spectra as shown in Fig. 1 for the SLS2 sample. X-ray thicknesses were extracted from the fitted rocking curves in (200) and (400) reflections, e.g. as shown in Fig. 3 for the SLS2 sample.

Figure 5 (a) The dashed line is the $\text{Fe K}_{\alpha 1}$ rocking curve for the

(200) reflection measured from the SLS1 sample shown also in Fig. 3(a). The solid line rocking curve was calculated by using the thickness of the individual periods measured by BS (Fig. 4) which gave the depth profile of strain shown in (b).

Figure 6 The depth distribution of strain and the Al concentration in the first period of the SLS2 sample. The strain profile was derived from the x-ray rocking curve, as explained in Fig. 3. The Al concentration profile was determined from the BS spectrum of Fig. 2 (see text). Excellent agreement exists between the two techniques.

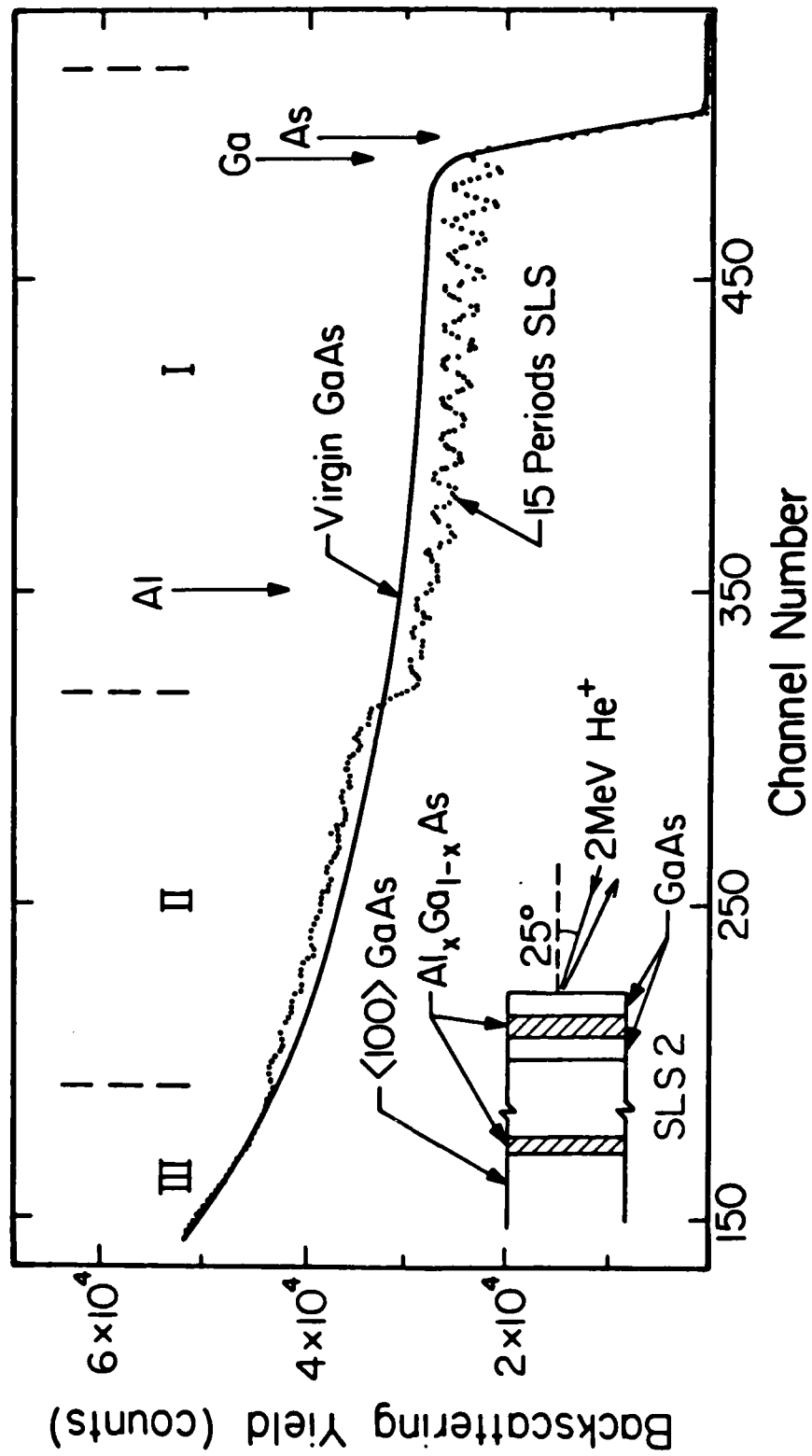


Fig. 1

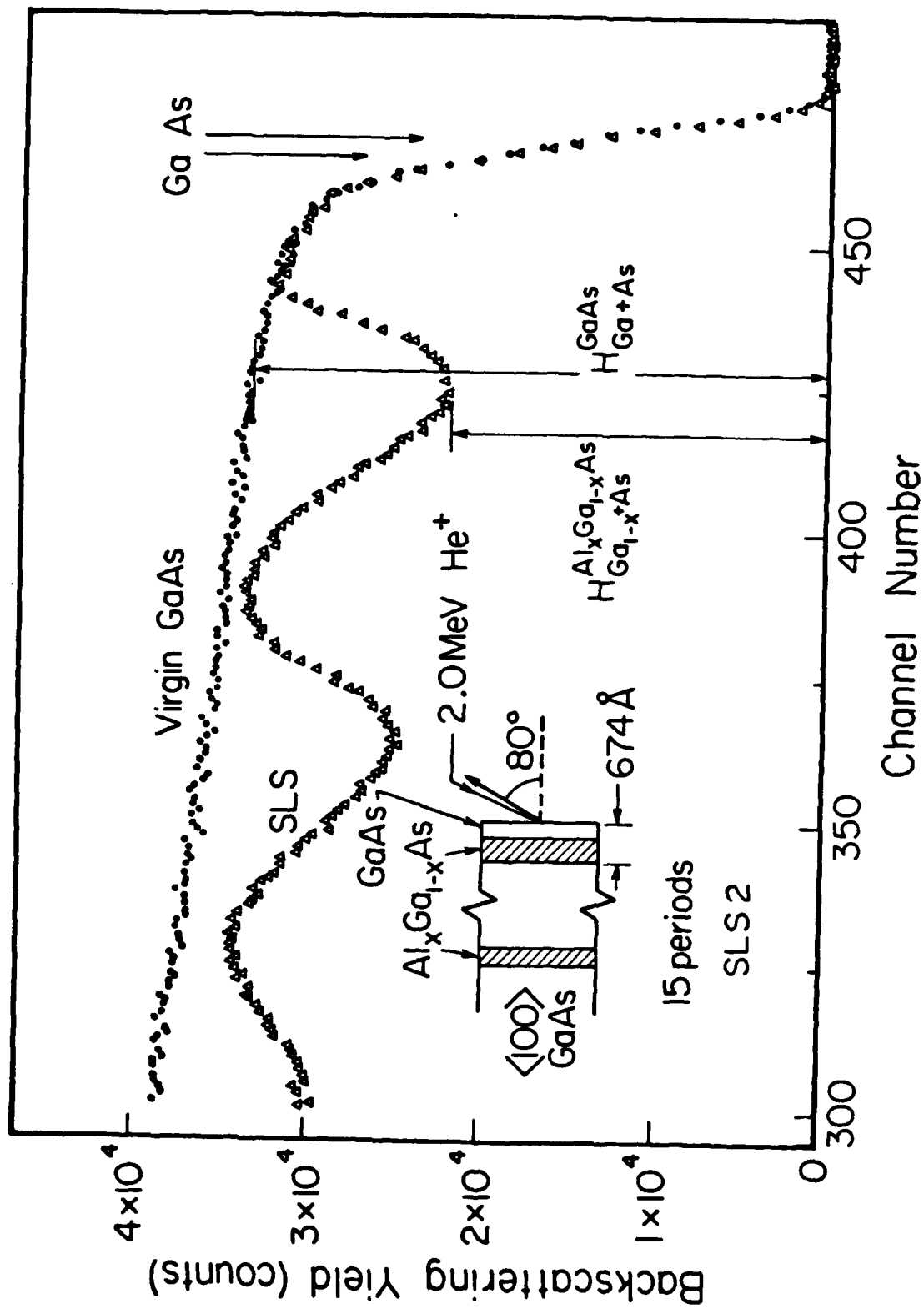


Fig. 2

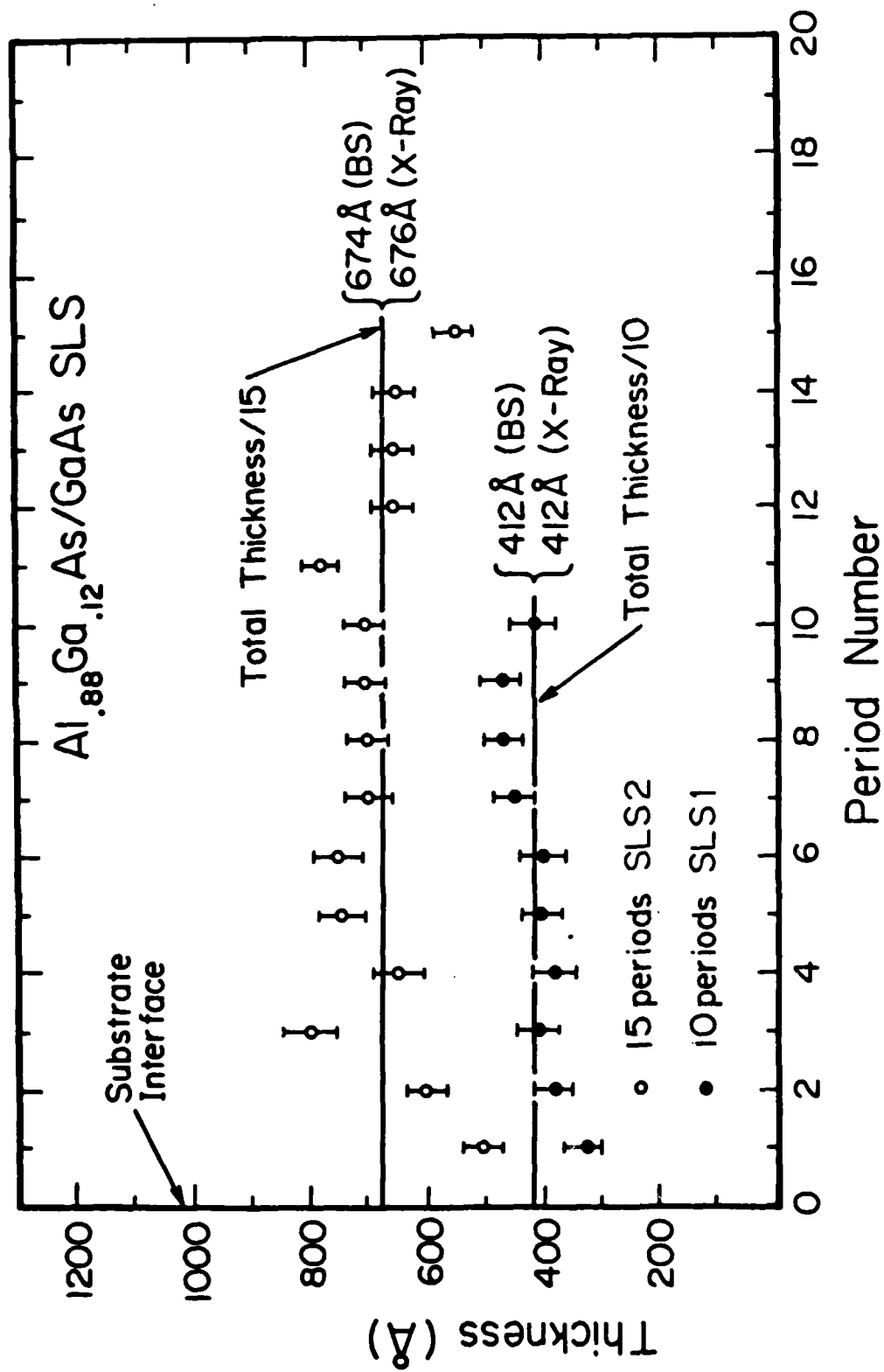


Fig. 3

AD-A147 449

X-RAY AND BACKSCATTERING ANALYSIS OF ION IMPLANTATION
PHENOMENA IN GAAS A... (U) CALIFORNIA INST OF TECH
PASADENA M A NICOLET ET AL. 04 AUG 84 MDA903-82-C-0348

3/3

UNCLASSIFIED

F/G 20/12 NL

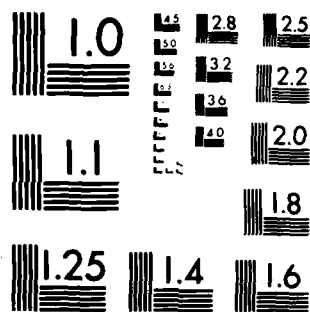


END

DATE
F/G 20/12

DTIC

12-84



MICROCOPY RESOLUTION TEST CHART
NATIONAL BUREAU OF STANDARDS-1963-A

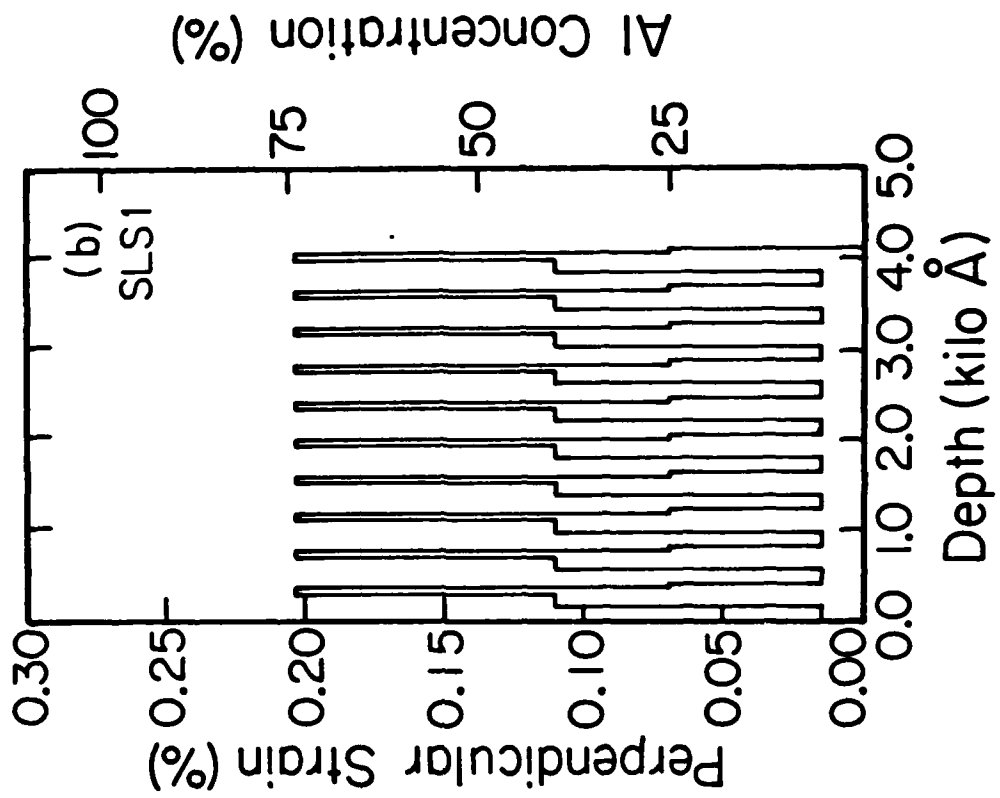
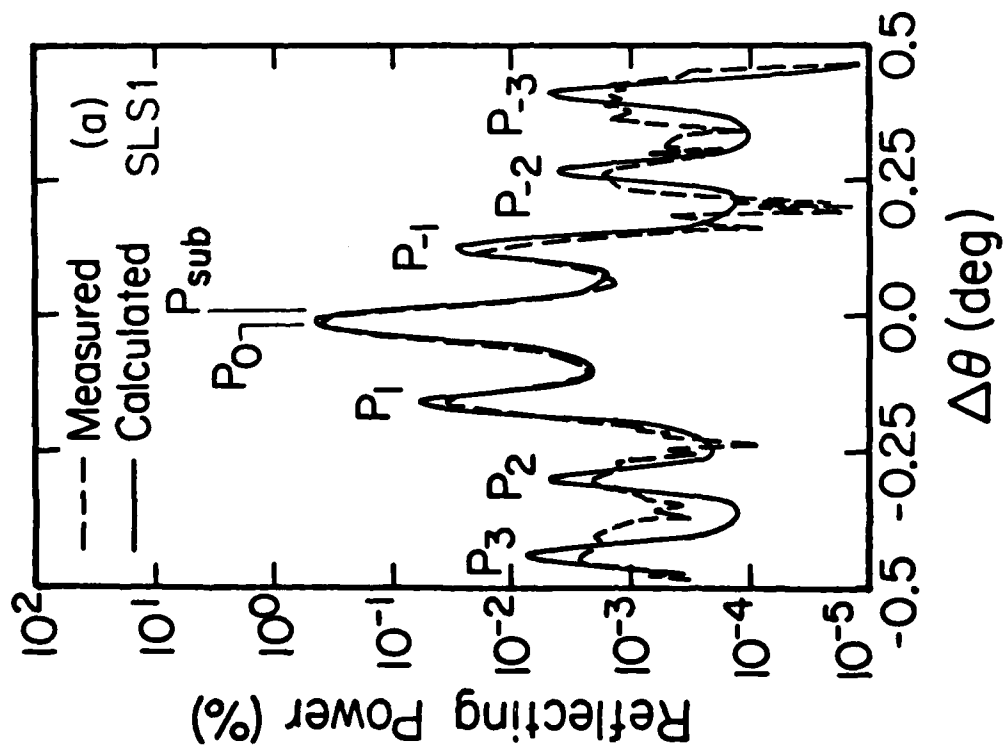


Fig. 4

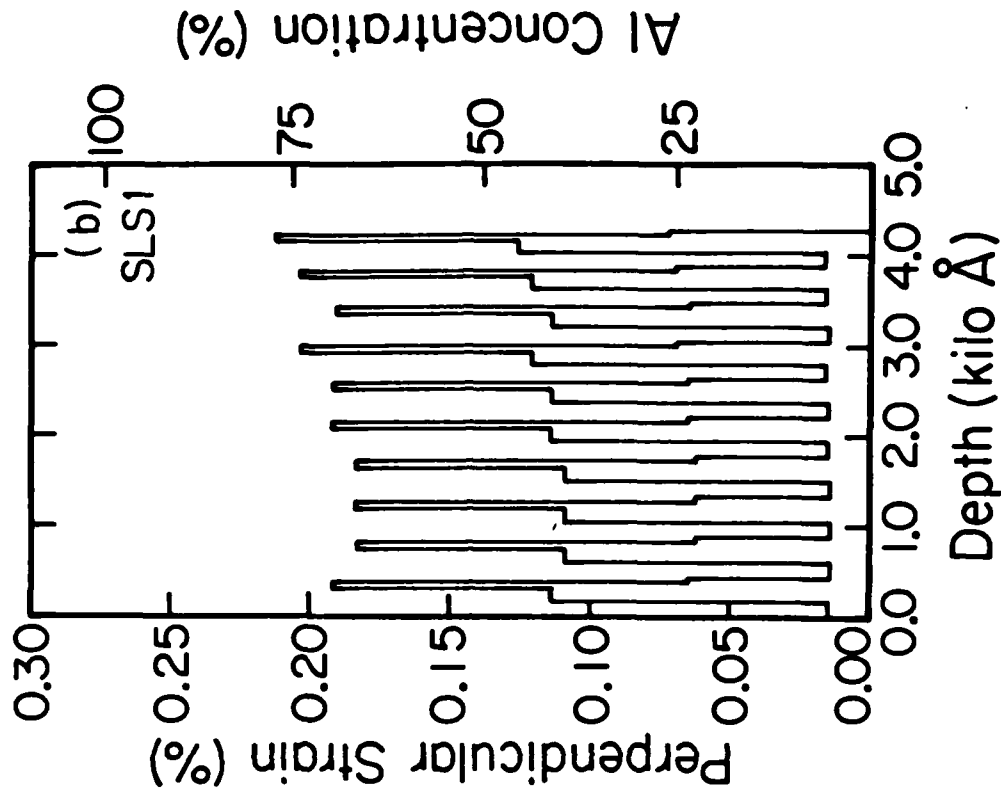
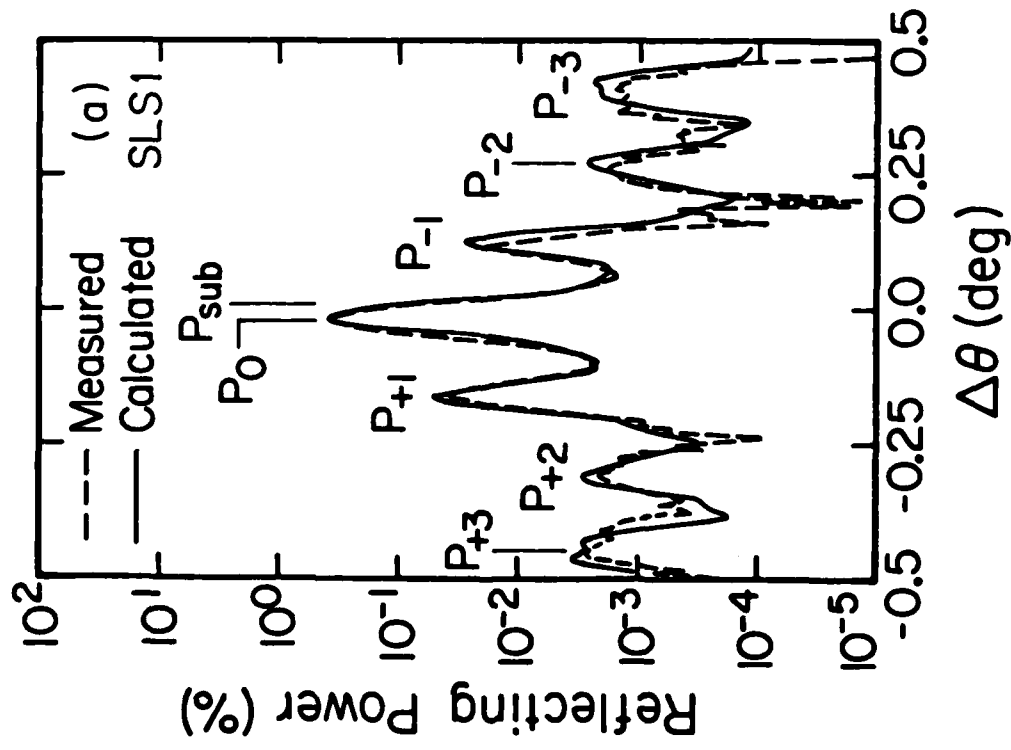


Fig. 5

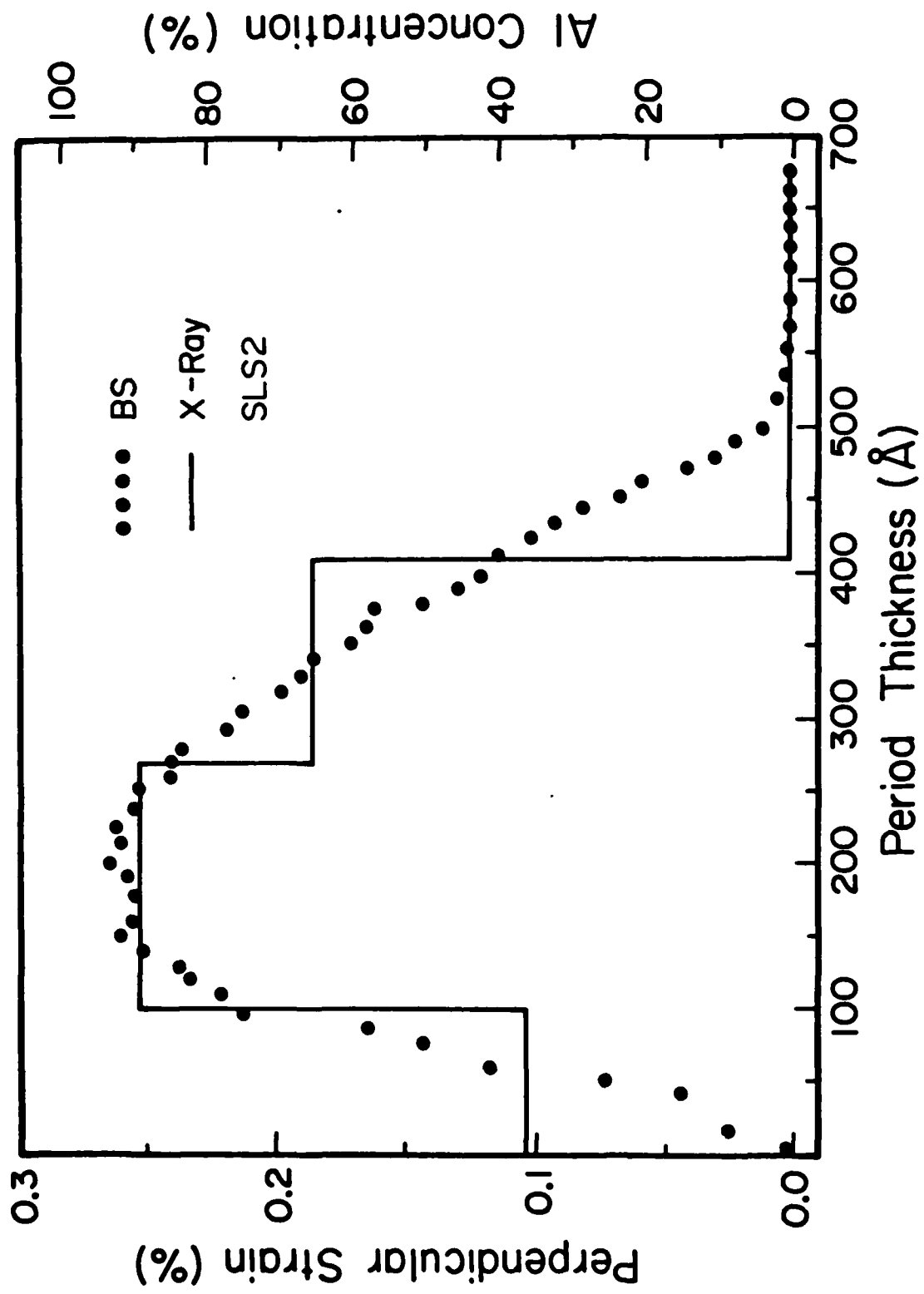


Fig. 6